DISSECTING CENTRIOLAR SATELLITE FUNCTION USING INDUCIBLE GENETIC TOOLS

by

Selin Yılmaz Karaoğlu

A Dissertation Submitted to the
Graduate School of Sciences and Engineering
in Partial Fulfillment of the Requirements for
the Degree of

Master of Science

in

Molecular Biology and Genetics

KOÇ ÜNİVERSİTESİ

31 July, 2025

Dissecting Centriolar Satellite Function Using Inducible Genetic Tools

Koç University

Graduate School of Sciences and Engineering

This is to certify that I have examined this copy of a master's thesis by

Selin Yılmaz Karaoğlu

and have found that it is complete and satisfactory in all respects,
and that any and all revisions required by the final
examining committee have been made.

Committee Members:

_____

Assoc. Prof. Elif Nur Fırat Karalar (Advisor)

_____

Assist. Prof. Ayşe Koca Çaydaşı

_____

Assoc. Prof. Umut Şahin

Date: 31 July, 2025

To cytoskeleton,

ABSTRACT

Dissecting Centriolar Satellite Function Using Inducible Genetic Tools

Selin Yılmaz Karaoğlu

Master of Science in Molecular Biology and Genetics

31 July, 2025

Centriolar satellites are membraneless granules that facilitate protein trafficking to the centrosome and primary cilium, but the principles governing their assembly, dynamics, and functional roles remain poorly defined. Here, we introduce two chemogenetic tools to manipulate satellite organization. First, chemically inducible Kin-14 motor protein-based trafficking system acutely concentrates satellite granules at the centrosome, altering client protein organization. This centrosomal foci created by PCM1 and other clients, behave like a solid compartment and does not dissolve during mitosis. Functionally, forced satellite accumulation disrupts mitotic progression, proper spindle formation, and chromosome congression. In our second system, we are utilizing a chemically inducible centriolar satellite dimerization assay to regulate the multimerization state of PCM1. Ligand-induced dimerization changes satellite organization by enlarging the granules and reducing their numbers. Notably, satellite multimerization prevents their mitotic dissolution and disrupts Hedgehog signaling but does not affect cilium assembly. Finally, we applied a high-throughput image-analysis pipeline to patient derived fibroblasts bearing mutations in ciliopathy related genes and showed that there are no significant differences in satellite number, intensity, or spatial distribution compared to control cells. Together, this thesis establishes various chemical assays for acute perturbation of centriolar satellites, demonstrate that dynamicity and multivalency are critical for proper centriolar satellite function, and indicate that satellite mislocalization and content is not a universal feature of ciliopathies.

ÖZETÇE

Sentriyoler Satelit Fonksiyonlarının Genetik Araçlar ile İncelenmesi

Selin Yılmaz Karaoğlu

Moleküler Biyoloji ve Genetik, Yüksek Lisans

31 Temmuz 2025

Sentriyoler satelitler, membransız granüller olarak sentrozoma ve primer silyuma protein taşınmasında görev alır; ancak bunların oluşumu, dinamikleri ve rolleri henüz tam olarak tanımlanmamıştır. Bu çalışmada, insan hücrelerinde satelitlerin organizasyonunu manipüle etmek için iki kemogenetik araç tanıtıyoruz. Öncelikle, kimyasal olarak indüklenen Kin-14 motor proteini tabanlı trafik sistemi, satelit granüllerini hızla sentrozoma yoğunlaştırıp diğer satelit proteinlerinin de organizasyonunu değiştirdi. PCM1 ve satelit proteinlerinden oluşan bu sentrozomal parçalar katı gibi davrandı ve mitoz sırasında çözünmedi. İşlevsel olarak, zorunlu sentrozomal kümelenmesi mitotik ilerlemeyi, doğru iğ oluşumunu ve kromozom kongresyonunu bozdu. İkinci sistemimizde ise PCM1'in multimerizasyon durumunu değiştirmek için kimyasal olarak indüklenen bir sentriyoler uydu dimerizasyon sistemi kullanıyoruz. Ligand kaynaklı dimerizasyon, granülleri büyütüp sayılarını azaltarak satelit organizasyonunu değiştirdi. Önemli olarak, satelit multimerizasyonu granüllerin mitoz esnasında çözünmesini engelledi ve Hedgehog sinyal iletimini bozdu, fakat silyum oluşumunu etkilemedi. Son olarak, silyopati hastalığı ile ilişkili genlerde mutasyonlar taşıyan hasta kökenli fibroblastlara uygulanan yüksek verimli görüntü analiz çalışması, satelit sayısı, yoğunluğu veya uzaysal (spatial) dağılım açısından kontrol hücreleriyle anlamlı farklılıklar göstermedi. Birlikte, bu çalışmalar sentriyoler uyduların akut pertürbasyonu için çeşitli kimyasal deneyler geliştirilmesini sağlayıp, satelitlerin dinamikliğinin ve multimerik regülasyonun mitotik ilerleme ve silya sinyal iletimi için kritik olduğunu göstermektedir. Bunun yanı sıra, satelitlerin içeriğinin ve hücre içerisinde yanlış konumlanmasının tüm silyopatilerde ortak bir özellik olmadığını göstermektedir.

ACKNOWLEDGMENTS

First, I would like to express my heartfelt gratitude to my advisor, Assoc. Prof. Elif Nur Fırat Karalar, for her support, guidance, and inspiring mentorship throughout my Master's studies. Her scientific vision and dedication have profoundly shaped both this thesis and my development as a researcher. She is a role model for me.

I am also deeply thankful to all the members of Cytolab including Jovana, Ezgi, Melis, Efe, Başak, Şeyma, Hande, İrem, Ece, Alper, and Hilal for their contribution and support. In particular, I would like to extend my warmest thanks to Başak and Ezgi for their mentoring, and I especially would like to thank Efe for his encouragement, generosity, and friendship.

I would like to express my appreciation to my thesis jury members, Assist. Prof. Ayşe Koca Çaydaşı and Assoc. Prof. Umut Şahin, for their time, valuable feedback, and thoughtful discussions that enriched this work.

I gratefully acknowledge the financial support provided by TÜBİTAK (Project no: 123N048, 124Z240), the European Research Council (ERC StG SatelliteHomeostasis), and the European Joint Programme on Rare Diseases (PREDICT: Towards a PREcise DIagnosis in Ciliopathies), which made this research possible.

I am especially thankful to Prof. Ronald Roepman and Dr. Mariam Aslanyan for their collaborative spirit, constructive input, and the opportunity to work together across institutions.

My deepest gratitude goes to my family including my mother Hatice, my father Zeynel, and my sister Ceren for their unconditional love, patience, and endless support.

Lastly, I want to thank my husband, İsmail, whose endless love, support, and encouragement have been my anchor through every challenge. This accomplishment is as much his as it is mine and I am sure we will build the best life possible together we begin this exciting new chapter in the Netherlands.

Work presented in this thesis has been published in the following journals:

Begar, E., Yilmaz, S., Seyrek, E., Arslanhan, M. D., Odabasi, E., & Firat-Karalar, E. N. (2025). Centriolar satellites are dynamic membrane-less organelles that assemble via a hierarchical pathway. bioRxiv, 2025-07.

LIST OF TABLES

LIST OF FIGURES

ABBREVIATIONS

ANOVA	Analysis of variance
ARL	ADP-ribosylation factor-like
ATP	Adenosine triphosphate
BCA	Bicinchoninic acid assay
BBS	Bardet–Biedl syndrome
BICD2	Bicaudal D homolog 2
BioID	Proximity-dependent biotin identification
BSA	Bovine serum albumin
CCDC	Coiled-coil domain-containing
CDK1	Cyclin-dependent kinase 1
CEP	Centrosomal protein
CETN	Centrin
DAPI	4′,6-Diamidino-2-phenylindole
DMEM	Dulbecco’s Modified Eagle’s Medium
DMSO	Dimethyl sulfoxide
DNA	Deoxyribonucleic acid
DYNC2H1	Dynein cytoplasmic 2 heavy chain 1
DYRK3	Dual-specificity protein kinase 3
EDTA	Ethylenediaminetetraacetic acid
FBS	Fetal bovine serum
FKBP	FK506-binding protein
FITC	Fluorescein isothiocyanate
FRAP	Fluorescence recovery after photobleaching
FRB	FKBP-rapamycin binding domain
GABARAP	Gamma-aminobutyric acid receptor-associated protein
GFP	Green fluorescent protein

GO	Gene onthology
GPCR	G protein-coupled receptors
gRNA	Guide RNA (for CRISPR/Cas9)
HEK	Human embryonic kidney
HEPES	4-(2-Hydroxyethyl)-1-piperazineethanesulfonic acid
HRP	Horseradish peroxidase
IF	Immunofluorescence
IFT	Intraflagellar transport
IDR	Intrinsically disordered region
IMCD3	Inner medullary collecting duct
INPP5E	Inositol polyphosphate-5-phosphatase E
IP	Immunoprecipitation
JBTS	Joubert syndrome
kDa	Kilodalton
Kin14	Minus-end directed kinesin-14 motor
LCA	Leber’s congenital amaurosis
LLPS	Liquid–liquid phase separation
mAb	Monoclonal antibody
MAPK	Mitogen-activated protein kinase
MIB	Mindbomb
MKS	Meckel-Gruber syndrome
mNG	mNeonGreen
MTOC	Microtubule organizing center
mTOR	Mammalian target of rapamycin
NA	Numerial aperture
nm	nanometer
nM	nanomolar
NPHP	Nephronophthisis
NSAF	Normalized spectral abundance factor
NT	No treatment
OFD	Orofaciodigital
PBS	Phosphate-buffered saline

PCD	Primary ciliary dyskinesia
PCR	Polymerase chain reaction
PCM	Pericentriolar material
PCM1	Pericentriolar material 1
PDGF	Platelet-derived growth factor
PEI	Polyethyleneimine
PIP	Phosphatifylinositol
PKD	Polycystic kidney disease
PLK1	Polo-like kinase 1
PMSF	Phenylmethylsulfonyl fluoride
PSM	Peptide spectrum match
RIPA	Radioimmunoprecipitation assay buffer
ROI	Region of interest
ROSA	Reverse orientation splice acceptor
RPE1	Retinal pigment epithelial
RT	Room temperature
SAG	Smoothened agonist
SD	Standard deviation
SDS	Sodium dodecyl sulfate
Shh	Sonic Hedgehog
SIM	Structural illumination microcopy
SLS	Senior–Løken syndrome
STED	Stimulated emission depletion
TBS	Tris-buffered saline
TXR	Texas red
UV	Ultraviolet
W/O	Wash-out
WT	Wild-type
WDR	WD-repeat

Chapter 1

1. INTRODUCTION

1.1. Mammalian Centrosome/Cilium Complex and Its Importance

The mammalian centrosome/cilium complex is composed of three components: the centrosome, the primary cilium, and the centriolar satellites (Arslanhan et al., 2020). Together, these structures function as a unit to regulate fundamental cellular processes such as cell polarity, signal transduction, cell proliferation, and motility, thereby ensuring proper development and tissue homeostasis in the organisms (Schatten, 2008). Disruption of the structure or function of the centrosome/cilium complex is implicated in a broad range of human diseases, including developmental disorders, cancer, and neurodegenerative disorders. In particular, genetic defects affecting the centrosome or cilium give rise to ciliopathies, a group of disorders caused by ciliary dysfunction, underscoring the critical importance of this organelle complex in human health and development (Badano et al., 2005).

1.2. The Centrosome

The centrosome is a membraneless organelle that serves as the primary microtubule-organizing center (MTOC) of animal cells. It plays central roles in organizing the interphase microtubule network, establishing cell polarity and adhesion, and forming the bipolar spindle during mitosis to ensure accurate chromosome segregation (Conduit et al., 2015). Structurally, each centrosome consists of two orthogonally arranged microtubule-based structures called centrioles, which are surrounded by an electron-dense protein matrix known as the pericentriolar material (PCM) (Bettencourt-Dias & Glover, 2007). Below, the main structural components of the centrosome and their function are described, as well as how the centrosome transitions to become the basal body of a cilium in quiescent cells.

1.2.1. Centrioles

Centrioles are barrel-shaped, microtubule-based structures typically about 200 nm in diameter and 400–500 nm in length. They are characterized by a nine-fold symmetric arrangement of microtubule triplets along their length. In human centrioles, the proximal portion contains nine microtubule triplets, whereas the distal portion is composed of nine doublet microtubules (Arslanhan et al., 2023). This microtubule scaffold gives the centriole an intrinsic polarity where the proximal end contains the older cartwheel assembly used for duplication, and the distal end is where appendage structures can form (Bettencourt-Dias & Glover, 2007).

Centrioles within a centrosome exist as a mother–daughter pair differing in age and maturity. The older mother centriole possesses distal appendages arranged in a nine-fold symmetric array, as well as subdistal appendages. Whereas the younger daughter centriole generally lacks these appendages until it matures in the next cell cycle. Subdistal appendages on the mother centriole act as anchor points for a subset of cytoplasmic microtubules, contributing to cell architecture and organelle positioning In addition, the distal appendages of the mother centriole are crucial for membrane docking during ciliogenesis, effectively enabling the mother centriole to attach to a vesicle or the plasma membrane and serve as a basal body for cilium formation. (Kumar & Reiter, 2021).

During the cell cycle, centrioles duplicate once per cycle to ensure each daughter cell inherits a centrosome with two centrioles. A new procentriole called daughter centriole forms orthogonally next to each pre-existing centriole in S phase, elongates through G2, and disengages in mitosis, followed by maturation that involve acquisition of appendages in the subsequent cell cycle. This strict duplication cycle normally limits centriole number to two per cell, a control vital for genomic stability (Firat-Karalar et al., 2014; Fırat-Karalar & Stearns, 2014).

1.2.2. Pericentriolar Material (PCM)

Pericentriolar material surrounds the centrioles, which is an amorphous protein-based matrix that concentrates factors required for microtubule nucleation and anchoring (Woodruff et al., 2014). Key components of the PCM include large coiled-coil proteins and scaffolding factors such as pericentrin and CEP152, as well as γ-tubulin ring complexes, which directly nucleate microtubule minus-ends. The PCM thus provides a platform to organize microtubules emanating from the centrosome and to orchestrate

signaling activities localized at the centrosome. For example, the PCM is involved in sequestering and regulating proteins that control cell-cycle progression and proteostasis (Comartin & Pelletier, 2016). The PCM can expand in size at the onset of mitosis to increase microtubule-nucleating capacity for spindle formation, and then it contracts after cell division. In summary, the PCM serves as a dynamic scaffold that both structurally integrates the centrioles into a single functional unit and functionally amplifies the centrosome's ability to organize the cytoskeleton and signaling molecules (Woodruff et al., 2014).

1.2.3. Functions of Centrosome

As the cell's main MTOC, the centrosome is best known for its function in nucleating and organizing microtubules. In interphase, the radial array of microtubules emanating from the centrosome helps position organelles and establishes cell polarity and directed cell migration. In polarized cell types like epithelial cells or neurons, centrosomes contribute to asymmetric organization of the microtubule cytoskeleton, thereby influencing the placement of the Golgi apparatus, nucleus, and other structures to define the front–rear or apical–basal polarity of the cell (Firat-Karalar & Stearns, 2015). During cell division, the centrosomes form the spindle poles. Their microtubule-nucleating activity is upregulated at mitotic entry to facilitate assembly of the bipolar mitotic spindle, ensuring accurate chromosome alignment and segregation (Prigent & Uzbekov, 2022).

Beyond microtubule organization, the centrosome is increasingly recognized as a signaling hub. It localizes certain cell cycle regulators such as kinases and ubiquitin ligases that monitor centriole duplication and spindle assembly checkpoints. It also concentrates misfolded proteins and proteasomes as components of the proteostasis machinery and forms aggresomes under stress conditions. This positioning may help cells manage protein quality control by coordinating with autophagy and proteasomal degradation pathways. Moreover, in some post-mitotic cells like neurons, centrosomes serve as platforms for signaling cascades; for instance, in developing neurons the centrosome and associated satellites help regulate dendrite branching by anchoring signaling proteins (Puram et al., 2011).

A remarkable feature of the centrosome is its ability to transform into a basal body to seed the formation of a primary cilium when cells exit the cell cycle (Arslanhan et al., 2020). Upon entry into G0 or quiescence, the cell's mother centriole migrates to the cell

surface and docks at the plasma membrane via its distal appendages. This docking event initiates the assembly of the primary cilium, a process known as ciliogenesis. The mother centriole, now referred to as the basal body, organizes the extension of the ciliary axoneme and recruits components necessary to build the ciliary membrane and transition zone (Schmidt et al., 2012).

1.3. The Primary Cilium

The primary cilium is a microtubule-based, antenna-like projection found on the surface of most mammalian cell types. Its main function is sensory and signaling where it serves as a hub for receiving and processing extracellular signals. The primary cilium is often described as a "cellular antenna" that coordinates signaling pathways crucial for development and homeostasis, including Hedgehog, Wnt, PDGF, and others (Singla & Reiter, 2006). By concentrating receptors and signaling molecules within its confined space, the cilium can spatially and temporally regulate signaling events that influence gene expression, cell fate decisions, and tissue patterning. In addition, specialized primary cilia in certain cells mediate mechanosensation. Given these critical roles, defects in ciliary structure or function lead to a range of diseases and developmental syndromes termed ciliopathies (Goetz & Anderson, 2010).

1.3.1. Cilium Assembly Pathways

Ciliogenesis can proceed via two pathways depending on the cell type, although both ultimately produce a similar ciliary organelle. The extracellular pathway is observed in many epithelial cells like lung airway and kidney collecting duct cells, the mother centriole directly attaches to the plasma membrane at the cell surface via its distal appendages (Tanos et al., 2013). Once docked, the mother centriole/basal body initiates polymerization of the axonemal microtubules that protrude outward as the ciliary shaft, pushing the ciliary membrane upward as the cilium elongates (Hagiwara et al., 2004). Essentially, the cilium grows openly into the extracellular space from the start.

In contrast, the intracellular pathway of ciliogenesis, first described in fibroblasts, smooth muscle cells, and certain retinal cells, involves an intermediate vesicle stage (Sorokin, 1962). In these cells, a small Golgi-derived periciliary vesicle is recruited to and docks on the distal appendages of the mother centriole, covering the centriole's distal end. Additional vesicles then fuse to form a larger ciliary vesicle that envelops the distal end of the centriole. The axoneme begins to assemble within this membrane-bound

compartment inside the cytoplasm (Westlake et al., 2011). As the axoneme elongates and the transition zone forms, the growing ciliary compartment is trafficked to the cell surface. Finally, the outer membrane fuses with the plasma membrane, thereby exposing the cilium, which can then continue to elongate outside the cell. A main event of the intracellular route is the formation of a ciliary pocket. The pocket is formed through the invagination of the cell membrane around the base of the emerging cilium, which may serve as a specialized region for vesicular trafficking and signaling at the cilium's base (Ghossoub et al., 2011).

Both ciliogenesis pathways involve common key steps such as mother centriole docking, axoneme polymerization, assembly of the transition zone and growth of the ciliary membrane, yet they differ in whether axoneme growth begins before or after the basal body contacts the plasma membrane. Notably, the choice of pathway correlates with cell type. For example, retinal pigment epithelial cells and fibroblasts typically use the intracellular pathway, whereas many polarized epithelial cells use the direct extracellular pathway as mentioned earlier (Goetz & Anderson, 2010). The molecular determinants that dictate which pathway a given cell employs are still under investigation.

1.3.2. Structure and Compartments of the Cilium

Although the cilium is a relatively small organelle, it is subdivided into distinct structural and functional compartments (Arslanhan et al., 2020). Understanding these compartments is key to appreciating how the cilium functions as a signaling organelle. The main ciliary structural elements and subdomains are outlined below.

Basal Body and Transition Zone

The basal body is formed by the docking of the mother centriole at the membrane, anchoring the base of the cilium. The transition zone is the region just above the basal body, characterized by Y-shaped protein linkers that connect the peripheral microtubule doublets to the ciliary membrane. The transition zone functions as a selective gate or diffusion barrier, controlling which proteins can enter or leave the ciliary compartment (Garcia-Gonzalo & Reiter, 2017). It is assembled from several multiprotein complexes, notably the Meckel-Gruber syndrome (MKS) module, the Nephronophthisis (NPHP) module, and the Joubert syndrome (JBTS) module, named after the ciliopathy syndromes caused by mutations in their components (Williams et al., 2011). These complexes cooperate to form a structural "gate" that restricts the free diffusion of proteins between

the ciliary membrane and the rest of the cell, thereby maintaining the unique composition of the cilium.

Axoneme

The axoneme is the core skeletal structure of the cilium, consisting of microtubules that extend from the basal body. In primary cilia, the axoneme has a "9+0" arrangement formed by nine outer microtubule doublets, whereas the motile cilia typically have a "9+2" arrangement formed by nine doublets plus along with a central pair and also includes dynein arms attached to the doublets (Deretic et al., 2023). The axoneme provides the scaffold along which molecular motors ferry cargo up and down the cilium and on which signaling molecules can be concentrated. The growth of the axoneme at its plus-end is a tightly regulated process which requires proper delivery of tubulin building blocks and microtubule-associated proteins via intraflagellar transport (Satir & Christensen, 2007).

Ciliary Membrane

The ciliary membrane is the specialized section of the cell's plasma membrane that wraps around the axoneme. It is continuous with the plasma membrane but has a distinct protein and lipid composition. Many receptors including Hedgehog, PDGF, somatostatin, and ion channels are specifically localized to the ciliary membrane (Gilula & Satir, 1972). The unique composition of the ciliary membrane is established and maintained by the transition zone barrier and by active trafficking mechanisms that target or retain certain proteins in cilia. Lipids such as phosphoinositides are also differentially distributed. For example, $PI(4,5)P_2$ is relatively low in the ciliary membrane while PI(4)P is enriched, which helps recruit cilia-specific membrane proteins and the BBSome. The ciliary membrane and the basal body region often form a ciliary pocket or invagination at the base, which is thought to facilitate endocytosis and exocytosis of ciliary membrane components (Garcia-Gonzalo et al., 2015).

Intraflagellar Transport (IFT) Machinery

Intraflagellar transport (IFT) is a bidirectional trafficking system that moves molecular cargo along the axoneme. IFT is essential for the assembly and maintenance of cilia depend. The transport is carried out by large protein complexes called IFT trains, which are composed of two multimeric sub-complexes, IFT-A and IFT-B, that link cargo

to molecular motors. Kinesin-2 motors drive anterograde IFT (from the base toward the tip of the cilium), carrying building materials needed for cilium assembly and delivering signaling receptors to the ciliary tip. At the tip, cargo is unloaded and sometimes processed, and the trains are then recycled back. The dynein-2 motor drives retrograde IFT (from the tip back to the base), carrying recycled components, signaling molecules that need to exit, or turnover products back to the cell body. IFT is essential for cilium growth and function. Without IFT, cilia either fail to assemble or are resorbed because proteins cannot be moved in and out efficiently (Pedersen & Rosenbaum, 2008).

BBSome Complex

The BBSome is a specialized protein complex named after Bardet-Biedl Syndrome (BBS) which is a human ciliopathy caused by mutations in its subunits. The BBSome is an octameric complex made up of BBS1, BBS2, BBS4, BBS5, BBS7, BBS8, BBS9, and BBIP1 that functions as an adaptor in ciliary trafficking, particularly for membrane proteins. It works in co-operation with IFT. While the BBSome can recognize membrane protein cargo and link them to the IFT trains, the trains transport them into the cilium (Jin et al., 2010). It also plays a role in removing specific receptors from the cilium, thereby tuning ciliary signaling. The BBSome is recruited to the basal body and ciliary compartment with the help of small GTPase ARL6/BBS3 and forms a coat-like structure that captures cargo proteins in vesicles that fuse with the ciliary membrane. In cells, loss of BBSome function leads to mislocalization of ciliary membrane proteins and dysregulation of signaling, explaining many features of Bardet-Biedl syndrome such as retinal degeneration, kidney cysts, obesity, and polydactyly due to widespread cilia dysfunction) (Liew et al., 2014).

These compartments work together to ensure that the cilium is assembled correctly and can fulfill its signaling duties. The transition zone gates the entry of molecules where the IFT trains and BBSome ferry required components in and out; the axoneme provides the structural support; and the ciliary membrane hosts the receptors and channels that receive external cues. The integrity of each part is critical.

1.3.3. Functions of Cilia

Sensory Signaling

The primary cilium is enriched with receptors and ion channels that detect various external stimuli. For instance, in Hedgehog signaling, the Patched and Smoothened receptors localize to the cilium; the presence of a ligand (Sonic hedgehog) triggers accumulation of Smoothened in the ciliary membrane and activation of downstream GLI transcription factors. Many other pathways (Wnt, Notch, GPCR signaling, etc.) have components that traffic through cilia or are regulated by ciliary presence, highlighting the cilium's broad importance in cell communication (Veland et al., 2009).

Developmental Patterning

Due to their role in signaling, cilia are also essential for embryonic development. Proper formation of limbs, brain structures, and organs often depends on ciliary signaling gradients. For example, cilia on embryonic node cells generate a left-right asymmetric fluid flow that is required for correct body axis specification (Nonaka et al., 1998). Mutations that ablate cilia can lead to developmental anomalies such as defects in organ positioning or neural tube formation (Lehman et al., 2008).

Mechanosensation

Some cilia can act as mechanosensors. In kidney epithelial cells, the bending of the primary cilium by fluid flow triggers mechanical activation of calcium channels in the ciliary membrane, initiating signaling cascades that influence cell proliferation and polarity in the kidney. Defects in this mechanosensory function are linked to polycystic kidney disease and abnormal fluid sensing leads to cyst formation (Prasad et al., 2014).

Motility

While the primary focus of this section is the non-motile primary cilium, it should be noted that motile cilia is essential for cells with multiple cilia. The structure of motile cilia is generally similar to primary cilia except that motile cilia have additional structural components to enable movement (Armengot et al., 2010). These structures perform crucial functions that rely on ciliary beating such as mucus clearance or cerebrospinal fluid circulation in airway epithelial cells and ependymal cells in the brain ventricles (Mitchison & Valente, 2017).

1.3.4. Roles of Cilia in Health and Disease

Cilia are involved in many specific biological processes. In development, cilia on embryonic cells are required for establishing left-right asymmetry and for the function of many morphogen signaling gradients (Nonaka et al., 1998). In adult tissues, cilia continue to mediate sensory functions. For example, photoreceptor cells of the retina have a modified cilium that is essential for phototransduction (Pazour et al., 2002) and olfactory neurons have multiple specialized cilia that detect odorants (Mair et al., 1982). In the brain, ependymal motile cilia circulate cerebrospinal fluid, and cilia on hypothalamic neurons detect signals and help regulate appetite and metabolism (Berbari et al., 2009). The diversity of cilia's roles means that different cell types can be affected in different ways when cilia are dysfunctional.

When there is a disruption in the structure or function of the cilia, cells and tissues cannot properly sense or respond to environmental cues. This gives rise to the class of diseases known as ciliopathies. Ciliopathies often have pleiotropic effects because cilia are ubiquitous in the body. For example, polycystic kidney disease (PKD) is a ciliopathy in which kidney tubule cells fail to sense fluid flow due to defective ciliary mechanosensors (Prasad et al., 2014), leading to abnormal cell proliferation and cyst formation. Bardet-Biedl syndrome (BBS), as noted, is caused by mutations in BBSome or related proteins and leads to retinal degeneration, obesity, kidney dysfunction, and polydactyly, among other symptoms (Liew et al., 2014). Joubert syndrome is another ciliopathy involving midbrain malformations and intellectual disability, linked to mutations in certain transition zone proteins. Meckel-Gruber syndrome (MKS) is caused by mutations in transition zone components of the MKS module. It is often lethal and involves kidney cysts and neural tube defects and. Primary ciliary dyskinesia (PCD) results from defects in motile ciliary components, leading to chronic respiratory infections and male infertility immotile cilia (Waters & Beales, 2011). This is not an extensive list, but it illustrates that when cilia are compromised, multiple organ systems can be affected.

1.4. Centriolar Satellites

Centriolar satellites are nanometer scale, electron-dense membraneless granules (Odabasi et al., 2020). They are typically visualized as punctate foci by immunofluorescence microscopy, often concentrated near the pericentriolar region with some scattered throughout the cytoplasm. They are responsible for trafficking, storing,

and sequestering proteins to the centrosome and basal body in ciliated cells. (Begar et al., 2025).

1.4.1. Discovery of centriolar satellites and PCM1 as the scaffolding protein

These electron-dense particles were first observed by electron microscopists in the 1950s, who noted "satellite" granules around centrioles (Bessis & Breton-Gorius, 1958). However, their molecular nature remained mysterious for some time. The breakthrough came in the mid-1990s with the identification of Pericentriolar Material 1 (PCM1), a ~230 kDa coiled-coil protein recognized by an autoantibody in human cells. PCM1 was found to localize to these centriolar "satellite" granules, and subsequent work confirmed by immunogold EM that PCM1 is a bona fide marker and structural component of centriolar satellites (Kubo et al., 1999).

Centriolar satellites are now defined as dynamic, protein-rich granules that localize in around centrosomes and cilia, moving along microtubules through the action of molecular motors dynein and kinesin. They also exhibit random diffusion in the cytoplasm and display dynamic behavior such as fusion and fission (Conkar et al., 2019).

1.4.2. Client Proteins

The main function of centriolar satellite is protein sequestration and trafficking to regulate their availability at the centrosome or cilium. The term "client proteins" refers to those proteins that depend on satellites for their proper localization or turnover. Experiments showed that numerous centrosome proteins failed to localize correctly to centrosomes when PCM1 was disrupted (Dammermann & Merdes, 2002). Over the last two decades, proteomic approaches have greatly expanded the list of satellite proteins. Proximity labeling and mass spectrometry for satellite proteins have identified hundreds of proteins associated with centriolar satellites. Well-known centriolar satellite components are called clients and they include PCM1, CEP290, CEP131, OFD1, CCDC14, CCDC66, CEP72, CEP90, SSX2IP, and many others, including several proteins that are encoded by genes mutated in microcephaly or ciliopathies (Gheiratmand et al., 2019). Thus, centriolar satellites contain lots of centrosomal and ciliary proteins, reinforcing the view that they are strongly tied to centrosome and cilium function.

The centriolar satellite proteome is highly enriched in proteins associated with ciliopathies. This indicates that satellites play active roles in assembling and maintaining the centrosome-cilium complex. Some proteins are stored in satellites until needed,

whereas others are actively ferried by satellites to the centrosome or basal body (Odabasi et al., 2019). In addition, satellites can protect certain proteins from degradation by sequestering them. Indeed, recent evidence suggests satellites influence proteostasis. For example, satellites can target specific proteins for degradation via autophagy or the ubiquitin-proteasome system (Prosser et al., 2022). One striking case is the autophagy protein GABARAP, where GABARAP is stabilized due to its interaction with satellite scaffolding protein PCM1. Without PCM1, GABARAP is improperly ubiquitinated by the satellite E3 ubiquitin ligase MIB1 and degraded, leading to impaired autophagosome formation (Joachim et al., 2017). This illustrates how satellites can regulate the levels of proteins and thereby intersect with cellular stress response pathways.

To summarize, centriolar satellites carry a large pool of centrosomal and ciliary proteins. They can actively transport these proteins toward or away from the centrosome/cilium, store/sequester proteins in an inactive state until needed, and even participate in proteostatic regulation by targeting proteins for degradation. Through these mechanisms, satellites fine-tune the composition of the centrosome and cilium and ensure the timely availability of key factors for processes like centriole duplication, centrosome maturation, and cilium assembly.

1.4.3. Tissue-Specific Regulation and Functions of Satellites

Centriolar satellites exhibit distinct spatial distributions depending on cell type and differentiation state, reflecting their tightly regulated roles in different cellular contexts. In epithelial and fibroblast cell lines like RPE1 and NIH3T3, satellites appear as a dense pericentrosomal cloud of PCM1-positive puncta within 1–2 μm of the centrioles, with fewer granules dispersed throughout the cytoplasm. This distribution facilitates efficient trafficking of centrosomal and ciliary proteins to the mother centriole/basal body during ciliogenesis or centriole duplication (Prosser & Pelletier, 2020).

In spermatogenic cells, satellite granules adopt a polarized localization along the growing flagellar axoneme and involve in the transport of flagellar proteins and centriole-derived components to the sperm tail (Wu et al., 2025). Loss of satellites in this context leads to mislocalization of axonemal assembly factors and defective flagellum formation.

In mammalian oocytes, which lack centrioles, PCM1 granules form discrete acentriolar microtubule-organizing centers (aMTOCs) and scattered throughout the ooplasm (Prodanova Hadzhinesheva et al., 2018).

In differentiated skeletal muscle cells (myotubes), centriolar satellites undergo a relocalization from centrosomal to non–centrosomal microtubule organizing centers (MTOCs). Instead of clustering tightly around the two centrioles, PCM1-positive satellite granules form a broad perinuclear shell around the nuclear envelope and extend along the myofibrils. This redistribution accompanies the loss of conventional centrosomal MTOC activity and the emergence of the nuclear envelope as the main MTOC in myotubes. There, satellite granules co-localize with nuclear envelope proteins and serve to concentrate tubulin nucleation factors at the nuclear surface, thereby supporting the microtubule array required for the contractile function (Odabasi et al., 2020; Viggars et al., 2023).

Together, these examples underscore that while the core composition of centriolar satellites is conserved, their subcellular localization patterns are highly adaptable, aligning with the unique structural and signaling demands of each cell type.

1.4.4. Role of Centriolar Satellites in Ciliogenesis

One of the most significant functions of centriolar satellites is their contribution to efficient ciliogenesis. Satellites promote ciliogenesis primarily by trafficking proteins to the basal body. When a cell exits the cell cycle and begins to form a primary cilium, centriolar satellites accumulate around the mother centriole and help recruit a suite of proteins needed at the ciliary base (Hall et al., 2023). For example, satellites carry transition zone proteins and basal body precursors that must be in place for a cilium to form. Upon cell cycle exit, the downregulation of MIB1-mediated ubiquitination allows satellite proteins like CEP290, CEP162, and TALPID3 to remain at the basal body in higher levels, aiding the construction of the ciliary transition zone (Tollenaere et al., 2015). It has been reported that cells lacking PCM1 display inefficient cilium formation and disrupted ciliary function (Odabasi et al., 2019).

The protein OFD1 localizes both to centrioles and centriolar satellites. An OFD1 mutant that cannot bind to PCM1 fails to localize properly and leads to defective ciliogenesis, implying that satellites normally help deliver OFD1 to centrioles for ciliogenesis (Tang et al., 2013). Another satellite protein, CEP72, cooperates with PCM1 and CEP290 to recruit the BBS complex proteins to the basal body, which is necessary for initiating ciliary membrane formation (Stowe et al., 2012).

Studies have also shown that centriolar satellites are required for the proper concentration of many ciliogenesis factors at the centriole, including microtubule

regulators, centriolar appendage proteins, and membrane trafficking proteins. For instance, satellites recruit the protein CP110 and play a role in removing CP110 from the mother centriole when ciliogenesis begins. This process is extremely important because failure to remove CP110 prevents axoneme extension in the cilia (Xie et al., 2023). Centriolar satellites also carry CCDC66, which is needed for ciliogenesis in retinal cells (Conkar et al., 2019). Mutation of CCDC66 causes retinal degeneration due to ciliary defects, again linking a satellite protein to ciliogenesis.

In summary, centriolar satellites act as key regulators of ciliogenesis. When satellites are dysfunctional, cells may eventually still form a cilium but the process is less efficient and the resulting cilium might not function properly. Thus, while a basic ciliogenesis process can occur without satellites in some contexts, satellites greatly enhance and safeguard the fidelity of cilium assembly and maintenance.

1.4.5. Mitotic Regulation of Centriolar Satellites

Centriolar satellites are highly dynamic during mitosis and are tightly regulated by the cell division cycle. In contrast to centrioles, satellites do not have a fixed number or persistent structural continuity through mitosis. Instead, satellites dissolve when cells enter mitosis and re-assemble after mitotic exit. During interphase, satellites are observed around the centrosome, actively involved in centrosome and cilium-related functions. However, as a cell prepares to divide, a dramatic reorganization occurs (Odabasi et al., 2020).

At the transition from G2 into mitosis, centriolar satellites undergo mitotic dissolution. Live-cell observations and biochemical studies indicate that numerous satellite particles converge toward the two spindle poles in early mitosis and then disassemble, releasing the client proteins into the cytoplasm or directly onto the mitotic centrosomes (Tollenaere et al., 2015). This dissolution is thought to be necessary for client protein to function in mitosis, and to prevent interference of bulky granules with spindle assembly. Then, after mitosis, new satellites gradually re-assembly around the centrosome of the daughter cells (Odabasi et al., 2020). This cell cycle dependent assembly and disassembly cycle suggests satellites are under strict regulatory control.

The centrosome/cilium complex in mammalian cells is currently considered as a structure formed by three components: centrosome, cilia, and centriolar satellites which together coordinate to execute vital cellular functions. The centrosome provides

architectural organization of microtubules, the primary cilium provides a sensory and signaling platform, and the centriolar satellites serve as dynamic hubs, regulating the composition of centrosome and cilium. This partnership is crucial for cellular homeostasis, development, and disease prevention.

Chapter 2

2. INDUCIBLE CENTROSOMAL RE-ROUTING OF CENTRIOLAR SATELLITES UNCOVERS THEIR TEMPORAL FUNCTIONS DURING MITOSIS

2.1. Introduction

2.1.1. Mitotic Regulation of Centriolar Satellites

Centriolar satellites normally cluster around the centrosome in interphase. However, as cells enter mitosis, these satellite granules dissolve and then reassemble upon mitotic exit **(Figure 2.1)**. Notably, this disassembly is not due to protein degradation, since the total levels of the major satellite proteins remain essentially unchanged during the cell cycle (Wang et al., 2013). This dynamic behavior suggests a tight mitotic regulation, ensuring that satellites break apart at the onset of mitosis and reform in the daughter cells as they return to interphase.

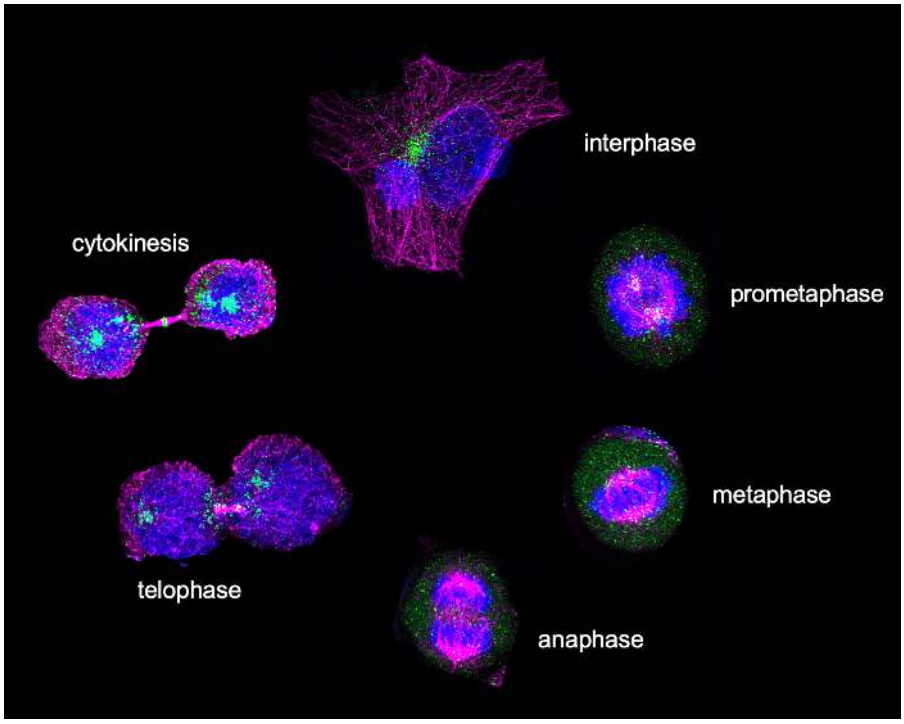

Figure 2.1 Mitotic dissolution of centriolar satellites in HeLa cells.

The dissolution of centriolar satellites in mitosis is thought to be functionally important for cell division. During mitosis, the centrosomes mature into spindle poles with a robust microtubule organizing center, and dispersing satellites may prevent any physical crowding or sequestration of factors at the spindle poles (Odabasi et al., 2020). This concept aligns with a broader principle where many membraneless organelles and biomolecular condensates in the cell undergo regulated disassembly at mitosis. By dissolving these structures, the cell creates a more homogeneous cytoplasm that allows proper chromosome segregation and spindle assembly (Rai et al., 2018).

2.1.2. Dissolution of Centriolar Satellite Granules by DYRK3

A dual-specificity kinase called DYRK3 plays an important role as a general "dissolvase" of biomolecular condensates. DYRK3 kinase activity increases in mitosis and drives the dispersal of several membraneless organelles by phosphorylation to create a more soluble state. Notably, the mitotic dissolution of satellites is abolished if DYRK3 is inhibited, underscoring that DYRK3 is a central regulator of this phase transition. The modifications done by DYRK3 are thought to disrupt PCM1's ability to oligomerize or to bind other satellite components, thereby promoting the dissolution of satellite granules (Begar et al., 2025; Rai et al., 2018).

2.1.3. The FKBP–FRB Dimerization System as a Tool to Study Organelle Positioning

Our understanding of organelle dynamics, including satellite behavior, has greatly benefited from tools that allow acute manipulation of organelle positioning. One such tool is the FKBP–FRB heterodimerization system, which exploits a chemically inducible protein interaction to reposition organelles or proteins in living cells. This system is based on the specific binding between two engineered protein domains: FK506-binding protein (FKBP12) and the FKBP–rapamycin-binding domain of mTOR (FRB). In the presence of the small molecule rapamycin, FKBP and FRB are forced into a tight heterodimer, effectively acting as a chemical "on-switch" for tethering two proteins together. Importantly, the FKBP–FRB interaction is essentially irreversible, meaning that a pulse of rapamycin will lock the two target proteins together (Kolos et al., 2018).

This rapamycin-inducible heterodimerization strategy has been widely used to study organelle behavior by artificially relocalizing proteins or even whole organelles. By fusing one of the pair (e.g. FRB) to a cellular landmark and the other (FKBP) to a protein of interest, researchers can rapidly drag the protein of interest to the chosen location with

rapamycin induction. For example, previous studies have attached FRB to an outer mitochondrial membrane protein and FKBP to a centrosomal or ciliary protein, so that adding rapamycin causes acute removal of that protein from the centrosome/cilium and sequesters it on mitochondria (Hong et al., 2018; Lin et al., 2013). Similarly, FKBP–FRB dimerization has been employed to recruit molecular motors to specific organelles. These approaches, often called "chemical trafficking" or "knocksideways" assays, allow tight spatiotemporal control over organelle positioning without genetic mutations (Aydin et al., 2020). The main caveat is the lack of reversibility, but the advantages in speed and specificity have made FKBP–FRB a preferred tool for organelle dynamics studies (Passmore et al., 2021).

2.1.4. A Chemical Trafficking Assay for Centriolar Satellites

Building on the FKBP–FRB system, recent work developed a specific satellite trafficking assay to investigate how centriolar satellites function when repositioned in the cell. In this approach, the satellite scaffold protein PCM1 was tagged with FKBP, while engineered motor protein fragments were tagged with FRB. By choosing motor domains with defined directionality, researchers achieved controlled movement of satellites either outward toward the cell periphery or inward toward the cell center. Specifically, a constitutively active fragment of kinesin-1 (Kif5B, amino acids 1–269) fused to FRB was used to direct satellites toward microtubule plus-ends at the cell periphery upon rapamycin addition. Conversely, a fragment of the dynein adaptor BICD2 (amino acids 1–198) fused to FRB was used to engage the dynein–dynactin complex and pull satellites toward microtubule minus-ends at the centrosomal region (Aydin et al., 2020).

However, the use of the BICD2 fragment to hijack dynein motors results in a significant setback which is the dominant-negative inhibition of the cell's native dynein–dynactin transport machinery. The truncated BICD2-N fragment competes with endogenous cargo adaptors for dynein binding, effectively sequestering dynein into complexes that cannot engage their physiological cargos. As a result, cells display widespread mislocalization of organelles normally dependent on dynein, including the Golgi apparatus, late endosomes, and lysosomes. Moreover, mitotic cells frequently exhibit fragmented Golgi and impaired spindle positioning, indicating that global dynein function is compromised by the overexpressed adaptor fragment (Nijenhuis et al., 2020).

2.1.5. Kinesin-14B as a Trafficking Tool

Due to the dominant-negative effects of BICD2, researchers started investigating how to achieve minus-end-directed transport efficiently without side effects. As mentioned earlier, the truncated BICD2 fragment competes with endogenous BICD adaptors, often displacing them from dynein–dynactin and thereby disrupting normal dynein function in the cell (Nijenhuis et al., 2020). This leads to cell-wide mislocalization of various organelles, complicating the interpretation of experiments.

To overcome these issues, researchers have developed an alternative strategy using a minus-end-directed kinesin motor derived from plants. In particular, a type VI kinesin-14 from the moss *Physcomitrella patens* (referred to as Kin14-VIb) has been utilized as a molecular tool for retrograde transport in animal cells. Using this moss kinesin motor to pull organelles inward has several advantages over the BICD2/dynein approach.

First, the kinesin-14 motor is a self-contained minus-end motor, it does not rely on the cell's dynein machinery or any co-factors, so it avoids perturbing the endogenous dynein/dynactin system. Second, the moss kinesin has very low homology to any mammalian proteins, meaning it is unlikely to interact with or dimerize with the cell's native motors or disrupt the mitotic spindle structure. Third, this particular kinesin-14 was found to be a highly processive and fast motor, even faster than typical mammalian minus-end motors. High speed and processivity ensure that cargoes can be rapidly and efficiently accumulated at the cell center. Lastly, by engineering the moss kinesin-14 into a dimer-of-dimers (tetramer) form utilizing a leucine zipper (GCN4), its force output is increased, enabling it to haul organelles just as robustly as the multi-component dynein complex.

The introduction of *Physcomitrella* kinesin-14b in organelle repositioning experiments has proven extremely effective. Unlike BICD2-based approaches, the usage of moss kinesin did not cause noticeable mislocalization of unrelated organelles or inhibition of endogenous transport pathways. By avoiding the dominant-negative sequestration of dynein, the kinesin-14 method preserves the normal cellular organization while still accomplishing the experimental goal of relocalizing the target organelle (Nijenhuis et al., 2020; Yoshida et al., 2019).

In conclusion, centriolar satellites are highly dynamic organelles whose localization are tightly regulated by the cell cycle. They dissolve during mitosis, likely to facilitate proper spindle assembly. The development of chemical and optical tools like the

FKBP–FRB system and engineered motors has enabled precise experimental manipulation of satellites, enabling us to study their roles in protein trafficking and mitotic progression.

2.2. Materials § Methods

2.2.1. Plasmids and clonings

pEGFP-PCM1-FKBP was previously cloned by amplifying full-length cDNA of Homo sapiens PCM1 (GenBank accession no:NP_006188.4) and using BamHI and KpnI enzymes.

pRosa26-Hygro-CAG-EGFP, hRosa26-Left-guide-Cas9, and hRosa26-Right-guide-Cas9 plasmids were gifts from Tamer Önder. PCM1-FKBP was cloned into pRosa26-Hygro-CAG-EGFP plasmid using BsrGI and MluI enzymes.

pWN236_pB80-FRB-GFP-GCN4-ppKin14Vib was a gift from Lukas Kapitein. pTwist-FRB-Flag-GCN4-Kin14 is synthesized from Twist Bioscience.

2.2.2. Cell culture and transfections

Human embryonic kidney (HEK293T, ATCC) and human cervical carcinoma cells (HeLa, ATCC) were cultured in DMEM supplemented with 10% FBS. All cell lines were maintained in a humidified incubator at 37C with 5% CO2.

HEK293T cells were transfected with plasmids using 1 μg/μL polyethylenimine. HeLa cells were transfected using either polyethylenimine or Lipofectamine 2000 transfection reagent (brand). Medium was changed four hours after transfection when Lipofectamine 2000 reagent is used.

2.2.3. Knock-in cell line generation

HeLa cells were co-transfected with pRosa26-Hygro-CAG-EGFP, hRosa26-Left-guide-Cas9, and hRosa26-Right-guide-Cas9 plasmids using Lipofectamine 2000 transfection reagent. 48 hours post-transfection, the cells were selected using 150 ug/mL Hygromycin B. Selection was carried out for 8 days until all control cells died. At the end of selection, colonies were picked using a pipette tip and screened with immunofluorescence for positivity.

2.2.4. Chemically inducible centriolar satellite trafficking assay

HeLa WT cells were seeded on coverslips and co-transfected with GFP-PCM1-FKBP and FRB-Flag-Kin14. 24 hours post-transfection, the cells were treated with 200 nM rapamycin for 1 hour. The rapamycin was washed out after 1 hour, and cells were incubated for at least another 5 hours for the complete re-routing of satellites and their clients. In some experiments, 24- or 48-hours incubation time is used.

2.2.5. Biotin-streptavidin affinity purification

For the BioID pulldown experiments, HEK293T cells were co-transfected with myc-BirA*-PCM1-FKBP and FRB-Flag-Kin14. Twenty-four hours post transfection, cells were incubated with DMEM-supplemented 10% FBS and 50 μM biotin for 18 hours. Cells were lysed in lysis buffer (50 mM Tris, pH 7.4, 500 mM NaCI, 0.4% SDS, 5mM EDTA, 1 mM DTT, 2% Triton X-100, protease inhibitors), and soluble fractions were incubated overnight at 4˚C with streptavidin agarose beads (Thermo Scientific, Waltham, MA). Beads were washed twice with wash buffer 1 (2% SDS in dH2O), once with wash buffer 2 (0.2% deoxycholate, 1% Triton X-100, 500 mM NaCI, 1 mM EDTA, and 50 mM HEPES, pH 7.5), once with wash buffer 3 (250 mM LiCI, 0.5% NP-40, 0.5% deoxycholate, 1% Triton X-100, 500 mM NaCI, 1 mM EDTA, and 10 mM Tris, pH 8.1), and twice with wash buffer 4 (50 mM Tris, pH 7.4, and 50 mM NaCI). 10% of the sample was analyzed by western blotting to assess pulldown, and 90% of the sample was analyzed by mass spectrometry.

2.2.6. Mass spectrometry and data analysis

Mass spectrometry was performed at Koc University Proteomics Facility. For mass spectrometry analysis, normalized spectral abundance factor (NSAF) values were calculated for each protein by dividing each Peptide Spectrum Match (PSM) by the total PSM count in that dataset. Proteins present only in one of the technical replicate datasets were excluded. The remaining proteins were analyzed using CRAPome contaminant repository, to remove proteins with a contamination percentage greater than 55%. NSAF values in the plusRapa condition were divided by the corresponding NSAF values from the minRapa condition to calculate an enrichment score for the proteins and later categorized as enriched if value is higher than 1 and depleted if value is lower. Finally,

proteins were organized according to their log2(Fold Change) values and an analyzed based on GO biological process.

2.2.7. Nocodazole wash-out

HeLa WT cells were seeded on coverslips and co-transfected with GFP-PCM1-FKBP and FRB-Flag-Kin14. 24 hours post-transfection, the cells were treated with 200 nM rapamycin for 1 hour and the cells were incubated for another 5 hours to induce complete re-routing of PCM1 and clients. After total of 6 hours incubation, cells were treated with 5 ug/mL of nocodazole for 1 hour at 37C to depolymerize the microtubules. For the wash-out, medium was discarded, and cells were washed with cold PBS three times gently. For the microtubule re-polymerization, warm medium was added, and the cells were fixed with ice-cold methanol at indicated time points.

2.2.8. Immunofluorescence

Cells were grown on glass coverslips for the immunofluorescence experiments. Coverslips were washed with PBS and the cells were fixed with either paraformaldehyde at room temperature or with ice-cold methanol at −20C for 10 mins. After washing the coverslips twice with PBS, cells were blocked with 3% BSA in PBS containing 0.1% Triton X-100 for permeabilization. For the immunostaining, cells were incubated with primary antibodies in blocking solution for 1 h at room temperature and then with secondary antibody solution containing DAPI. After washing out the excess antibodies with PBS, cells were mounted using Mowiol mounting medium. Full list of primary and secondary antibodies used for immunofluorescence experiments in this chapter are listed Appendix Table 1.

2.2.9. Microscopy

Fluorescence microscopy was performed with Leica DMI8 inverted fluorescence microscope system equipped for four-color imaging with 405, 488, 561, and 633 nm LED light source and four filters (DAPI, FITC, TXR, and Cy5), HC PL APO CS2 63X 1.4 NA oil objective. Images were acquired with 5-20% light source power and 10-200 ms exposure time with 2X2 binning. The system was controlled with the Leica Application Suite X Software (Leica).

Confocal microscopy was performed with Leica TCS SP8 or Stellaris 8 laser scanning inverted confocal microscope system equipped for four-color imaging with 405,

488, 561, and 633 nm laser lines, four detection channels (1 photomultiplier tube and 3 Hybrid Detectors), HC PL APO CS2 63X 1.4 NA oil objective and an incubation chamber. Pinhole diameter was set to 1 µm. Images were acquired with 0.2–0.5 µm z-spacing, line averaging set to 2–323 and 400/600 Hz unidirectional xyz scan mode. An image format of 1,024x1,024 pixels and an additional 1–4x optical zoom was used for sample acquisition. The system was controlled with the Leica Application Suite X Software (Leica). Post-processing was performed using the Huygens Professional (Scientific Volume Imaging) or LAS X Lightening.

ZEISS Lightsheet microscope was used for time-lapse imaging experiments. The microscope was equipped for three-color imaging with 488, 568, and 633 nm laser lines. Images were taken at 100x1400 pixels format. Focus sheet was adjusted to 0, focus waist to 60, and aberration control to 170. Tilt X-axis value was set to-0,019 and tilt Y-axis to 0,004. Cells were maintained at 37C with 5% CO_2.

2.2.10. Live imaging of inducible centrosomal re-routing of centriolar satellites

For the time lapse imaging of satellite re-routing, HeLa WT cells were plated on Ibidi µ-Slide 8 well dishes, co-transfected with GFP-PCM1-FKBP and FRB-Flag-Kin14, then imaged with Stellaris 8 laser scanning inverted confocal microscope at 37C with 5% CO2 with a frequency of 2 minutes per frame for 1 hour, with 0.5 µm step size in 1024 x 1024 pixels format. The cells were treated with rapamycin between the first and second imaging frames.

2.2.11. Live imaging of mitosis

For the time lapse imaging of mitosis, HeLa cells stably expressing GFP-PCM1-FKBP were plated on Ibidi µ-Slide 8 well glass bottomed slides, transfected with FRB-Flag-Kin14, and treated with SiR-tubulin (Cytoskeleton) with 1:10,000 dilution overnight. 6 hours before imaging, cells were treated with either vehicle control (DMSO) or 200 nM of rapamycin. The cells were imaged with ZEISS Lightsheet microscope at 37C with 5% CO2 with a frequency of 4 minutes per frame for 18 hours, with 0.4 µm z-spacing using 488 and 633 nm lasers at 5% power with 20 ms exposure time.

2.2.12. Live and apoptotic cell detection with Muse Cell Analyzer

HeLa hR26 cells were seeded in 12 well plates and transfected with FRB-Flag-Kin14. Cells were treated with vehicle control or rapamycin for 6, 24, and 48 hours. At

the end of treatment, cells were trypsinized, collected and 100 uL of cell suspension was incubated with 100 uL of Muse Annexin V & Dead Cell Reagent (Cytek) for 20 minutes at room temperature. Control cells are used for the gating for live/dead calibration and for apoptotic cell calibration. Cell number and apoptotic cell percentages were acquired from flow cytometry analysis of Muse Cell Analyzer device.

2.2.13. Image Analysis and Quantifications

Pericentrosomal levels of proteins

All pericentrosomal level quantifications were performed in ImageJ. Regions of interest (ROIs) encompassing the centrosome were drawn using the gamma-tubulin staining as a marker. The corresponding signals from other channels and from the background were measured from the cytoplasm using the Analyze > Measure function. For the analysis, the background signal was subtracted from pericentrosomal signal. Statistical analysis was conducted by normalizing the mean value of the treatment condition to the mean of the control for each biological replicate.

Aster size and microtubule density

Aster size and microtubule density quantifications were performed in ImageJ. Centrin1 staining was used as centrosome marker and ROIs encompassing the microtubule aster were drawn using the α-tubulin staining. The aster area was measured using the Analyze > Measure > Area function. The microtubule density within the asters were obtained by measuring the fluorescence intensity of the aster area and subtracting the cytoplasmic background using Analyze > Measure > Mean. Statistical analysis was conducted by normalizing the mean value of each condition to the mean of the control-0min time point for each biological replicate.

Mitotic index and cells at different cell cycle stages

Mitotic index and cells at different cell cycle stages were quantified using images taken randomly from five different areas on the coverslip. Annotations > counting function of LasX software was used to quantify the total cell number and mitotic cells from DAPI staining as the nuclei and α-tubulin staining as the microtubule marker.

Chromosome congression index

Chromosome congression index was measured using the Annotations > um function of LasX software. The width and length of chromosome at the metaphase stage was measured from the DAPI channel. The congression index was calculated by dividing the width to the length of the chromosomes.

Total spindle length and half-spindle length ratio

Total spindle length and half-spindle ratio was measured using the Annotations > um function of LasX software. The total spindle length was obtained by measuring the length of microtubules from α-tubulin channel from one pole to the other. The half-spindle length was obtained by measuring the length of the half-spindles from one pole until the chromosomes. The ratio was calculated by dividing the longer spindle (PCM1 positive) length to the shorter one (PCM1-negative).

2.2.14. Statistical analysis

Prism 10 software (GraphPad Software, La Jolla, CA) is used to calculate p-values and determine statistical significance. To compare two groups that exhibit Gaussian distribution, parametric unpaired two-tailed Student's t-test was used. When the sample does not have Gaussian distribution, nonparametric Mann-Whitney test is applied. Error bars in the graphs indicate the standard deviation (SD), and statistical significance levels were denoted as follows: ns: $P>0.05$, *:$P<0.05$, **:$P<0.01$, ***:$P<0.001$ and ****:$P<0.0001$.

2.3. Results

2.3.1. Development and validation of inducible centriolar satellite trafficking assay

Centriolar satellites are membraneless granules concentrated around the centrosome in most mammalian cells. Apart from their pericentrosomal pool, they also have a cytoplasmic pool displaying either motor dependent mobility or Brownian motion to perform distinct functions within the cell. To uncover the temporal functions of the centriolar satellites, we have come up with a chemically inducible satellite trafficking assay by re-routing the cytoplasmic pool of the satellites to the centrosome. This trafficking assay utilizes the widely employed irreversible heterodimerization between the FK506-binding protein (FKBP) and FKBP-rapamycin binding (FRB) domain of

mTOR, mediated by the small molecule rapamycin. We adapted this system to our study by generating an FKBP fusion of centriolar satellite scaffold protein PCM1 and an FRB fusion of minus-end directed motor protein **(Figure 2.2)**.

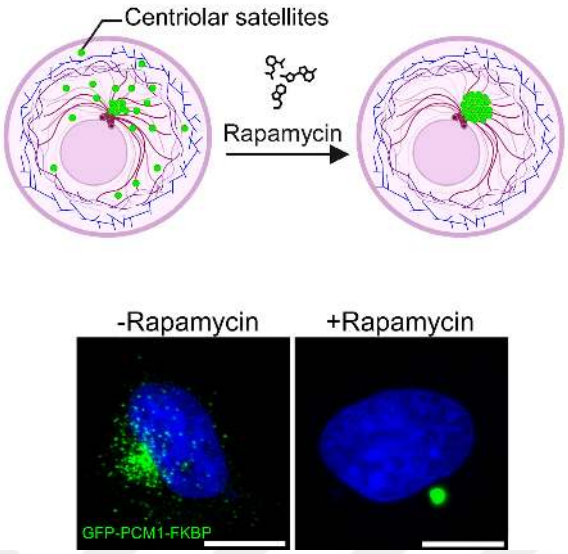

Figure 2.2 Design of the satellite trafficking assay.

Satellite granules are re-routed to the centrosome upon rapamycin treatment and form a large foci around the pericentrosomal region. Created with BioRender.

The previous study published by (Aydin et al., 2020) utilized the dynein/dynactin cargo adaptor bicaudal D homolog 2 (BICD2) to re-route the satellites to centrosome. However, the expression of BICD2 alone led to an unexpected dispersal of satellites throughout the cytoplasm, consistent with previous studies reporting the dominant negative effect of BICD2 on dynein-dynactin function (Nijenhuis et al., 2020). To overcome the disruption of centriolar satellite localization by BICD2, we made use of the minus-end directed type VI kinesin-14b motor protein (Kin14) derived from the moss Physcomitrella patens, which is more processive and faster than mammalian kinesin-14 motors. We tagged the FRB-Kin14(861-1312) with Flag and PCM1-FKBP with GFP for the trafficking assay **(Figure 2.3)**.

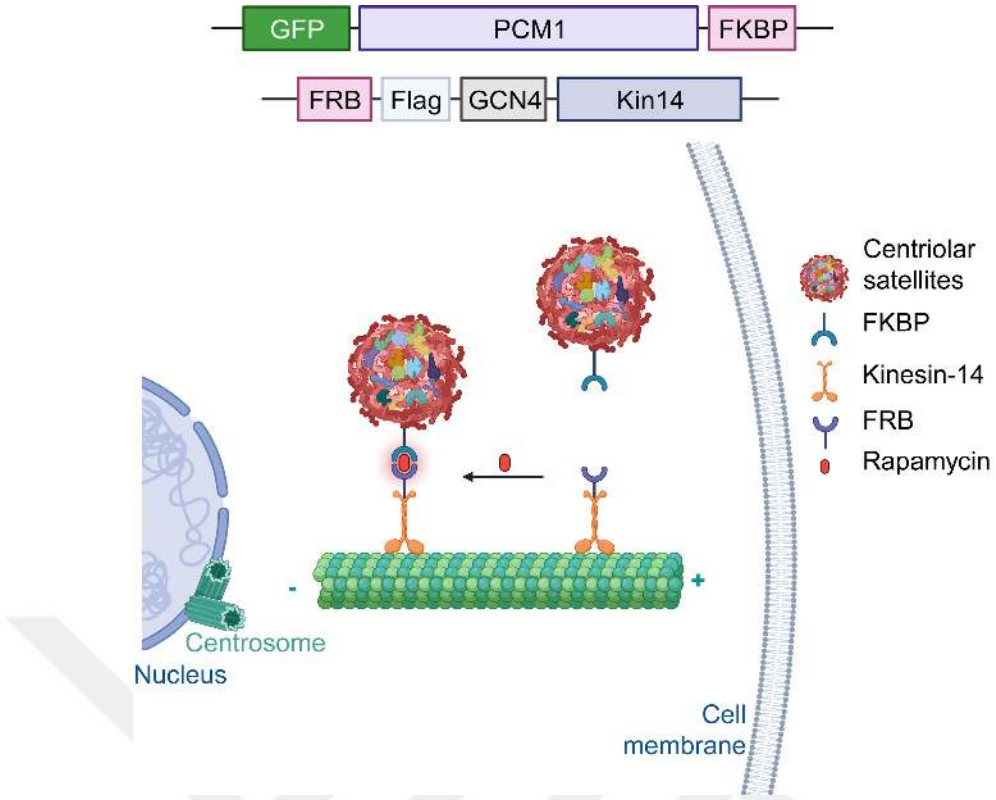

Figure 2.3 Development of the chemically inducible centriolar satellite trafficking assay.

Plasmid constructs designed for the satellite trafficking assay. FKBP fusion of centriolar satellites are targeted to the centrosome utilizing FRB fusion of minus end-directed motor protein Kinesin-14. Created with BioRender.

To test the satellite trafficking assay, we co-transfected GFP-PCM1-FKBP and FRB-Flag-GCN4-Kin14 constructs in HeLa cells. In the minus rapamycin (control) condition, centriolar satellites exhibited their endogenous-like localization within the cell and the Kin14 had a weak microtubule pattern along with a centrosomal pool. Upon rapamycin treatment, we observed a striking accumulation of centriolar satellite granules around the centrosome, forming a large pericentrosomal punctum that co-localized with Flag-Kin14 **(Figure 2.4.A)**. To assess whether Kin14 alone affects satellite distribution, we transfected the cells with only the Flag-Kin14 plasmid. In this condition, centriolar satellites preserved their typical endogenous localization, indicating that Kin14 does not exert a dominant-negative effect on satellite positioning, in contrast to BICD2 **(Figure 2.4.B)**.

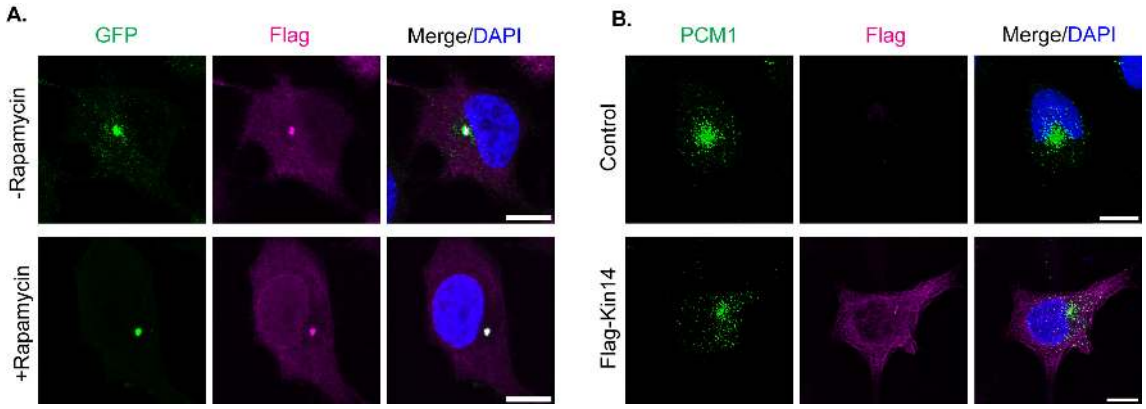

Figure 2.4 Validation of the chemically inducible centriolar satellite trafficking assay.

A. Confirmation of satellite trafficking assay with the co-transfection of GFP-PCM1-FKBP and FRB-Flag-Kin14. Both GFP and Flag co-localize at the centrosome upon rapamycin treatment. **B.** Kin14 expression alone does not affect endogenous PCM1 localization confirmed with Flag and PCM1 immunostainings.

Since the satellite trafficking experiments were carried out in wild-type cells, we examined the localization of endogenous PCM1 following the re-routing of the centriolar satellites. Endogenous PCM1 localization was almost identical to the GFP-PCM1-FKBP localization in both minus and plus rapamycin conditions, likely due to the presence of two known self-dimerization domains located in the N-terminal region of PCM1 **(Figure 2.5.A, Appendix Figure 1)**. Importantly, rapamycin treatment resulted in an approximately five-fold increase in the pericentrosomal levels of PCM1, demonstrating the efficiency and robustness of the satellite trafficking assay **(Figure 2.5.B)**. This efficiency was further supported by live-cell imaging of GFP-PCM1-FKBP during the centrosomal re-routing. The satellites formed a prominent granule within 10 minutes and a complete re-routing was observed within 1 hour **(Figure 2.5.C)**.

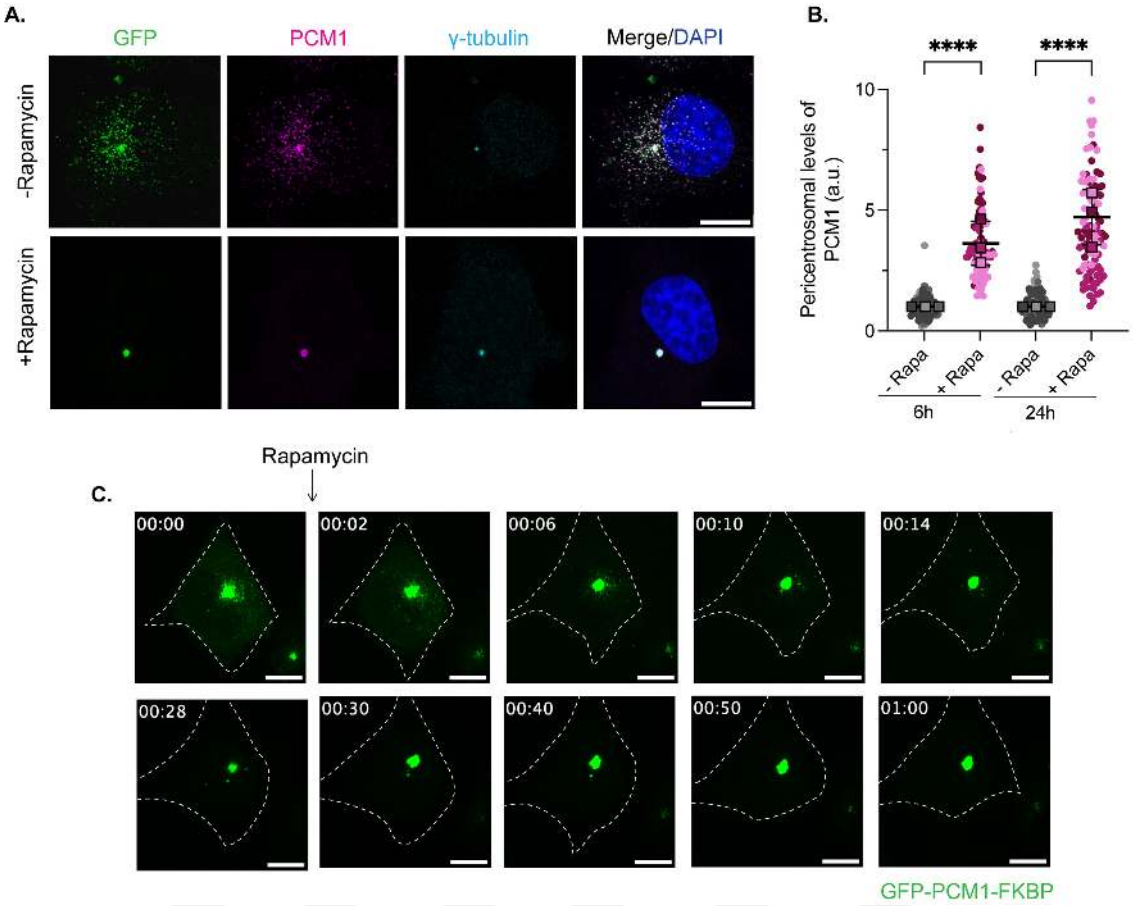

Figure 2.5 Inducible satellite trafficking assay targets PCM1 to the centrosome using Kin14 motor protein.

A. Cells co-transfected with GFP-PCM1-FKBP and FRB-Flag-Kin14 were treated with rapamycin to induce trafficking assay. Centrosomal re-routing of satellites were confirmed with GFP (marks GFP-PCM1-FKBP), PCM1 (marks GFP-PCM1-FKBP and endogenous PCM1), and γ-tubulin (centrosome) staining. **B.** Pericentrosomal fluorescence intensity of the PCM1 is measured using Fiji. The data represents three biological replicates, with n = 30 per replicate. *:p<0.05, **:p<0.01, ***:p<0.001****:p<0.0001, ns: not significant. **C.** Still images representing satellite granule re-routing to the centrosome upon rapamycin treatment in time-lapse imaging. Scale bar: 10 μm.

Together, these results show that chemically induced centriolar satellite trafficking assay effectively disrupts the spatial organization of satellite granules within the cell and enables the investigation of the effect of acute, temporally controlled satellite depletion.

2.3.2. Centriolar satellites spatiotemporally regulate client proteins

Centriolar satellites are scaffolds for the trafficking, sequestration, and regulation of numerous client proteins involved in diverse cellular functions such as ciliogenesis, mitotic progression, and response to cellular stress. By sequestering clients in a spatiotemporally regulated manner, satellites prevent aberrant activation or depletion of centrosomal components, hence maintaining cellular homeostasis (Begar et al., 2025). Given that the pericentrosomal localization of satellites is critical for proper client regulation, we investigated how centrosomal re-routing of centriolar satellites affects the localization of the client proteins. To this end, we co-expressed GFP-PCM1-FKBP and Flag-Kin14-FRB in cells, and measured pericentrosomal levels of several client proteins before and after centrosomal re-routing of satellites **(Figure 2.6.A and B)**.

For this analysis, we chose client proteins having different functions and localizing to the different regions of the centrosome. CEP131 has a very prominent centriolar satellite localization and is implicated in protein trafficking, ciliogenesis, and stress response. Upon centrosomal re-routing of the satellites, pericentrosomal levels of CEP131 increased to three-fold on average. CEP72 is another client protein with prominent satellite localization that has higher pericentrosomal levels upon rapamycin treatment compared to control.

CEP120, CEP290, and CETN1 are clients with prominent centriole pool with CEP120 being enriched in the daughter centriole. These proteins are implicated in centriole elongation, ciliary transition zone gating, and centriole core structure, respectively. Their pericentrosomal levels are increased more than two-fold upon centrosomal re-routing of satellites. MIB1 is a ubiquitin ligase which is important for protein turnover and has a weak satellite pool in the control cells. Upon rapamycin treatment, pericentrosomal levels of MIB1 increased approximately five-fold.

CEP63 localizes to the proximal end of the mother centriole and is implicated in centriole duplication. Its pericentrosomal levels did not change at the earlier time-point but showed accumulation at the centrosome twenty-four hour after re-routing. We used CEP164 as a negative control since it is a distal appendage protein and does not have centriolar satellite pool. The pericentrosomal levels of CEP164 did not change significantly upon re-routing of satellites as expected.

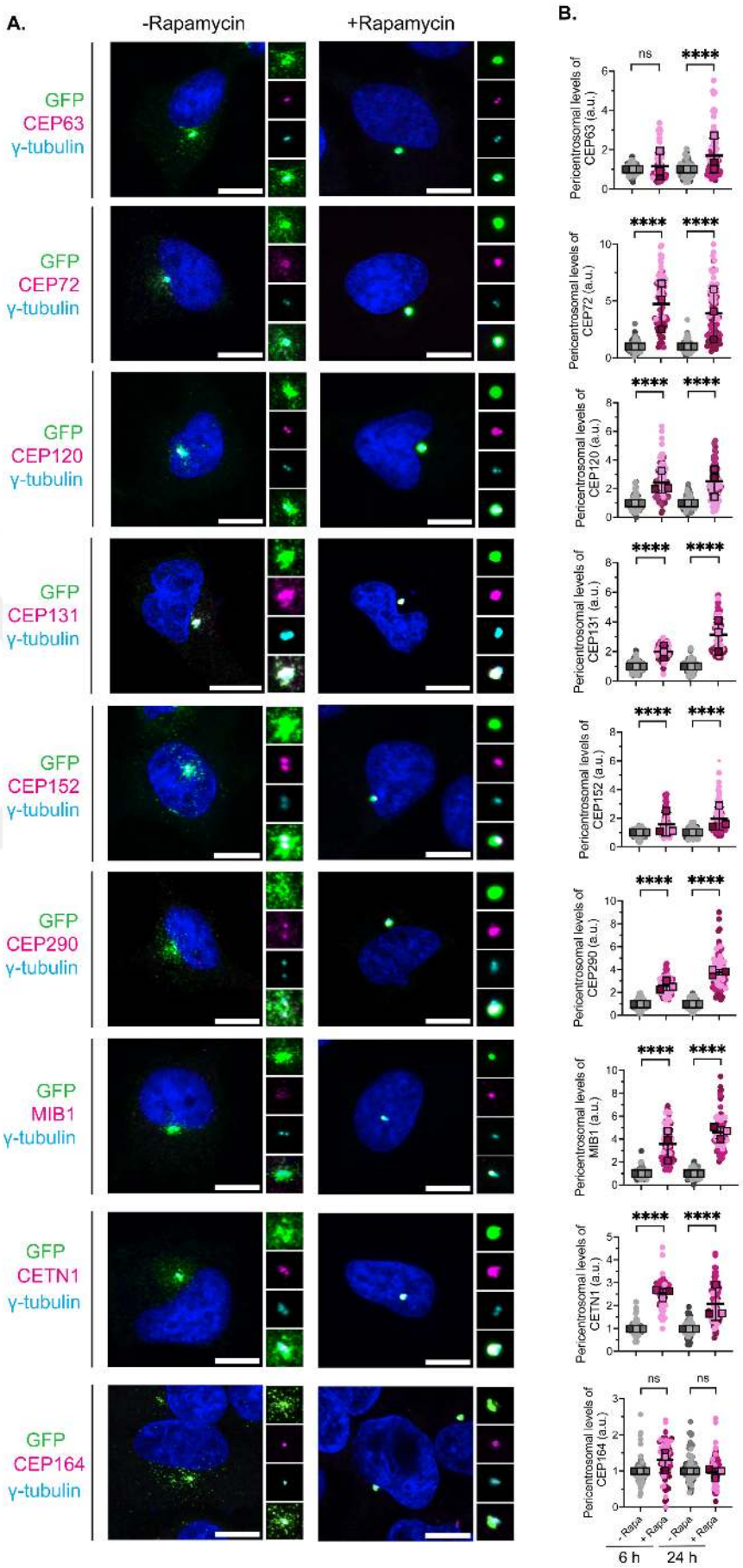
A.
-Rapamycin
+Rapamycin
GFP
CEP63
γ-tubulin
GFP
CEP72
γ-tubulin
GFP
CEP120
γ-tubulin
GFP
CEP131
γ-tubulin
GFP
CEP152
γ-tubulin
GFP
CEP290
γ-tubulin
GFP
MIB1
γ-tubulin
GFP
CETN1
γ-tubulin
GFP
CEP164
γ-tubulin
B.
Pericentrosomal levels of CEP63 (a.u.)
Pericentrosomal levels of CEP72 (a.u.)
Pericentrosomal levels of CEP120 (a.u.)
Pericentrosomal levels of CEP131 (a.u.)
Pericentrosomal levels of CEP152 (a.u.)
Pericentrosomal levels of CEP290 (a.u.)
Pericentrosomal levels of MIB1 (a.u.)
Pericentrosomal levels of CETN1 (a.u.)
Pericentrosomal levels of CEP164 (a.u.)
ns
****
- Rapa
+ Rapa
6 h
24 h

Figure 2.6 Client proteins are spatiotemporally regulated by centriolar satellites. The change in the localization and pericentrosomal levels of several client proteins upon centrosomal re-routing of centriolar satellites. **A.** HeLa cells co-transfected with GFP-PCM1-FKBP and FRB-Flag-Kin14 were treated with rapamycin for 1 hour and fixed after 24 hours. Cells were immunostained for GFP, γ-tubulin, and indicated client proteins. Insets show pericentrosomal region. Scale bar: 10 μm. **B.** Pericentrosomal fluorescence intensity of indicated client proteins at 6- or 24-h treatment conditions were measured with Fiji. Average intensity of clients in the control cells is normalized to 1. The data represents three biological replicates, with n = 30 per replicate. *:$p<0.05$, **:$p<0.01$, ***:$p<0.001$****:$p<0.0001$, ns: not significant.

All together, these results show that client proteins were selectively trafficked to the centrosome in response to the inducible re-routing of satellites **(Figure 2.6A, B, and Appendix Figure 2)**. These findings support the proposed functions of centriolar satellites in storage, sequestration and trafficking, and prove that client proteins are regulated by centriolar satellites in a spatiotemporally controlled manner.

2.3.3. Centrosomal re-routing alters centriolar satellite interactome

To determine how centriolar satellite interactome changes upon centrosomal re-routing, we performed proximity labeling in cells co-expressing PCM1-FKBP and FRB-Kin14 in control and rapamycin treated cells. We generated Myc-BirA* fusion of PCM1-FKBP and allowed BioID system to biotinylate proteins that are in the proximity of centriolar satellites **(Figure 2.7.A)**. Then, we analyzed the proximity interaction list to obtain proteins that have enriched or depleted interaction with centriolar satellites upon centrosomal re-routing.

Upon Gene Onthology analysis, we observed decrease in the interaction levels of proteins related with regulation of transcription, protein transport, actin organization, microtubule organization, and cell division. When we analyzed the proteins with increased interaction with PCM1, we obtained proteins related with proteins transport, cilium assembly, and microtubule-based movement, and cell division **(Figure 2.7.B)**.

In conclusion, centrosomal re-routing of centriolar satellites selectively reshapes their interactome, decreasing associations with transcription, cytoskeletal, and cell division regulators while increasing interactions with proteins involved in transport, cilium assembly, and microtubule-based processes.

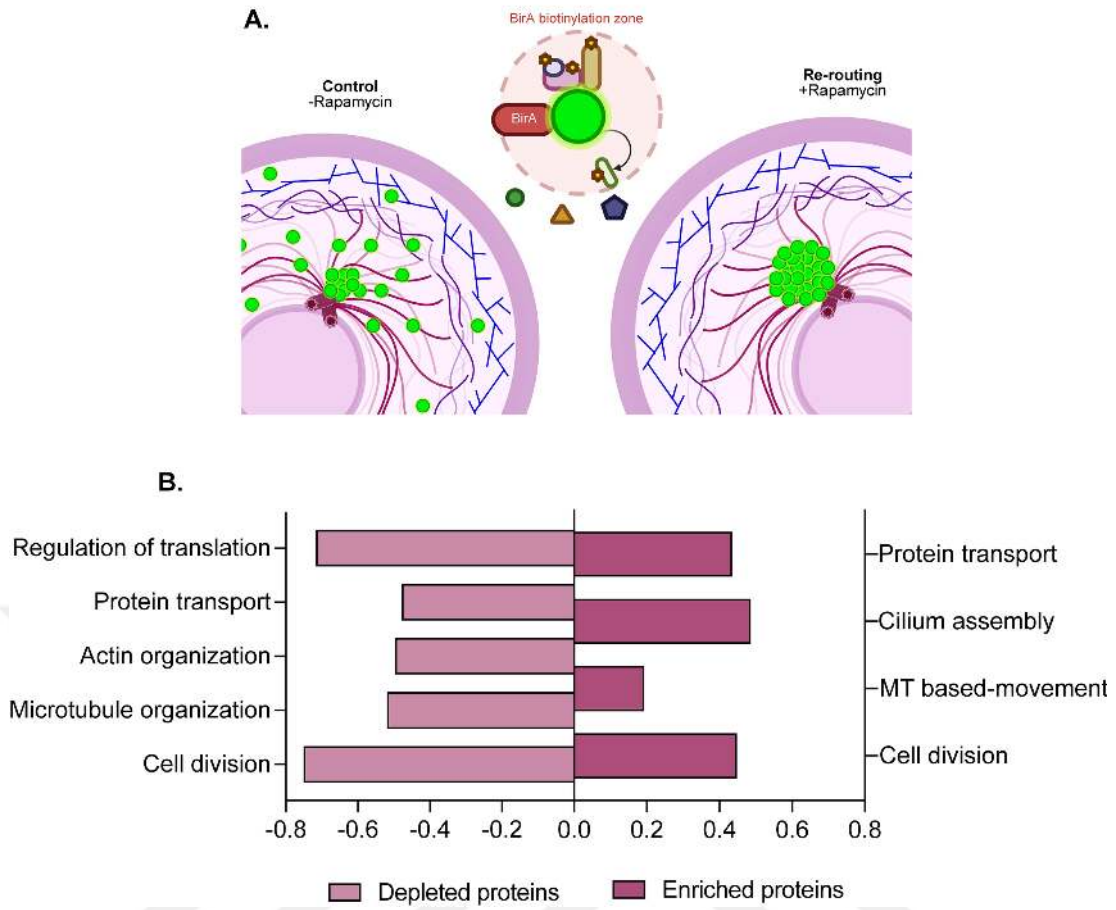

Figure 2.7 Centriolar satellite interactome changes upon centrosomal re-routing.
A. Experimental setup for proteomics of centriolar satellites before and upon centrosomal re-routing that utilizes the proximity dependent biotinylation. **B.** Depletion and enrichment levels of proteins upon centrosomal re-routing of centriolar satellites categorized according to biological process.

2.3.4. Preferential distribution of centriolar satellites on mother centriole

We have showed that the chemically induced centriolar satellite trafficking assay allows spatiotemporal control over client protein localization. To assess the consequences of this perturbation, we first examined the distribution of re-routed satellites on individual centrioles. Our trafficking assay relies on minus-end directed motility of Kin14 along microtubules. Therefore, we hypothesized that centriolar satellites should converge on mother centriole upon rapamycin treatment, since microtubules are anchored to the subdistal appendages of mother centriole. To test this, we co-expressed GFP-PCM1-FKBP and Flag-Kin14-FRB and immunostained the cells for CEP120 which is enriched on daughter centriole and CEP164 as a mother centriole marker.

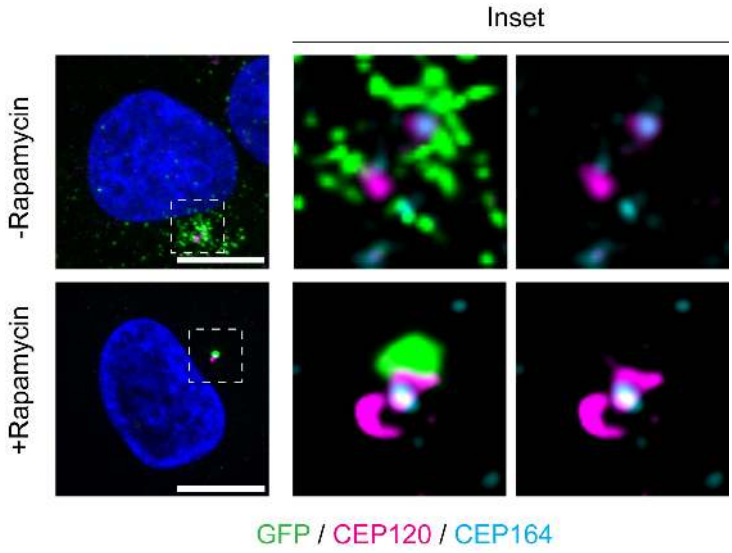

Figure 2.8 Satellites cluster around mother centriole.

HeLa cells co-transfected with GFP-PCM1-FKBP and FRB-Flag-Kin14 were treated with rapamycin for 1 hour and fixed after 6 hours. Cells were immunostained for GFP, CEP120 (enriched in daughter centriole), and CEP164 (mother centriole). Insets show pericentrosomal region. Scale bar: 10 μm.

In the absence of rapamycin, centriolar satellites were distributed around both centriole dots. After induction of centrosomal re-routing by rapamycin, PCM1 granules specifically localized around the CEP164-positive mother centriole **(Figure 2.8)**, proving our hypothesis. Notably, CEP120 signal intensity was similar at both centrioles, likely due to the recruitment of CEP120 by satellites as shown in **Figure 2.6A and B**, which results in its increased levels at mother centriole.

2.3.5. Centriolar satellite re-routing does not affect microtubule nucleation

The mother centriole is the main microtubule organizing center (MTOC) in the cell, and it regulates the microtubule network by (1) microtubule anchoring and (2) microtubule nucleation (Sanchez & Feldman, 2017). Since we have showed increased centriolar satellite accumulation at the mother centriole, we next investigated how this enrichment affects microtubule nucleation. To do so, we co-expressed GFP-PCM1-FKBP and Flag-Kin14-FRB, induced centrosomal re-routing with rapamycin, and then treated the cells with nocodazole to depolymerize microtubules. Following nocodazole washout, we allowed re-polymerization of microtubules and fixed the cells after 1, 2, and 3 minutes.

Cells were immunostained for α-tubulin and Centrin 1 to quantify the aster size and microtubule density at the asters.

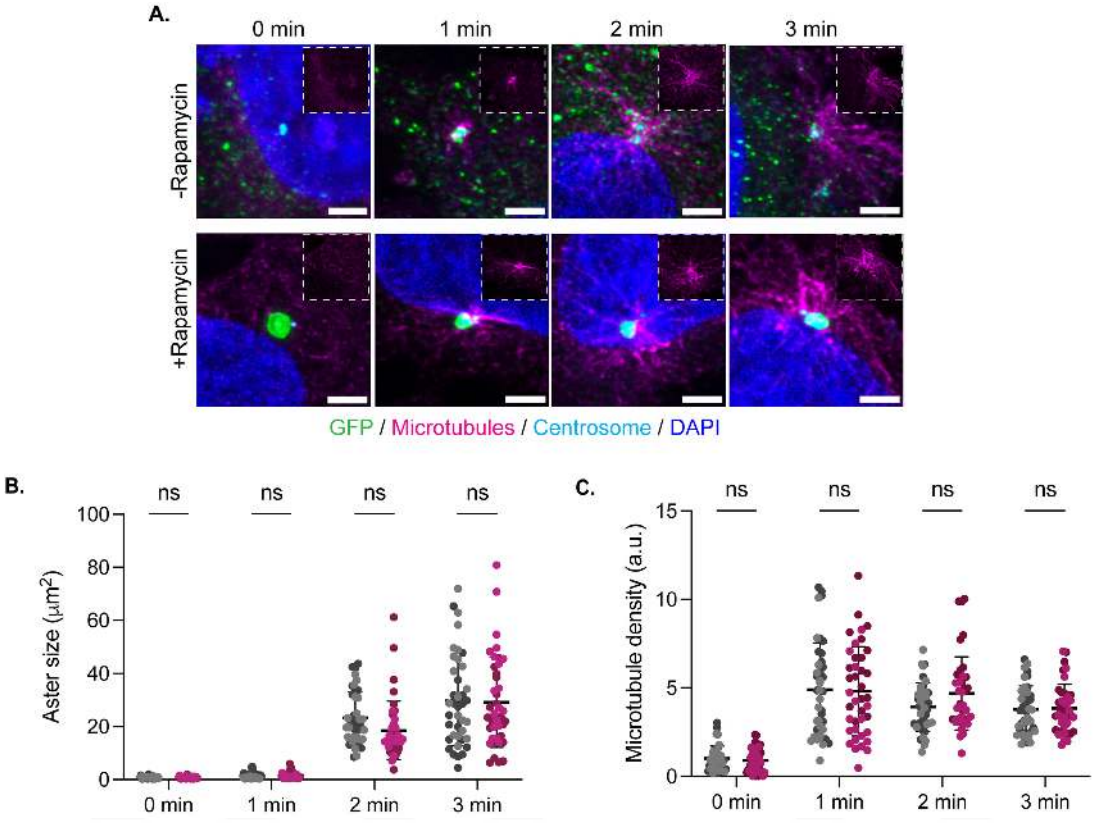

Figure 2.9 Centriolar satellite clustering does not inhibit microtubule nucleation.

A. HeLa cells co-transfected with GFP-PCM1-FKBP and FRB-Flag-Kin14 were treated with rapamycin for 1 hour and after 6 hours, microtubules were depolymerized with 5 ug/mL of nocodazole for 1 hour. Cells were fixed and immunostained for GFP, α-tubulin, and Centrin1. Insets show pericentrosomal region. Scale bar: 2 μm. **B.** Aster size is measured with Fiji encompassing the growing microtubule aster area. The data represents three biological replicates, with n = 20 per replicate. **C.** Microtubule density is quantified by measuring average the α-tubulin fluorescence intensity within the aster area using Fiji. All measurements normalized to the minus rapamycin 0 min time-point. The data represents three biological replicates, with n = 20 per replicate. *:p<0.05, **:p<0.01, ***:p<0.001****:p<0.0001, ns: not significant.

The microtubule nucleation was observed by 1 minute, as small α-tubulin-positive asters formed around the centrosome **(Figure 2.9.A)**. Aster size increased over-time in both control and the rapamycin treated cells with no significant difference between

conditions **(Figure 2.9.B)**. The fluorescence intensity of α-tubulin peaked at 1 minute time-point and then decreased as the asters expanded in size. Notably, the microtubule density in rapamycin treated cells was higher than in control at the 2-minute time-point, although control cells reached similar intensity levels by 3 minutes **(Figure 2.9.C)**.

Overall, these results show that despite the preferential re-routing and accumulation of satellites to the mother centriole, the intrinsic microtubule nucleation capability of the cell is not perturbed.

2.3.6. Re-routed centriolar satellites on the centrosome do not dissolve during mitosis

Centriolar satellite integrity and composition adapts to different cellular cues such as stress, ciliogenesis, and cell cycle progression (Begar et al., 2025). Upon mitotic entry, PCM1 granules disassemble into the cytoplasm and release client proteins so that they can perform their mitosis related functions. Clients whose levels are shown to be regulated by satellites **(Figure 2.6.A and B)** including CEP63, CEP152, CEP120, CEP72, and CETN1 have well-characterized roles in mitosis. However, how centriolar satellites contribute to mitosis besides sequestering centrosomal proteins remains unclear.

Previous studies investigating the role of centriolar satellites in mitosis using RPE1 and IMCD3 PCM1 KO cells did not report defects in cell proliferation or mitotic progression. However, these studies were done with chronic depletion where compensatory mechanisms could possibly play a role. To address this limitation and probe the acute effect of centriolar satellite perturbation on mitosis, we generated a GFP-PCM1-FKBP knock-in cell line and applied our inducible satellite trafficking assay to re-route them to the centrosome. Then, we monitored the localization of satellite granules and the mitotic behavior of the cells with fixed imaging and in real-time.

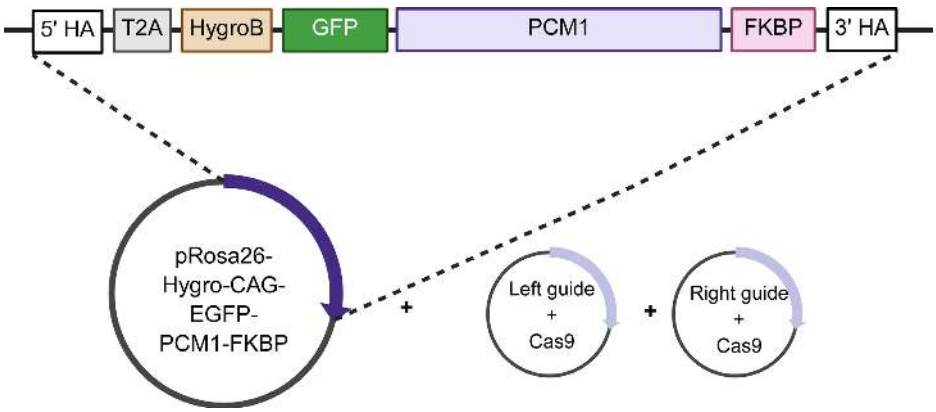

Figure 2.10 GFP-PCM1-FKBP knock-in cell line generation.

Schematic representation of pRosa26-Hygro-CAG-EGFP-PCM1-FKBP plasmid and the knock-in principle utilizing Rosa26 locus homology arms.

We utilized the human ROSA26 safe-harbor knock-in strategy to constitutively express GFP-PCM1-FKBP in HeLa WT cells (thereafter HeLa hR26 cells) using CRISPR/Cas9 **(Figure 2.10)**. The genomic integration of PCM1 sequence to ROSA26 locus is confirmed by PCR reaction using specific primers. Satellite-like localization of GFP-PCM1-FKBP is also confirmed by immunostaining for GFP and PCM1 **(Appendix Figure 3)**. We transfected HeLa hR26 cells with Flag-Kin14-FRB, induced centrosomal re-routing of satellites with rapamycin for 6 hours, then investigated the localization of satellite granules at different mitotic stages.

GFP-PCM1-FKBP granules in the control condition behaved similarly to endogenous satellite granules in interphase cells, concentrating around the centrosome and distributed throughout the cytoplasm in a lesser extent. Upon mitotic entry, majority of the granules were disassembled in metaphase, anaphase, and telophase, then reassembled at cytokinesis as cells exited mitosis. In contrast, rapamycin-treated cells exhibited different granule dynamics. They remained as large pericentrosomal punctum throughout all mitotic stages, co-localizing with one or both spindle poles in an uneven distribution **(Figure 2.11)**. Overall, the inducible centrosomal re-routing of centriolar satellites disrupted their mitotic regulation.

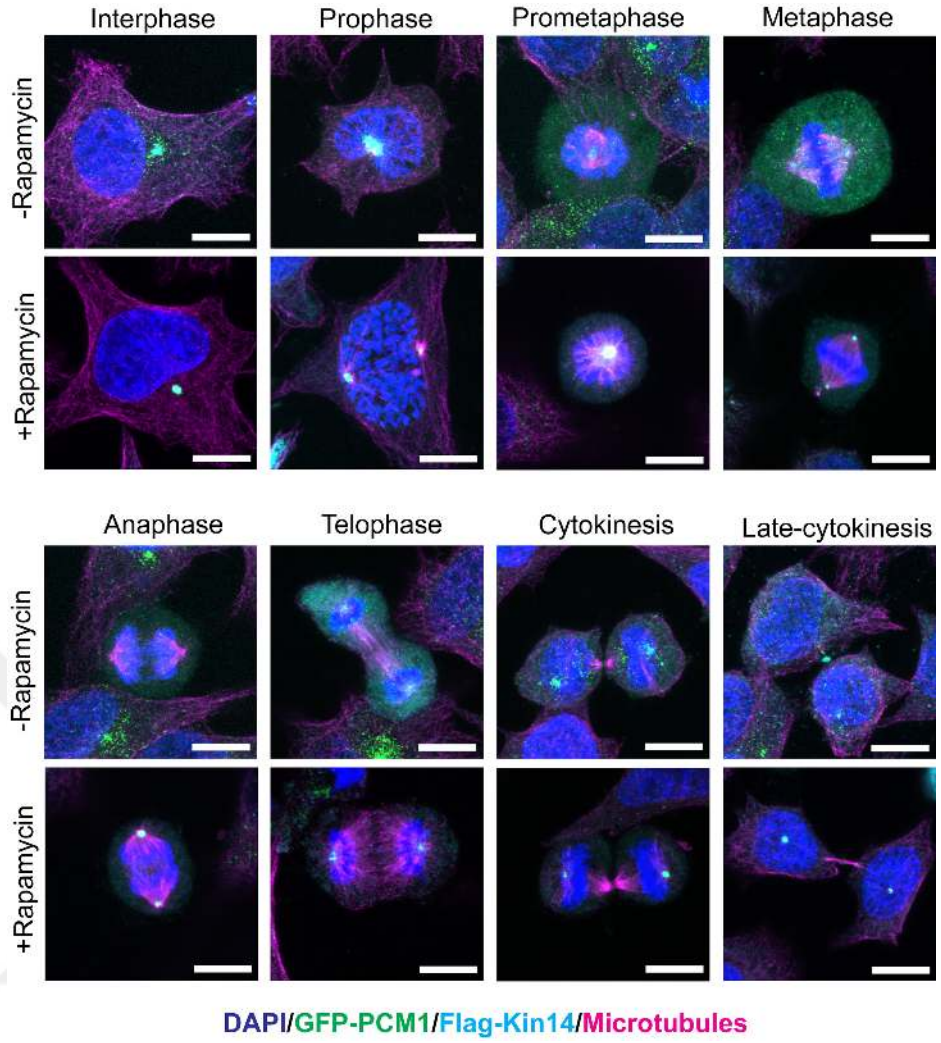

Figure 2.11 Mitotic behavior of centriolar satellites in control and rapamycin treated cells.

HeLa hR26 cells transfected with FRB-Flag-Kin14 were fixed after rapamycin treatment and stained with GFP, Flag, and α-tubulin antibodies. Satellites dissolve in metaphase and reassemble upon mitotic exit in control cells. Upon centrosomal re-routing, satellite foci remain intact at the pericentrosomal region throughout mitosis. Scale bar: 10 μm.

2.3.7. Centriolar satellite re-routing induces metaphase arrest in live cells

To elucidate the fate of the cells that have persistent satellite puncta at the centrosome, we performed live-cell imaging to capture mitotic events. We transfected HeLa hR26 cells with Flag-Kin14-FRB, induced centrosomal re-routing of satellites with rapamycin for 6 hours and set up time-lapse imaging with 4 minutes intervals. Satellite granules were dynamic in the control condition, rapidly disassembling and reassembling

upon cellular cues. Although light sheet fluorescence microscopy is ideal for fast imaging of living cells, HeLa hR26 cells were susceptible to phototoxicity, hence even the control cells had longer mitotic times (average duration = 86 mins) than expected. The frequency of mitotic events was low in the rapamycin treated condition; majority of the cells stayed in interphase. We categorized different phenotypes in the mitotic cells as no spindle formation (22%), metaphase arrest (56%), and successful division (22%). As a result, majority of the mitotic cells having the large satellite puncta was displaying metaphase arrest. Successful division events were rare, but when we compared the mitotic and cytokinetic times of cells, we observed that cells treated with rapamycin had longer mitotic durations. **(Figure 2.12.A)**.

We then wanted to assess the longer-term effects of satellite mislocalization on cell proliferation upon rapamycin treatment and performed flow cytometry based live and apoptotic cell counting. For this purpose, we transfected HeLa hR26 cells with Flag-Kin14-FRB, induced centrosomal re-routing of satellites with rapamycin and collected the cells at 6-, 24-, and 48-hours post-treatment. The live cell numbers in both conditions were similar at earlier time-points, but the cell viability decreased significantly at 48-hour condition in rapamycin treated cells. The apoptotic cells were detected from the annexin V levels with a fluorescence-based assay with flow cytometry. The apoptotic cell percentage between two conditions was similar at 24-hour, but the apoptotic cell percentage is increased almost two-fold compared to control at 48-hour **(Figure 2.12.B)**.

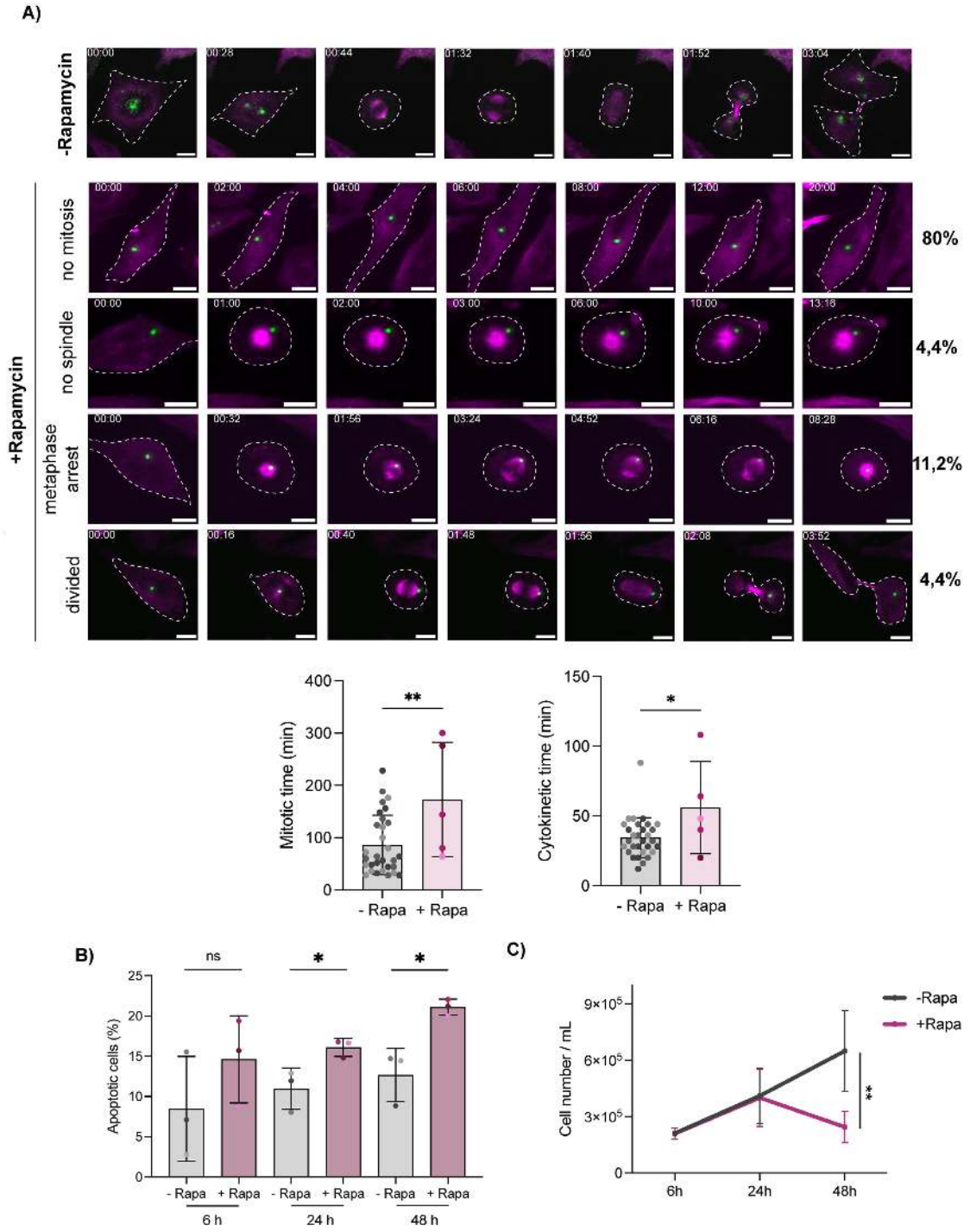

Figure 2.12 Centriolar satellites do not dissolve during mitosis upon centrosomal re-routing.

A. Time-lapse imaging of centriolar satellites in control and rapamycin treated cells. HeLa hR26 cells transfected with FRB-Flag-Kin14 were treated with rapamycin and after 6 hours, time-lapse imaging started. Cells were treated with SiR-tubulin O/N to visualize microtubules. Cells were imaged in every 4 mins during 18 hours of live cell. Cells displaying different phenotypes over the course of mitosis were classified and quantified accordingly. The data represents three biological replicates. Cell edges are outlined. Scale

bar: 10 μm. **B.** Live and apoptotic cells were assayed using flow cytometry in control and rapamycin treated cells. HeLa hR26 cells transfected with FRB-Flag-Kin14 were treated with rapamycin for 1 hour and collected at 6-, 24-, and 48-h time points. Cells were mixed with Muse Annexin V & Dead Cell reagent and apoptotic cells were counted using flow cytometry in a time-dependent manner. The data represents three biological replicates.

Overall, analysis of live cells revealed that mispositioning of satellites resulted in metaphase arrest during mitosis, decreased cell viability and increase in apoptosis over time.

2.3.8. Mislocalization of satellites leads to disruption in proper spindle formation and chromosome congression

Next, we probed the mitotic behavior of these cells with fixed imaging and immunofluorescence. We first quantified the mitotic index and found that rapamycin treated cells exhibited significantly lower mitotic index compared to control **(Figure 2.13.A)**. Then, we quantified the percentage of cells at each mitotic phase in control versus rapamycin treated condition. While control cells were displaying a relatively heterogeneous distribution over each mitotic phase, rapamycin treated cells were mostly at either pro-metaphase or metaphase, indicating a mitotic arrest phenotype **(Figure 2.13.B)**.

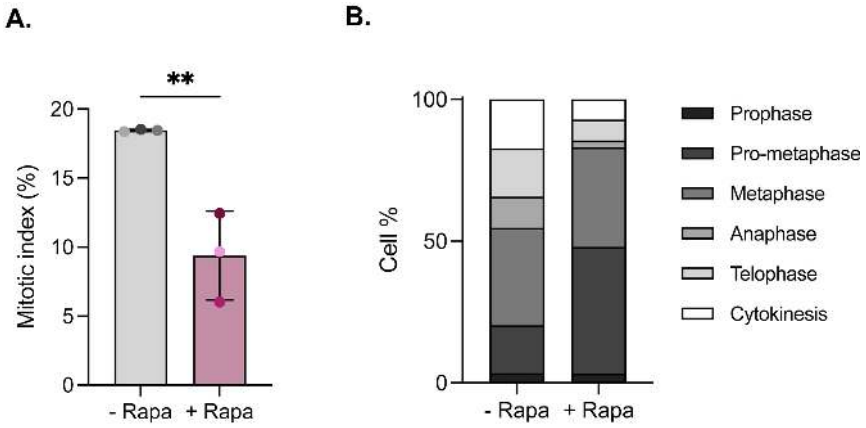

Figure 2.13 Effect of centrosomal re-routing on mitotic index and mitotic progression.

A. Mitotic index was calculated by dividing the number of mitotic cells to the total cell number. The index of cells decreased significantly upon rapamycin treatment. The data represents three biological replicates. **B.** Mitotic cells were counted and categorized according to cell cycle stages. The data represents three biological replicates.

Focusing on metaphase, we categorized and quantified the satellite puncta depending on their behavior during mitosis as localizing to spindle poles equally, unequally, or to one spindle pole only. Majority (48% of cells) of rapamycin-treated cells exhibited one pole localization, while there are also two-pole localization with equal (18%) and unequal levels (34%). Notably, we observed uneven spindle length in cells displaying one pole satellite localization **(Figure 2.14.A)**. When we quantified the total spindle length, we did not observe any significant difference between control versus rapamycin treated cells **(Figure 2.14.B)**.

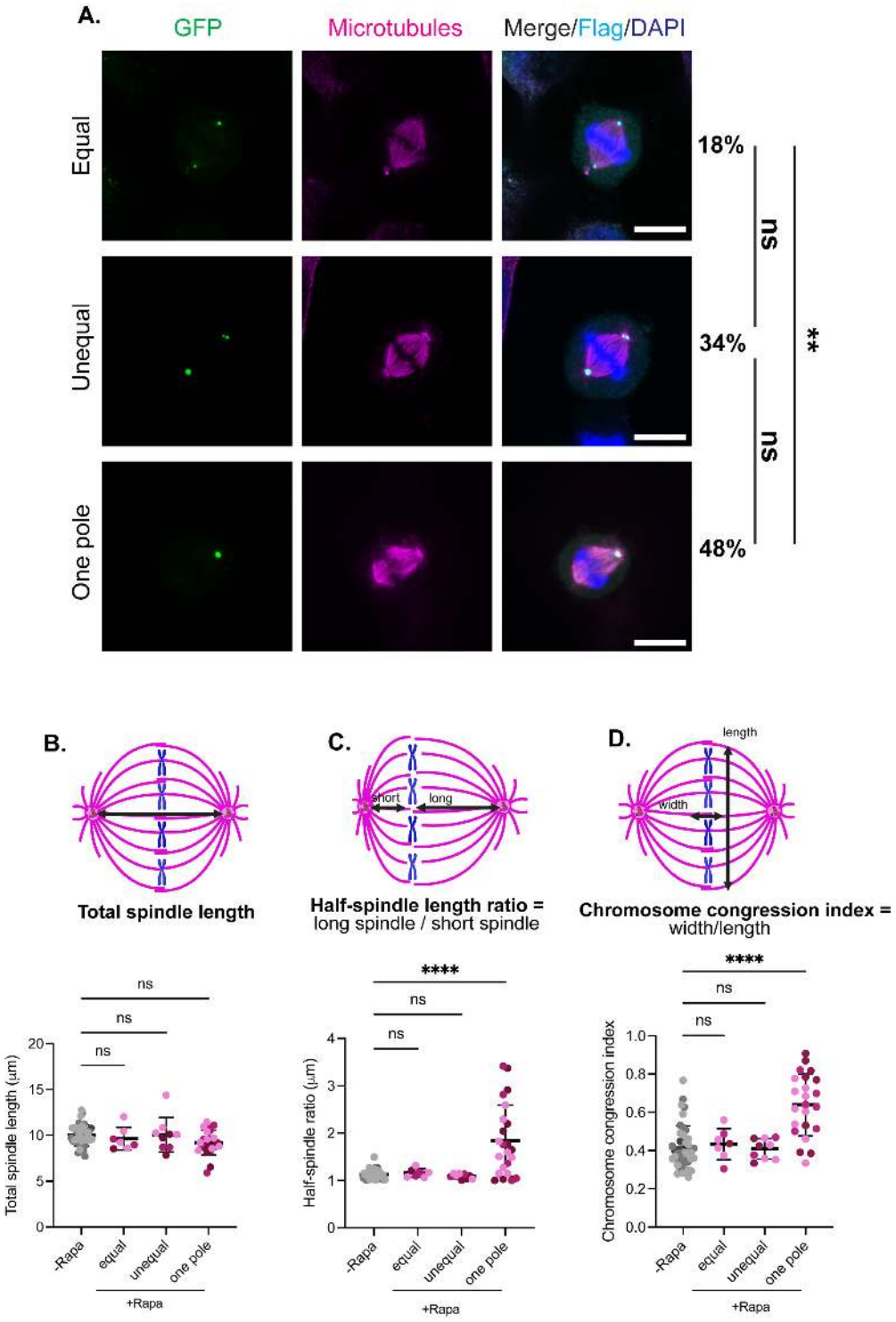

Figure 2.14 Satellite clustering at the centrosome results in asymmetric half spindle formation and chromosome congression defects.

A. Centriolar satellite distribution on spindle poles in rapamycin treated cells. Satellite foci at the pericentrosomal area displayed three distinct phenotypes: equal or unequal distribution on both poles, or only present at one pole. The data represents three biological replicates. Scale bar: 10 µm. **B.** Effect of centrosomal re-routing on total spindle length.

Spindle lengths were measured from one pole to the other using the α-tubulin staining. The data represents three biological replicates, with n > 17 per replicate. Created with BioRender. **C.** Effect of centrosomal re-routing on half-spindle length ratio. Half-spindle lengths were measured starting from one pole until the chromosome area using the α-tubulin staining. The half-spindle length of the PCM1-positive pole was divided by the PCM1-negative pole. The data represents three biological replicates, with n > 17 per replicate. **D.** Effect of centrosomal re-routing on chromosome congression. The width and length of the congressed chromosomes was measured using the DAPI staining. The congression index was calculated by dividing the width to length. The data represents three biological replicates, with n > 17 per replicate.

We then calculated the half-spindle length ratio by dividing the long half-spindle length to the short half-spindle length. This value was around 1 in control cells since both half-spindle microtubule lengths are similar. We also observed the same pattern in cells where re-routed satellites localize to both poles independent of their equal or unequal segregation. However, we calculated significantly higher half-spindle length ratio values for cells with one pole satellite localization, reflecting asymmetric half-spindle formation. Importantly, the longer half-spindle originated from the pole bearing the satellite punctum **(Figure 2.14.C)**. Finally, since proper spindle formation is essential for chromosome alignment during mitosis, we then calculated the chromosome congression index. The index of the rapamycin treated cells were much higher than control cells, suggestion a disruption in chromosome alignment **(Figure 2.14.D)**.

Together, we showed that centrosomal re-routing of centriolar satellites during mitosis results in spindle asymmetry, metaphase arrest, and defective chromosome congression, proposing a crucial role for satellite dynamics in maintaining mitotic fidelity.

2.4. Discussion

Our work establishes a system to manipulate centriolar satellite positioning and dynamics and uses it to test the direct link between satellite localization and function. The main advantage of our system is providing an acute mislocalization, because it allows studying temporal functions which is not possible with the previous loss of function studies. By fusing the satellite scaffold protein PCM1 to FKBP and recruiting it to centrosome with a rapamycin inducible FRB-tagged minus-end directed Kinesin-14b

motor, we overcame the dominant-negative effects caused by BICD2-based approaches. The resulting assay achieved approximately a five-fold enrichment of satellites at the centrosome within an hour, providing a rapid alternative to chronic protein depletion or long-term depletion by RNAi that are often overcamed by compensatory mechanisms.

Acute clustering of satellites also resulted in accumulation of diverse client proteins including CEP131, CEP72, and CEP290 while leaving the mother centriole marker CEP164 unaffected. These data reinforce the idea that satellites act as tunable storage sites that buffer centrosomal protein dosage and prevent ectopic activation. Notably, clients with weak satellite pools, such as MIB1, also showed increased accumulation at the pericentrosomal region, suggesting that satellites can rapidly sequester proteins in response to cellular cues rather than only serving as a storage site.

Following re-routing, satellites are clustered specifically on the mother centriole, consistent with minus-end directed motor protein movement. Similar mother-specific enrichment has been reported during centriole remodeling and may ensure that cargo delivery is spatially restricted to the mature centriole. Notably, this asymmetric accumulation did not compromise microtubule nucleation, implying that basal MTOC activity is either buffered against satellite re-routing or uses distinct pericentrosomal territories.

In most vertebrate cells, centriolar satellites dissolve as cells enter mitosis, a process driven by mitosis-specific phosphorylation of PCM1. DYRK3 adds phosphates that weaken the multivalent PCM1-client interactions thereby releasing its content to the cytosol (Rai et al., 2018; Wang et al., 2013). The clearance of pericentrosomal area from satellites allows spindle-assembly factors to function properly. Our chemically inducible trafficking assay overrides this dissolution by creating hyper-multimerized clusters that resist phosphorylation-driven disassembly. With this assay, we uncovered a requirement for satellite dynamicity during mitosis deduced from asymmetric spindles, disruption in chromosome congression, metaphase arrest, and increase in apoptosis. These phenotypes contrast with earlier reports with chronic PCM1 deletion in RPE1 or mIMCD3 cells (Odabasi et al., 2019), highlighting how acute interference allows dissecting acute dependencies that long-term adaptations conceal. But what is the underpinning mechanism of asymmetrical half-spindles if microtubule nucleation is not affected by satellite re-routing? Mechanistically, large satellite foci may sequester centriole-associated regulators such as CEP63 or CEP152, or disrupt dynein loading at spindle poles, both of which are required for symmetrical spindle microtubule formation.

One of the limitations of this study would be the off-target effects of rapamycin. Rapamycin is an mTOR inhibitor that negatively affects mitotic progression. Could the mitotic defects observed in this study might be simply due to the inhibition of mTOR pathway rather than a result of centrosomal satellite accumulation? Firstly, prolonged exposure (> 12 hours) is associated with inhibition of mitosis due to the G1/S arrest and not metaphase arrest. Moreover, mTOR activity is physiologically downregulated by CDK1-dependent mechanisms during mitosis (Odle et al., 2020), so additional inhibition by rapamycin is often fails to alter spindle dynamics in the short term treatments with higher concentrations such as 300 nM for 30 minutes like it is used in this study (Ryan et al., 2021). However, repeating some functional experiments using rapalog, a rapamycin derivative that does not bind endogenous mTOR (Abdel-Magid, 2019), or assessing the mTOR activity by checking its phosphorylation levels would rule out the off-target effects caused by rapamycin even though a very short treatment (1 hour) was used in this study.

Centriolar satellites are also implicated other cellular processes such as ciliogenesis or stress response. Since HeLa cells are non-ciliated, extending this system into ciliating cells like RPE1 or mIMCD3 would allow us to study the effects of satellite mislocalization on cilium assembly, ciliary content regulation, and ciliary signaling in physiologically relevant contexts. Satellites normally scatter within minutes upon UV, heat-shock, or transciptional stress via p38-MAPK cascade that phosphorylates CEP131 and drives cargo dissociation. This system provides a unique method to block the scattering of satellites and study what would be the functional consequences when satellites cannot scatter upon stress.

2.5. Conclusion

In conclusion, our results demonstrate that the chemically inducible centriolar satellite trafficking assay effectively disrupts the spatial organization of satellite granules within the cell and enables the investigation of the effects of acute, temporally controlled satellite depletion. We show that client proteins are selectively trafficked to the centrosome in response to inducible re-routing of satellites, supporting their roles in storage, sequestration, and trafficking, and highlighting the spatiotemporal regulation of client proteins by centriolar satellites. Notably, despite the preferential re-routing and accumulation of satellites at the mother centriole, the intrinsic microtubule nucleation capacity of the cell remains unaffected. However, inducible centrosomal re-routing

disrupts the mitotic regulation of satellites which is shown by persistent satellite foci on centrosome. Time-lapse imaging of mitotic events revealed that mispositioning of satellites leads to metaphase arrest which is also supported by the spindle asymmetry and disruption in chromosome congression. Altogether, these findings propose a role for centriolar satellite dynamics in maintaining mitotic fidelity and proper cell division.

Chapter 3

3. INDUCIBLE DIMERIZATION OF CENTRIOLAR SATELLITES DISRUPTS HEDGEHOG SIGNALING

3.1. Introduction

3.1.1. Membraneless Organelles

Cells contain numerous membraneless organelles such as nucleolus, Cajal bodies, P-bodies, and stress granules, which lack a surrounding lipid membrane. These structures form via liquid–liquid phase separation (LLPS), a process in which specific biomolecules demix from the cytosol or nucleoplasm to create a concentrated droplet phase. LLPS is driven by multivalent interactions among proteins and nucleic acids, often involving intrinsically disordered regions (IDRs) or repetitive interaction motifs.

Above a critical concentration, these multivalent interactions induce a phase transition, segregating components into a dense phase while excluding others. The resulting condensates typically display liquid-like properties where they fuse upon contact, round up due to surface tension, and allow dynamic exchange of components with the surroundings. LLPS thus offers cells a way to organize biochemical reactions in compartmentalized yet highly dynamic microdomains, without the barrier of a membrane (Hirose et al., 2023).

3.1.2. Centriolar Satellites as Membraneless Organelles

Centriolar satellites are membraneless organelles that has the potential to form by phase separation. Live-cell imaging reveals that satellites behave like liquid droplets since individual granules can fuse and split, and exhibit mostly diffusive, dynamic movement (Conkar et al., 2019). This liquid-like behavior suggests an underlying phase-separation mechanism. Consistently, in vitro studies have shown that fragments of PCM1 can spontaneously phase-separate into liquid droplets, which readily coalesce into larger droplets and exchange components with the surrounding solution (Zhao et al., 2021). Thus, centriolar satellites meet the hallmarks of membraneless organelles formed by LLPS.

Functionally, satellites serve as dynamic hubs near the centrosome by sequestering, modifying, and trafficking centrosome and cilia related proteins. By concentrating specific client proteins, satellites regulate their availability to the centrosome, for example, storing and releasing factors required for ciliogenesis or centrosome stability. The membraneless nature of satellites likely allows rapid assembly or dissolution in response to cellular signals, ensuring flexible control of centrosome-associated processes (Begar et al., 2025).

3.1.3. Dimerization Domains of PCM1

The multivalent properties of PCM1 allows it to form higher-order assemblies like the centriolar satellite granules. Human PCM1 is a large (~228 kDa) protein enriched in coiled-coil regions and disordered segments. Notably, PCM1 contains two distinct self-association domains (approximately amino acids 201–494 and 745–1128) that mediate self-interactions. These domains enable PCM1 proteins to bind one another and form oligomeric complexes which creates a molecular network that scaffolds satellite granules (Kubo & Tsukita, 2003).

The importance of PCM1's dimerization or oligomerization capacity was demonstrated with overexpression studies in which PCM1 fragments that lacked the C-terminus but retained the internal binding regions led to formation of large PCM1 aggregates in cells. Truncated PCM1 proteins were shown to bind to each other via two separate regions, driving self-aggregation and recruiting endogenous PCM1 into the assemblies (Kubo & Tsukita, 2003). The extensive intrinsically disordered regions (IDRs) in PCM1 may further contribute by mediating weak multivalent interactions such as electrostatic and hydrophobic contacts, enhancing the phase separation potential.

In addition, PCM1 has various protein–protein interaction motifs like C-terminal conserved domain and LC3-interacting region that tether client proteins (Wirth et al., 2019). Thus, PCM1 serves as a multivalent hub in which self-associates to form a molecular scaffold and simultaneously captures many client proteins. This multivalency is crucial for nucleating centriolar satellite condensates.

3.1.4. Inducible Dimerization System to Study Multivalency of Organelles

A powerful experimental strategy to probe phase separation in cells is to artificially induce clustering of a protein of interest and observe if condensates form. One such tool utilizes a modified FK506-binding protein domain, FKBP12(F36V). The F36V

mutation allows FKBP12 to bind a synthetic chemical dimerizer (such as AP20187) that does not bind the wild-type protein. In essence, the cell-permeable ligand acts as a molecular crosslinker that homodimerizes FKBP-F36V domains with very high affinity. These dimers could also be dissociated by other competitor ligands (such as AP22542) which makes the system reversible (Clackson et al., 1998). By fusing FKBP(F36V) to a target protein, researchers can acutely control the protein's valency. Addition of the ligand brings two proteins together, potentially triggering a phase-separated assembly if the protein has inherent multivalent interaction capacity.

This approach has been used to mimic and analyze membraneless organelles in previous studies. One example is the clustering of signaling proteins via FKBP(F36V) ligand which lead to the formation of punctate cytosolic bodies and activate signaling pathways, demonstrating that condensate formation can drive functional outcomes (Mabe et al., 2014). Such chemically inducible systems are valuable for dissecting the mechanistic requirements of phase separation. Moreover, reversibility of ligand binding means the induced condensates can be dissolved by ligand withdrawal, letting researchers observe dynamic assembly/disassembly cycles.

In summary, centriolar satellites exemplify how cells exploit multivalent interactions and liquid–liquid phase separation to organize pericentrosomal space without a membrane barrier. By leveraging chemogenetic tools such as the FKBP-F36V dimerization system, we can now probe the mechanistic underpinnings of satellite formation and dissect the causal relationships between condensate assembly and cellular function.

3.2. Materials § Methods

3.2.1. Plasmids and clonings

Full-length cDNAs of Homo sapiens PCM1 (GenBank accession no: NP_006188.4) was used. The sequence was amplified and cloned into pCDH-EF1α-mNG using BamHI and NotI enzymes. FKBP(F36V) was amplified from pCDNA3.1(+)-miniTurboID-6xGGSGlinker-FKBPF36V-2xHA (Addgene plasmid #200641) and cloned into pCDH-EF1α-mNG-PCM1 using NotI enzyme. pCDNA3.1(+) miniTurboID-6xGGSG linker-FKBPF36V-2xHA was a gift from Justin English & Fleur Ferguson (Addgene plasmid # 200641 ; http://n2t.net/addgene:200641 ; RRID:Addgene_200641)

3.2.2. Generation of chemically inducible centriolar satellite dimerization cell line

pCDH-mNG-PCM1 FL-FKBP(F36V) was co-transfected with envelope (pMD2-VSVG) and packaging (pLVpsPAX2) plasmids using PEI in HEK293T cells. 48 hours after transfection, the medium was collected and virus particles were concentrated using 50% PEG6000, 4 M NaCl, and 1X PBS. RPE1::PCM1 KO cells were seeded in 12 well plate and infected with the concentrated virus. After 2 days, the heterogeneous pool was screened, and single cell dilution was done to generate single cell colonies. Colonies were screened with immunofluorescence and all the functional experiments were carried out using the same clonogenic line.

3.2.3. Chemically inducible centriolar satellite dimerization assay

RPE1::PCM1 KO cells stably expressing mNG-PCM1-FKBP(F36V) are used for the inducible dimerization system. To dimerize the satellite granules, cells were treated with 250 nM of B/B Homodimerizer (AP20187) for at least 4 hours. To dissociate the dimerized granules, the cells were washed with PBS 2 times after dimerizer treatment and consequently treated with 1 uM of wash-out ligand (AP22542) for at least 1 hour. The treatment duration varied among different experiments (e.g. for cilium assembly, 24 h; for Sonic hedgehog stimulation, 48 h; for live imaging of mitosis, 18 h).

3.2.4. Immunofluorescence

Cells were grown on glass coverslips for the immunofluorescence experiments. Coverslips were washed with PBS and the cells were fixed with either paraformaldehyde at room temperature or with ice-cold methanol at −20C for 10 mins. After washing the coverslips twice with PBS, cells were blocked with 3% BSA in PBS containing 0.1% Triton X-100 for permeabilization. For the immunostaining, cells were incubated with primary antibodies in blocking solution for 1 h at room temperature and then with secondary antibody solution containing DAPI. After washing out the excess antibodies with PBS, cells were mounted using Mowiol mounting medium. Full list of primary and secondary antibodies used for immunofluorescence experiments in this chapter are listed table in Appendix Table 1.

3.2.5. Microscopy

Confocal microscopy was performed with Leica TCS SP8 or Stellaris 8 laser scanning inverted confocal microscope system equipped for four-color imaging with 405, 488, 561, and 633 nm laser lines, four detection channels (1 photomultiplier tube and 3 Hybrid Detectors), HC PL APO CS2 63X 1.4 NA oil objective and an incubation chamber. Pinhole diameter was set to 1 μm. Images were acquired with 0.2–0.5 μm z-spacing, line averaging set to 2–323 and 400/600 Hz unidirectional xyz scan mode. An image format of 512x512 or 1,024x1,024 pixels and an additional 1–4x optical zoom was used for sample acquisition. The system was controlled with the Leica Application Suite X Software (Leica). Post-processing was performed using the Huygens Professional (Scientific Volume Imaging).

3.2.6. Ciliogenesis in dimerization system

For the ciliogenesis experiment, cells were treated with B/B homodimerizer for 4 hours and treated with W/O ligand for 1 hour (after B/B homodimerizer treatment is completed). Then, cells were incubated in serum depleted media containing either B/B homodimerizer or W/O ligand for 24 hours.

3.2.7. Sonic hedgehog pathway activation in dimerization system

For the Sonic hedgehog experiment, cells were treated with B/B homodimerizer for 4 hours and treated with W/O ligand for 1 hour (after B/B homodimerizer treatment is completed). Then, cells were incubated in serum depleted media containing either B/B homodimerizer or W/O ligand for 24 hours. After the starvation, 50 nM of SAG was added, and the cell were incubated for another 24 hours.

3.2.8. Live imaging of inducible dimerization of satellites

For the time lapse imaging of satellite dimerization/dissolution, the cells were plated on Ibidi μ-Slide 8 well dishes and imaged at 37C with 5% CO2 with a frequency of 2 minutes per frame until 1 hour, then 20 minutes per frame until 4 hours, with 0.5 μm step size in 512 x 512 pixel format. The cells were treated with corresponding dimerizer and wash/out ligands between the first and second frames.

3.2.9. Live imaging of mitosis in dimerization system

For the live mitosis imaging, the cells were plated on Ibidi µ-Slide 8 well dishes and treated with SiR-tubulin (Cytoskeleton) with 1:10.000 dilution overnight. The next day, the cells were treated with B/B homodimerizer for 4 hours and treated with W/O ligand for 1 hour (after B/B homodimerizer treatment is completed), then immediately taken for live cell imaging. They were imaged at 37C with 5% CO2 with a frequency of 10 minutes per frame, with 0.7 µ m step size and 512 x 512 pixel format.

3.2.10. Quantification of dimerized granule properties

Imaris for Cell Biologists (v.10.0, Oxford Instruments) module was used for quantifying the granule number and volume properties in chemically inducible centriolar satellite dimerization assay. Microscopy images in Leica Image File format first converted into Imaris compatible file format using Imaris File Converter. Then, the Z-stacks were opened in Imaris in their native format and automatically reconstructed into a multi-channel 3D model during input, requiring no further image pre-processing. To designate individual granules, the Surface creation tool was used to generate a ROI. In the Surface creation wizard, the source channel was set to “Green Channel-Ch2” and the surfaces detail value was adjusted manually according to the granule size. Background subtraction (absolute intensity thresholding) was used to separate the cell in the foreground from the background environment. Any adjustments to the surface shape were made by altering the surface extraneous noise around the periphery during detection. Split touching objects function (morphological split) was used to differentiate individual granules in contact with each other. All values related were directly exported from the software.

3.2.11. Ciliary Quantifications

Ciliogenesis quantifications were done using Leica Application Suite X Software. Cells were counted using the Annotations > counting function from DAPI staining as the nuclei marker and the cilia were counted using acetylated tubulin and Arl13b as ciliary axoneme and ciliary membrane markers. Cilia length was also measured using the Annotations > um function of this software from acetylated tubulin channel.

3.2.12. Statistical analysis

Prism 10 software (GraphPad Software, La Jolla, CA) is used to calculate p-values and determine statistical significance. To compare two groups that exhibit Gaussian distribution, parametric unpaired two-tailed Student's t-test was used. When the sample does not have Gaussian distribution, nonparametric Mann-Whitney test is applied. To compare more than two groups, un-paired ordinary one-way ANOVA test is used. Error bars in the graphs indicate the standard deviation (SD), and statistical significance levels were denoted as follows: ns: P>0.05, *:P<0.05, **:P<0.01, ***:P<0.001 and ****:P<0.0001.

3.3. Results

3.3.1. Development and validation of centriolar satellite dimerization assay

Centriolar satellites adapt to different cell types and physiological states by regulating their content and spatiotemporal behavior (Begar et al., 2025). Their intracellular and intercellular heterogeneity were previously reported, however the mechanisms underpinning this plasticity are yet to be discovered (Kubo & Tsukita, 2003). To elucidate the relationship between centriolar satellite granule properties and their cellular functions, we developed an inducible tool that can selectively manipulate satellite granule number and size. Through this manipulation, we disrupt the centriolar satellite homeostasis and assess the effect of this perturbation on different cellular processes such as mitosis, ciliogenesis, and ciliary signaling.

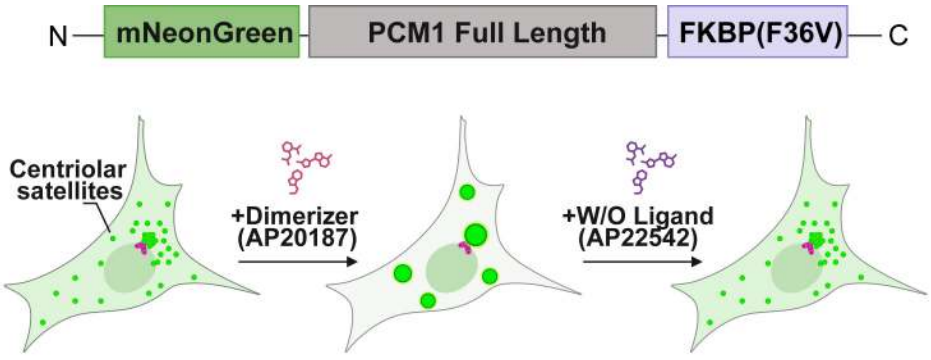

Figure 3.1 Development of the inducible centriolar satellite homodimerization system.

Design of the satellite dimerization system. mNeonGreen (mNG) tagged PCM1 is fused with FKBP(F36V) mutant which dimerizes upon dimerizer (AP20187) treatment. After

the dimers are formed, they can be dissociated with wash-out ligand (AP22542). Created with BioRender.

To manipulate centriolar satellite granules in cells, we utilized a reversible chemically inducible dimerization system that can dimerize the monomeric proteins. This assay is using the F36V mutant of FK506-binding protein (FKBP-F36V) that can homodimerize upon AP2018 (dimerizer) treatment and can dissociate the dimers upon AP22542 (wash-out ligand) treatment. We adapted this system to our study by generating an FKBP-F36V fusion of centriolar satellite scaffold protein PCM1 and designed a lentiviral expression construct by tagging PCM-FKBP-F36V with mNeonGreen (mNG) and generated RPE1::PCM1 KO cells stably expressing this homodimerizable satellite construct **(Figure 3.1)**.

We then used the dimerizer drug for merging individual satellite granules together, and the W/O ligand to dissociate them as confirmed by immunostaining of mNG and PCM1 **(Figure 3.2.A)**. We quantified the number and size of the satellite granules upon dimerizer and following W/O ligand treatments. Dimerizer treatment induced PCM1 homodimerization, resulting in a significant decrease in granule number and an increase in mean granule volume. Upon W/O ligand treatment, granules dissociated and returned to their physiological number and size **(Figure 3.2.B)**. Dimerization and dissociation of satellite granules upon drug treatments is also confirmed by live imaging. It took four hours for satellite granules to completely dimerize and one hour was adequate for their dissociation **(Figure 3.2.C)**.

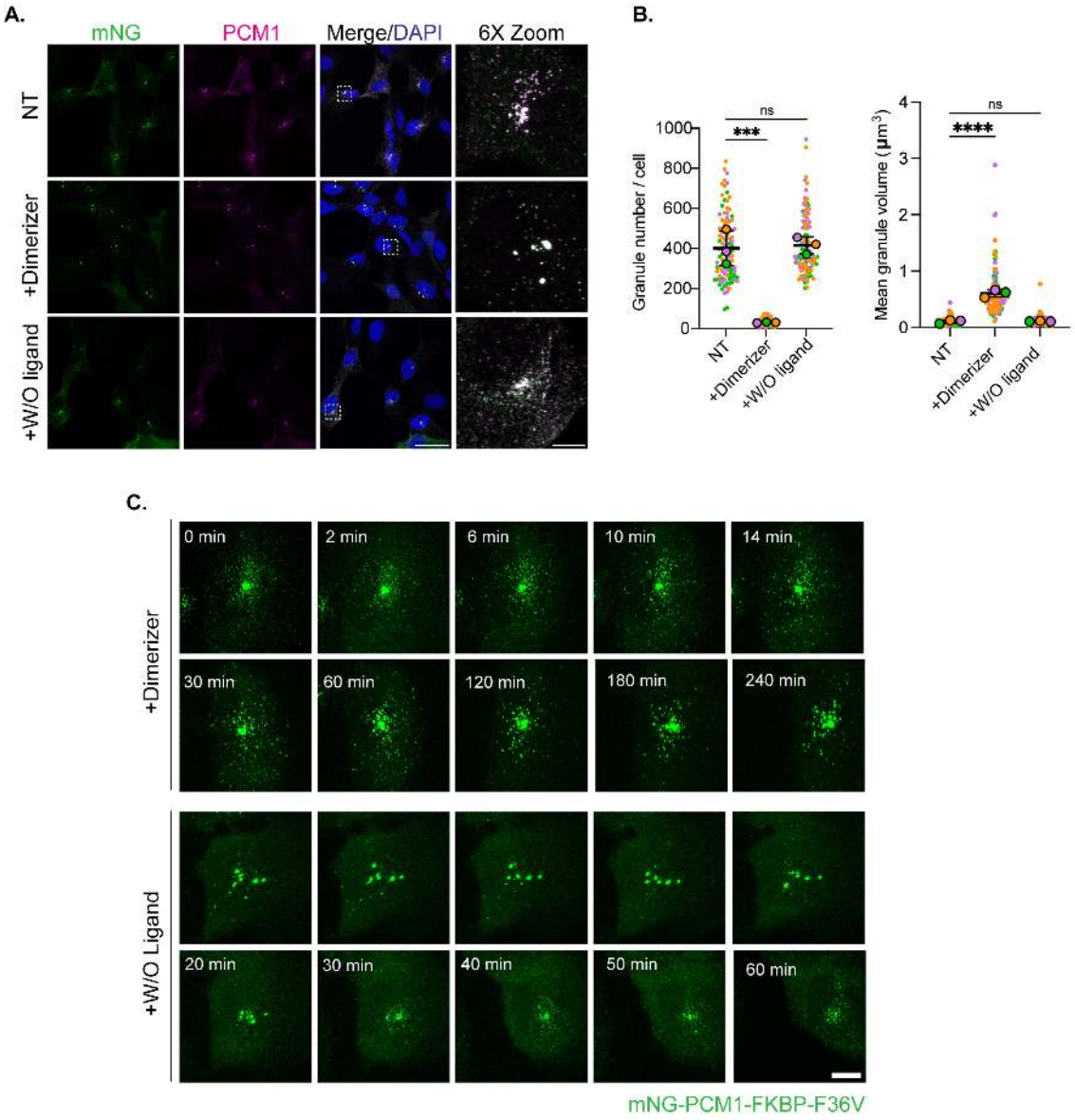

Figure 3.2 Inducible homodimerization of PCM1 changes centriolar satellite granule properties.

A. Representative images of satellite granule manipulation in No treatment (NT), +Dimerizer, and +W/O ligand conditions in RPE1 PCM1 KO cells stably expressing mNG-PCM1-FKBP(F36V). Cells were treated with dimerizer for 4 hours and with wash-out ligand for 1 hour following dimerizer treatment. After the treatments, the cells were fixed with and stained for mNG and PCM1 antibodies. Scale bar: 30 µm. The insets show enlarged satellite area. Scale bar: 5 µm. **B.** Centriolar satellite granule quantifications. Granule number (mean NT=403, BB=35, and WO=417), volume (mean NT=0.107, BB=0.603, and WO=0.114 μm^3), and mean intensity after dimerizer and wash-out ligand treatments are quantified using Imaris Image Analysis Software. The data represents three biological replicates, with n = 35 per replicate. **C.** Still images representing satellite

granule dynamicity upon dimerizer and wash-out ligand treatments in time-lapse imaging. Scale bar: 10 µm.

All together, these results show that the reversible chemically induced satellite dimerization assay effectively manipulates the PCM1 multimerization and confirms the role of regulated dimerization in controlling centriolar satellite granule number and size.

3.3.2. Manipulation of satellite homeostasis affect their mitotic behavior

Centriolar satellites disassemble in response to mitotic cues, releasing their clients into the cytoplasm. Upon mitotic exit, they re-assemble into granules and sequestering centrosomal proteins (Odabasi et al., 2020; Rai et al., 2018). Considering the importance of their dynamic behavior for mitotic fidelity as shown in Chapter 1, we decided to investigate the behavior of PCM1 granules upon dimerizer treatment.

We induced homodimerization of PCM1 granules in RPE1::PCM1 KO cells stably expressing mNG-PCM1-FKBP-F36V and probed the localization and behavior of satellites at different mitotic stages with fixed and time-lapse imaging.

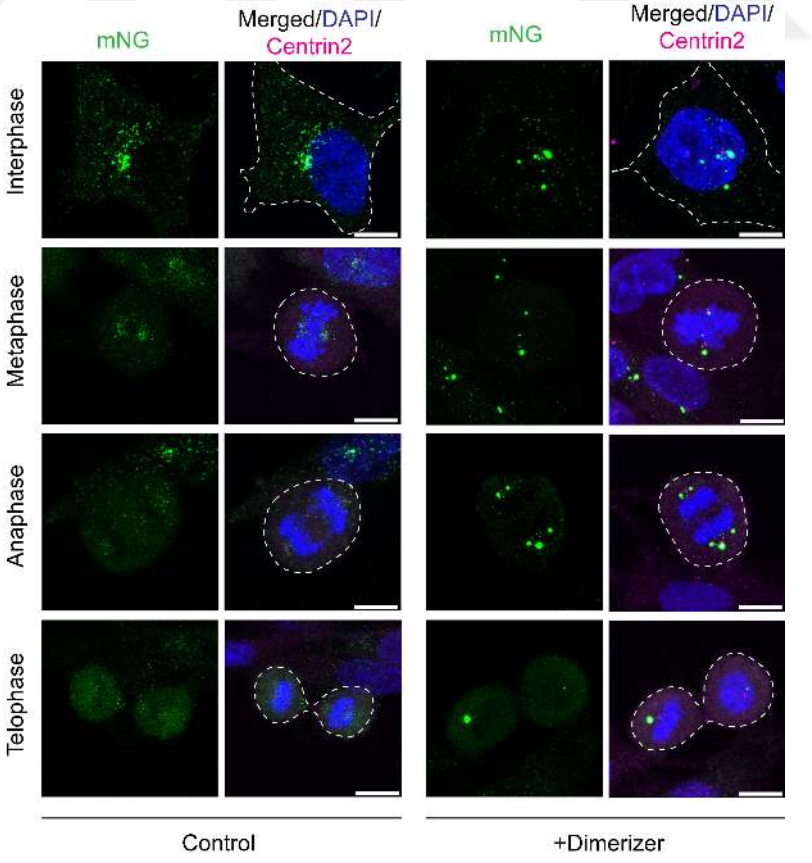

Figure 3.3 Dimerized satellite granules persist during mitosis and randomly segregate into daughter cells.

Representative images of satellite granules in control and dimerizer treated cells at interphase, metaphase, anaphase, and telophase stages. Cells were fixed and stained for DAPI, mNG, and Centrin2. Scale bar: 10 μm.

In no treatment (control) condition, majority of the satellite granules were dissolved during mitosis as expected, while a small portion of them remained intact and localizing around the spindle poles. However, in the dimerizer treated condition, all the granules remained intact, did not necessarily localize to the poles, and were randomly distributed upon cell division **(Figure 3.3)**. Similar mitotic behavior is also observed with time-lapse imaging. Homodimerized satellite granules did not dissolve, and most importantly, they were randomly localizing to the daughter cells resulting in unequal distribution of satellites in daughter cells **(Figure 3.4)**.

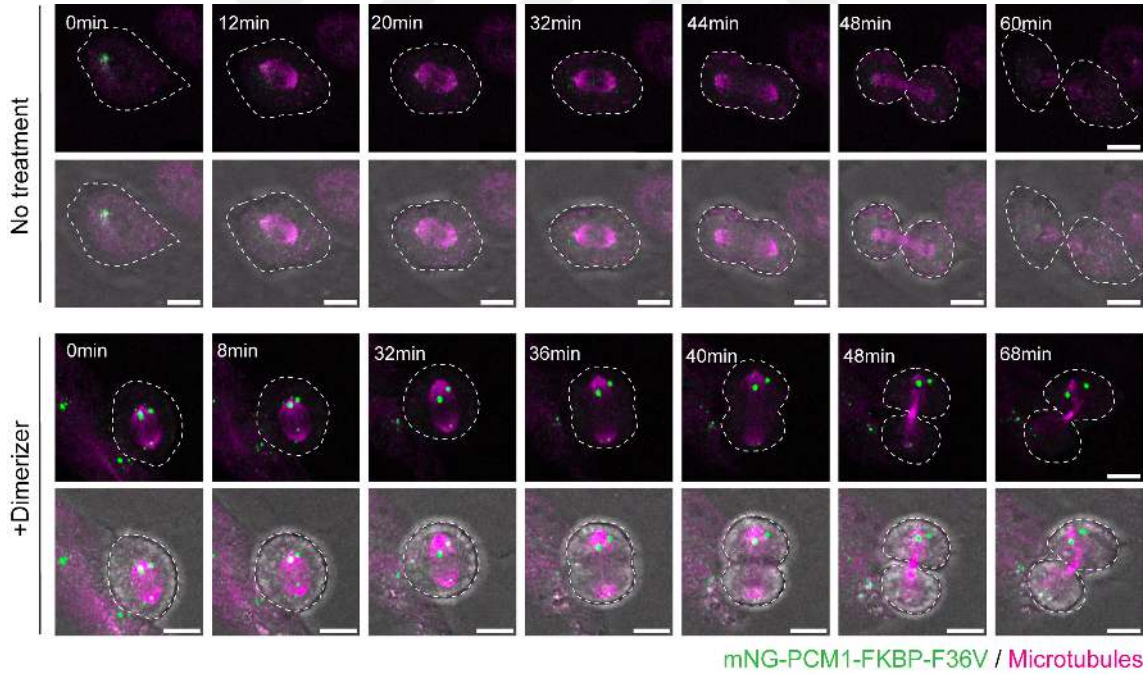

Figure 3.4 Live imaging of satellite granules in control and dimerizer treated cells during mitosis.

Still images show persistent centriolar satellite granules (green) during mitosis in dimerizer-treated cells. Both conditions were also treated with SiR-tubulin to show spindle microtubules. Cells were imaged for every 4 minutes for 18 hours. Scale bar: 10 μm.

In summary, inducible PCM1 homodimerization prevents the dynamic behavior of satellites during mitosis, resulting in persistent and randomly distributed foci among cells. This shows that PCM1 multimerization is crucial for satellite homeostasis.

3.3.3. Inducible dimerization of PCM1 disrupts ciliary signaling

As the third component of mammalian centrosome/cilium complex, centriolar satellites are important for ciliogenesis, ciliary content regulation, and ciliary signaling. However, the extent to which cells rely on satellites for these functions differs by cell type. Kidney cells (mIMCD3) exhibit decreased ciliation percentage, decreased IFT88 recruitment within cilia, and defects in sonic hedgehog pathway upon PCM1 knockout. However, PCM1 is essential for the ciliogenesis of retinal cells (RPE1) since its deletion completely abolishes cilium formation (Odabasi et al., 2019).

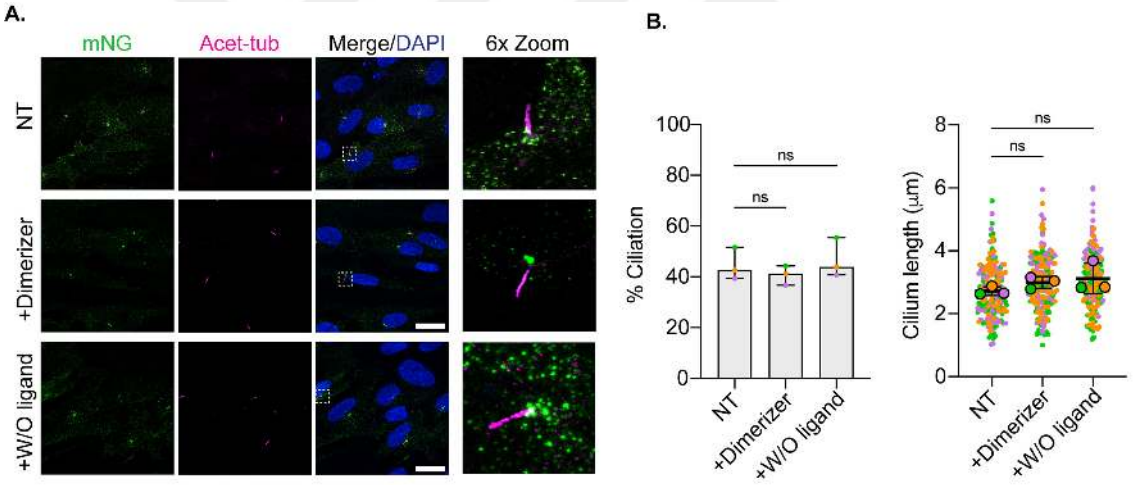

Figure 3.5 Centriolar satellite dimerization does not affect ciliogenesis and cilium length.

A. Representative images of ciliated RPE1 PCM1 KO cells stably expressing mNG-PCM1-FKBP(F36V) treated with dimerizer and subsequent wash-out ligand in serum depleted medium. Cells were fixed and stained for mNG and acetylated tubulin. Scale bar: 20 µm. Insets show enlarged satellite/cilium region. **B.** Quantification of ciliogenesis and cilium length in control, dimerizer, and wash-out ligand treated cells 24 hours post serum starvation. The data represents three biological replicates, with n = 35 per replicate.

Therefore, to correlate centriolar satellite granule properties and functions, we induced dimerization in RPE1 cells stably expressing mNG-PCM1-FKBP-F36V and assessed cilium formation and ciliary signaling. Cells were treated with the dimerizer drug, left in serum depleted medium for twenty-four hours to induce cilium assembly, then immunostained with acetylated tubulin antibody as a marker of cilia **(Figure 3.5.A)**. The ciliation frequency was similar between control, +dimerizer, and +w/o ligand conditions. Similarly, there was no significant difference in cilium lengths **(Figure 3.5.B)**.

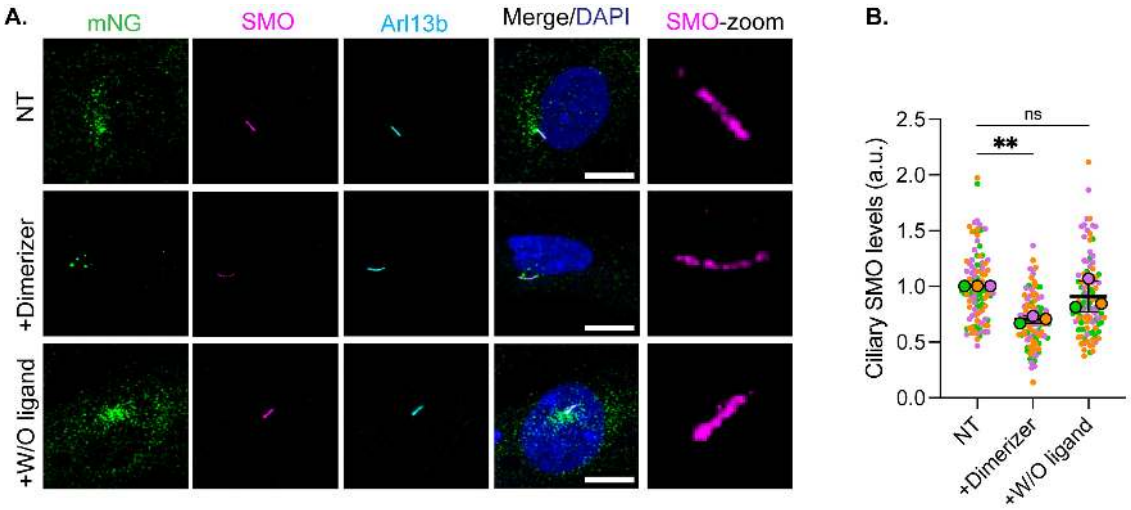

Figure 3.6 Dimerization of centriolar satellites disrupts ciliary Sonic hedgehog signaling.

A. Representative images of ciliated RPE1 PCM1 KO cells stably expressing mNG-PCM1-FKBP(F36V) treated with dimerizer and subsequent wash-out ligand in serum depleted medium. Sonic hedgehog pathway is activated by treating the cells with 50 nM of Smoothened agonist SAG for 24 hours. Cells were fixed and stained for mNG, SMO, and Arl13b. Scale bar: 10 μm **B.** Quantification of ciliary SMO levels in control, dimerizer, and wash-out ligand treated cells 48h hours post serum starvation with 24 hours of SAG treatment. The data represents three biological replicates, with n = 35 per replicate.

To test the effect of inducible dimerization of satellites on ciliary signaling, we decided to activate the Sonic Hedgehog signaling and assess the response of the cells by measuring the Smoothened levels on the ciliary membrane. Cells were treated with the dimerizer drug and left in serum depleted medium for twenty-four hours to induce cilium assembly. After serum starvation, cells were treated with Hedgehog agonist SAG for

another twenty-four hours and then immunostained for Smoothened and Arl13b as a ciliary marker **(Figure 3.6.A)**. Quantitative analysis showed that cells treated with the dimerized had impaired response to the Sonic Hedgehog pathway as shown with the decreased ciliary smoothened levels **(Figure 3.6.B)**. Notably, this perturbation could be reversed by treatment of w/o ligand which dissociates the satellite granules.

In summary, inducible dimerization of centriolar satellites does not perturb cilium assembly but significantly inhibits ciliary Sonic hedgehog signaling. These results emphasize that satellite homeostasis and dynamicity is crucial for proper ciliary signal transduction.

3.4. Discussion

By fusing PCM1 to FKBP-F36V and triggering dimerization, we could acutely cluster centriolar satellites into fewer, larger granules without altering PCM1 abundance. Wash-out of the ligand rapidly restored granule number and size to the physiological levels, demonstrating satellite plasticity. This assay supports a model in which PCM1 acts as a modular scaffold whose valency sets a biophysical threshold for phase separation of satellites, similar to other LLPS-organelles.

In most vertebrate cells, most satellite granules dissolve as cells enter mitosis. Forced PCM1 dimerization overrides this since granules remain intact, fail to localize at the poles, and are inherited asymmetrically by daughter cells. These data shows that PCM1 multimerization state affects satellite dissociation although post-translation modifications are not disrupted. Failure to disassemble likely traps client proteins away from spindle poles in which functional consequences are yet to be discovered. However, these findings are also similar to studies involving stress granules and P-bodies, where timely dissolution is required for cell cycle progression (Rai et al., 2018).

Dimerizer treatment had no effect on the frequency or length of cilia. In contrast, the same satellite perturbation reduced Sonic hedgehog pathway activation. This inconsistency could be explained by several possible mechanisms. Firstly, RPE1 cells are completely dependent on PCM1 for cilium formation (Wang et al., 2016). In this chemically induced dimerization assay, PCM1 is still present, it is just clustered into bigger granules. So, they might still contribute to the mother centriole docking and axoneme formation. Moreover, as stated earlier, cilium assembly is a one-off event, it happens once in each G0 cycle. If centriolar satellites and IFT machinery are at the right

place at the right time, cilium assembles (Mirvis et al., 2018). However, ciliary signaling demands fine-tuned trafficking (Ho & Stearns, 2021). So, dimerized satellite granules could be spatially restricted or not enough dynamic to support the frequent and fast cargo exchange needed for Sonic hedgehog signaling. Also, the dimerized granules may sequester intraflagellar transport adaptors such as IFT88 or membrane remodeling factors needed for Smoothened import, hence impairing the ciliary signaling.

3.5. Conclusion

In conclusion, our findings demonstrate that the reversible, chemically induced satellite dimerization assay effectively manipulates PCM1 multimerization and confirms the role of regulated dimerization in controlling the number and size of centriolar satellite granules. We show that inducible PCM1 homodimerization disrupts the dynamic behavior of satellites during mitosis, leading to persistent, randomly distributed foci across cells, underscoring the importance of PCM1 multimerization for satellite homeostasis. Furthermore, while inducible dimerization of satellites does not impair cilium assembly, it significantly inhibits ciliary Sonic Hedgehog signaling. Together, these results highlight the critical role of centriolar satellite homeostasis and dynamicity in maintaining both mitotic regulation and proper ciliary signal transduction.

Chapter 4

4. CENTRIOLAR SATELLITE ORGANIZATION IN PATIENT-DERIVED FIBROBLAST CELLS

4.1. Introduction

4.1.1. Ciliopathies

Ciliopathies are a group of inherited disorders caused by genetic mutations that disrupt the formation or normal function of cilia (Mill et al., 2023). Nearly all vertebrate cells possess a primary cilium, so ciliary dysfunction can affect multiple organ systems such as the retina, kidneys, and brain which leads to a variety of clinical features. Such pleiotropic involvement underlies why ciliopathies often present with clinical variability, with patients exhibiting combinations of retinal degeneration, renal disease, cerebral anomalies, liver fibrosis, obesity, diabetes, or skeletal dysplasia. The genetic basis of ciliopathies is also highly heterogeneous since over 180 disease-causing genes have been identified until now (Waters & Beales, 2011).

4.1.2. Types of Ciliopathy Diseases

Leber's Congenital Amaurosis (LCA) is a severe congenital retinal dystrophy. It is caused by the mutations in ciliary proteins, such as CEP290. CEP290 encodes a transition zone protein of photoreceptor cilia, and different CEP290 mutations can also manifest as other ciliopathies. Nephronophthisis (NPHP) is an autosomal recessive cystic kidney disease characterized by chronic tubulointerstitial nephropathy. NPHP is caused by mutations in any of at least a dozen NPHP genes like NPHP1, NPHP4, NPHP5, and NPHP6/CEP290 encoding nephrocystin proteins that localize to primary cilia or centrosomes. Certain NPHP gene mutations also cause Senior–Løken syndrome, a variant of NPHP combined with retinal degeneration.

Bardet–Biedl Syndrome (BBS) is a multisystem ciliopathy marked by retinitis pigmentosa, obesity, polydactyly, renal anomalies, and hypogonadism. BBS is genetically heterogeneous, with at least 24 known genes (e.g. BBS1, BBS10, BBS4, MKKS/BBS6, ARL6, TRIM32) encoding components of the basal body or BBSome complex. Joubert

Syndrome (JBS) is a ciliopathy defined by a distinctive midbrain–hindbrain malformation, leading to hypotonia, ataxia, developmental delay, and often retinal and renal involvement. Mutations in over 30 ciliary genes can cause Joubert syndrome. JBS exhibits extreme genetic heterogeneity: Many Joubert-associated genes are shared with other ciliopathies, reflecting overlapping molecular pathways. Meckel–Gruber Syndrome (MKS) is one of the most severe ciliopathies, presenting prenatally with lethal features which is caused by mutations in several cilia-related genes (Reiter & Leroux, 2017).

4.1.3. Phenotypic and genotypic overlaps in ciliopathy patients

There is significant phenotypic overlap between different ciliopathies, as many share core clinical features. For instance, progressive retinal degeneration is seen not only in retinal diseases like LCA or retinitis pigmentosa, but also in syndromic disorders such as BBS, Joubert, Senior–Løken and some forms of NPHP (Bujakowska et al., 2017). Likewise, renal cystic disease is a common thread in NPHP, MKS, Joubert, and BBS, and liver fibrosis may appear in Joubert, BBS, and MKS. Skeletal abnormalities occur in BBS, Joubert, and MKS. These overlapping symptoms reflect the fact that many different ciliary proteins are involved in shared developmental pathways (Handa et al., 2020).

Besides the clinical overlap, there is also genotypic overlap because the same gene can be mutated in multiple distinct ciliopathy syndromes. CEP290 is an important example, with alleles of this single gene implicated in LCA as well as in Joubert, Senior–Løken and MKS. Similarly, TMEM67 mutations can cause either Joubert or Meckel–Gruber syndrome. Inversely, mutations in different genes can produce nearly identical phenotypes. In some cases, patients carry mutations in two ciliopathy genes and a blended phenotype, where individuals with simultaneous mutations in a Joubert-related gene and a BBS gene have manifested combined features not seen in either syndrome alone (Davis & Katsanis, 2012). This genetic complexity makes it difficult to predict clinical outcomes purely from genotype. As a result, the clinical boundaries between certain ciliopathy diagnoses can blur, with substantial patient-to-patient variability.

4.1.4. Impact and Diagnostic Challenges

Although each ciliopathy is individually rare, together they impose a significant health burden. Many ciliopathies present early in life with severe consequences like childhood blindness or childhood renal failure requiring transplantation. The most severe forms are perinatal lethal (Hyland & Brody, 2021), whereas others lead to lifelong

disability and require multidisciplinary care. These disorders thus have high medical and social impact despite their rarity.

Clinically, diagnosis is challenging because patients often have multisystem symptoms that evolve over time and there is extensive overlap between syndromes. As a result, many patients remain without a clear molecular diagnosis, complicating counseling and management (Modarage et al., 2022). That is why cellular assays have stimulated interest as diagnostic tools. By assessing the functional state of a patient's cilia in cultured cells, these assays can provide pathogenic evidence beyond DNA sequencing. Recent efforts have standardized such high-content imaging assays to improve reproducibility, measuring parameters like the percentage of ciliated cells and cilium length in an automated fashion (Doornbos et al., 2021), which could be also applied for evaluating centriolar satellite granule properties. These functional readouts can validate whether a variant of uncertain significance truly disrupts cilia, thus helping confirm diagnoses when genetic results are ambiguous.

4.2. Materials § Methods

4.2.1. Cell culture

Human control cell and the patient cells were cultured in DMEM supplemented with 20% FBS and 1% Pen-Strep in T25 flasks. All cell lines were maintained in a humidified incubator at 37C with 5% CO_2.

4.2.2. Nocodazole treatment

Control cells were seeded on coverslips in 24 well plates. When the cells reached enough confluency, they were treated with 5 ug/mL of nocodazole for 1 hour at 37C to depolymerize the microtubules. After treatment, cells were washed with cold PBS three times gently and fixed with ice-cold methanol.

4.2.3. Cilium assembly experiment

Control and patient cells were seeded on coverslips in 12 well plates. When the cells reached 80-90% confluency, their medium were replaced serum depleted medium to induce ciliogenesis. After 24 hours of treatment, cells were fixed with ice-cold methanol for 10 minutes at room temperature while shaking.

4.2.4. Immunofluorescence and Microscopy

Cells were grown on glass coverslips for the immunofluorescence experiments. Coverslips were washed with PBS and the cells were fixed with ice-cold methanol at −20C for 10 mins. After washing the coverslips twice with PBS, cells were blocked with 3% BSA in PBS containing 0.1% Triton X-100 for permeabilization. For the immunostaining, cells were incubated with primary antibodies in blocking solution for 1 h at room temperature and then with secondary antibody solution containing DAPI. After washing out the excess antibodies with PBS, cells were mounted using Mowiol mounting medium. Full list of primary and secondary antibodies used for immunofluorescence experiments in this chapter are listed table in Appendix.

Confocal microscopy was performed with Leica TCS SP8 or Stellaris 8 laser scanning inverted confocal microscope system equipped for four-color imaging with 405, 488, 561, and 633 nm laser lines, four detection channels (1 photomultiplier tube and 3 Hybrid Detectors), HC PL APO CS2 63X 1.4 NA oil objective and an incubation chamber. Pinhole diameter was set to 1 μm. Images were acquired with 0.2–0.5 μm z-spacing, line averaging set to 2–323 and 400/600 Hz unidirectional xyz scan mode. An image format of 1,024x1,024 pixels and an additional 1–4x optical zoom was used for sample acquisition. The system was controlled with the Leica Application Suite X Software (Leica).

4.2.5. Image Analysis and Quantification

Image analysis (signal identification, segmentation, filtering, relating, masking, and measuring) of all microscopy data was done with CellProfiler pipeline **(Appendix Figure 4)**. Thresholding parameters were adjusted manually according to the image output. Cell number, cell area, granule number, granule intensity and voronoi tiling information was obtained from the CellProfiler pipeline.

Results were obtained in excel format and further analyzed with a Python code to merge all measured granule properties and to calculating the Wiener entropy value. Results were obtained in excel format and plotted in Graphpad Prism.

Statistical analysis

Prism 10 software (GraphPad Software, La Jolla, CA) is used to calculate p-values and determine statistical significance. To compare two groups that exhibit Gaussian distribution, parametric unpaired two-tailed Student’s t-test was used. When the sample

does not have Gaussian distribution, nonparametric Mann-Whitney test is applied. To compare more than two groups, un-paired ordinary one-way ANOVA test is used. Error bars in the graphs indicate the standard deviation (SD), and statistical significance levels were denoted as follows: ns: P>0.05, *:P<0.05, **:P<0.01, ***:P<0.001 and ****:P<0.0001.

4.3. Results

4.3.1. Development and validation of centriolar satellites quantification pipeline

We developed an image-analysis pipeline in CellProfiler to quantify centriolar satellite properties and link satellite homeostasis and function. Because centriolar satellites are nanometer scale, liquid-like granules that undergo fusion and fission, and concentrated around pericentrosomal region; accurate segmentation and size measurements can be challenging. To optimize our image analysis pipeline and identify reliable measurable features, we designed an experiment contrasting two phenotypes: one is the endogenous satellite distribution, and the other is aberrant, dispersed distribution induced by nocodazole treatment. Since localization of granules depend on microtubule presence, we depolymerized microtubules with nocodazole to scatter satellite granules inside the cell and confirmed this phenotype by immunostaining for PCM1 and α-tubulin **(Figure 4.1.A)**.

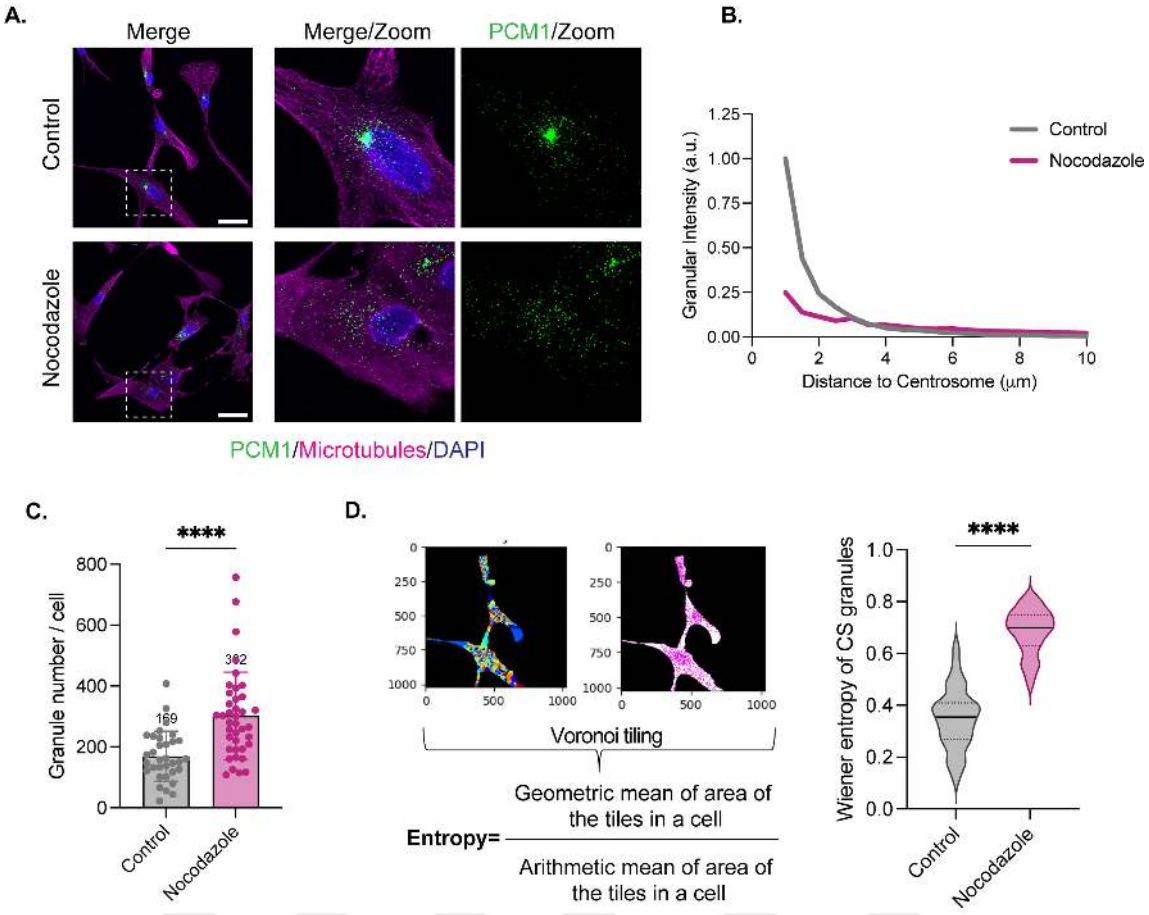

Figure 4.1 Centriolar satellite quantification pipeline confirms scattering of granules upon nocodazole treatment.

A. Control fibroblast cells are either treated with vehicle control or nocodazole to disrupt microtubule network. Cells were fixed and immunostained for PCM1 (centriolar satellites) and α-tubulin (microtubules). **B.** Microscopy images were analyzed by CellProfiler using the "satellite quantification pipeline" and Python is used for further calculations. Granular intensity vs distance to centrosome graph was plotted by measuring the fluorescence intensity of PCM1 in each centrosome-centered co-centric ring. Intensity of control PCM1 in the first co-centric ring is normalized to 1. **C.** Granule number in each cell is measured in CellProfiler using the "satellite quantification pipeline". Each dot represents the granule number in one cell. n=33. **D.** Voronoi tiling detection was performed in CellProfiler using the "satellite quantification pipeline" and the entropy calculations were performed in Python. Entropy value is between 0-1 while lower values represent order and higher value represent disorder. n=33. *:p<0.05, **:p<0.01, ***:p<0.001****:p<0.0001, ns: not significant.

Using the "satellite quantification pipeline", we optimized object detection parameters to extract four key parameters: fluorescence intensity, granule number, distance from centrosome, and Voronoi-tile area. We then exported these data for downstream analysis in Python script. Whole image analysis pipeline is schematized in **Appendix Figure 4**. Plotting granule intensity versus distance to centrosome revealed a clear pericentrosomal clustering gradient, with lower intensities at greater distances **(Figure 4.1.B)**. Consistent with satellite dispersion upon microtubule loss, nocodazole treatment produced a two-fold increase in granule number per cell **(Figure 4.1.C)**, validating our image analysis workflow.

Lastly, we quantified the spatial distribution of centriolar satellites by calculating their entropy, a metric of order/disorder patterns. Since satellite localization is tightly regulated upon cellular cues, changes in distribution could reflect functional states. To calculate the entropy, we first generated Voronoi tiling of the cell area, partitioning cytoplasm according to each satellite granule. From the resulting tile areas, we calculated the entropy as the ratio of the geometric mean to the arithmetic mean of all tile areas. This ratio was between 0 and 1, while being close to 0 considered as an organized distribution and being close to 1 is considered as disorganization. Consistent with scattered granule localization, nocodazole treated cells exhibited significantly higher entropy values, reflecting increased spatial disorganization **(Figure 4.1.D)**.

4.3.2. Ciliopathy mutations do not disrupt centriolar satellite organization in patient-derived cells

After validating the "satellite quantification pipeline", we analyzed patient-derived cell lines having mutations in various ciliopathy genes. Cells were immunostained for PCM1 (satellites), Arl13b (cilia), and Centrin 2 (centrioles/centrosome) antibodies. In all patient cell lines, satellites displayed similar intensity and endogenous-like localization by clustering around centrosome with a minor cytoplasmic pool **(Figure 4.2)**.

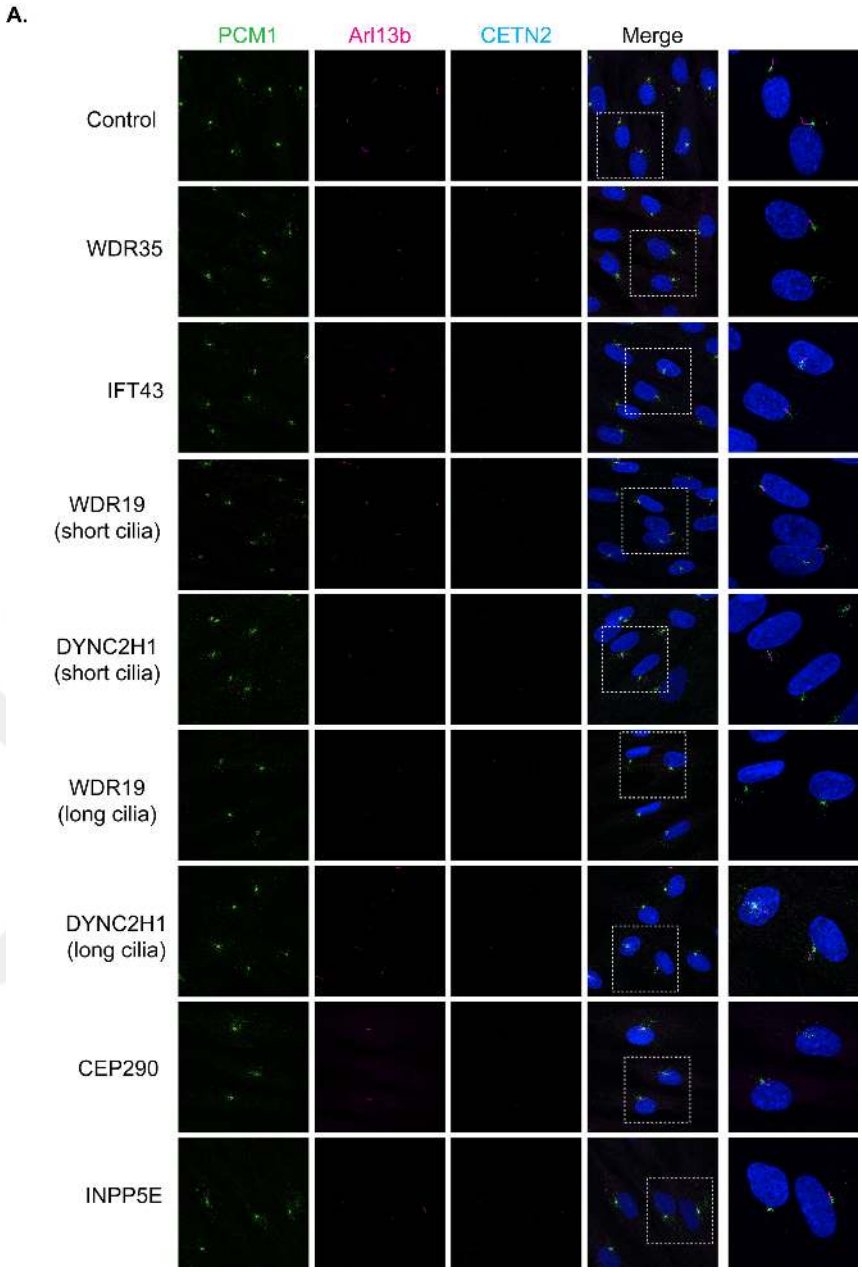

Figure 4.2 Centriolar satellite localization in ciliopathy patient-derived fibroblast cells.

Cells were serum starved, fixed, and immunostained for PCM1 (centriolar satellites), ARL13b (cilia), and CETN2 (centrosome). The mutated genes in each patient cell are indicated on the left.

We normalized the granule intensity of patient cells to control cell line and plotted the intensity values over distance to centrosome. The patient cells displayed decreased granular intensity around pericentrosomal region except CEP290 mutated cell line which

had higher intensity. However, none of these differences were statistically significant **(Figure 4.3.A)**.

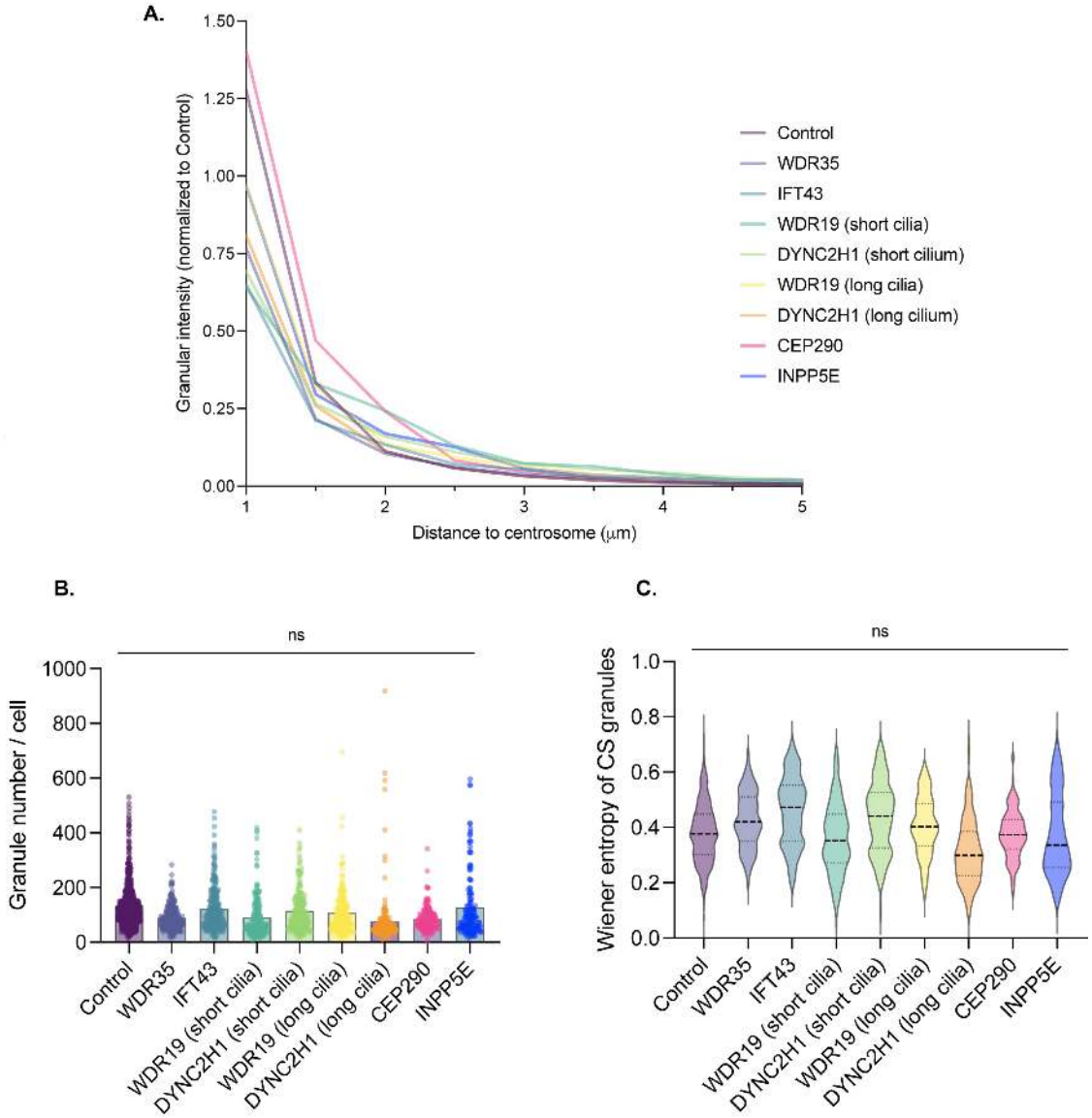

Figure 4.3 Quantification of centriolar satellites in ciliopathy patient cells.

A. Microscopy images were analyzed by CellProfiler using the "satellite quantification pipeline" and Python is used for further calculations. Granular intensity vs distance to centrosome graph was plotted by measuring the fluorescence intensity of PCM1 in each centrosome-centered co-centric ring. Intensity of PCM1 granules in patient cells is normalized to the average intensity in control. The data represents three biological replicates, n > 34. **B.** Granule number in each cell is measured in CellProfiler using the "satellite quantification pipeline". Each dot represents the granule number in one cell. The data represents three biological replicates, n > 34 per replicate. **C.** Voronoi tiling

detection was performed in CellProfiler using the "satellite quantification pipeline" and the entropy calculations were performed in Python. Entropy value is between 0-1 while lower values represent order and higher value represent disorder. The data represents three biological replicates, n > 34 per replicate. *:p<0.05, **:p<0.01, ***:p<0.001****:p<0.0001, ns: not significant.

We next plotted granule number per cell for each patient cell and found no significant differences between patient and control cell lines (**Figure 4.3.B**). Finally, Voronoi-based entropy analysis revealed similar entropy values across all cell lines, indicating conserved spatial distribution of satellites **(Figure 4.3.C)**, as previously confirmed by immunofluorescence.

4.4. Discussion

By comparing endogenous satellite organization with the nocodazole-induced dispersion phenotype, we demonstrated that the CellProfiler pipeline robustly identifies four biologically meaningful parameters: fluorescence intensity, granule number, distance to centrosome, and Voronoi-tile entropy.

An automated cellular image analysis pipeline yields consistent, quantitative measurements for every cell in each image, minimizing observer bias and revealing subtle phenotypic changes that manual inspection might miss. This high-throughput approach enhances diagnostic precision and enables unbiased comparisons of patient cell phenotypes.

Our results showed that patient fibroblasts with various ciliopathy mutations (WDR35, IFT43, WDR19, DYNC2H1, CEP290, INPP5E) had similar centriolar satellite intensity, number, and pericentrosomal clustering to control. This aligns with reports that WDR35 (IFT121) loss does not disrupt satellite organization (Quidwai et al., 2021). Likewise, acute depletion of IFT-A complex components such as IFT43 and IFT144 reduces pericentrosomal satellite protein levels at minimal levels (Fu et al., 2016). Although CEP290 knockdown disperses PCM1 satellites (Kim et al., 2008), our CEP290-mutant cells did not show significant satellite disorganization, suggesting partial retention of CEP290 function or compensation. Similarly, disrupting the ciliary motor DYNC2H1 or the ciliary enzyme INPP5E, which are not core satellite components, did not markedly affect satellite distribution.

To increase the sensitivity of this pipeline, super-resolution microscopy could be employed. Conventional fluorescence microscopy is diffraction-limited (~200 nm), whereas techniques like 3D-SIM or STED achieve higher resolution. Super-resolution imaging can reveal nanoscale changes in satellite granule size or positioning that standard imaging might not resolve (Schermelleh et al., 2019). Incorporating such methods would likely improve detection of subtle differences in satellite organization.

Finally, connecting our satellite results with ciliary parameters such as ciliogenesis percentage, cilium length, and ciliary function could further improve interpretation. Centriolar satellites are required for efficient ciliogenesis and proper trafficking of ciliary proteins (Odabasi et al., 2019). Correlating satellite properties with each cell's ciliation status, cilium length, or ciliary signaling readouts may uncover relationships hidden in bulk analysis. For example, cells with IFT-A mutations have severely reduced ciliogenesis (Fu et al., 2016) but still normal satellites; analyzing whether non-ciliated cells accumulate satellites differently could reveal subtle effects. Such integrated analyses would link satellite homeostasis to ciliary structure and function in these patient cells.

4.5. Conclusion

In summary, our optimized image-analysis pipeline successfully quantified centriolar satellite properties measured by granule intensity, number, and spatial entropy, providing an in vitro phenotypic quantification tool for ciliopathy patients. Despite subtle, non-significant variations in pericentrosomal intensity, all mutant lines exhibited satellite distributions indistinguishable from controls, indicating that these mutations do not evidently impair satellite homeostasis.

BIBLIOGRAPHY

Abdel-Magid, A. F. (2019). Rapalogs Potential as Practical Alternatives to Rapamycin. *ACS Med Chem Lett*, *10*(6), 843–845.

Armengot, M., Milara, J., Mata, M., Carda, C., & Cortijo, J. (2010). Cilia motility and structure in primary and secondary ciliary dyskinesia. *American journal of rhinology & allergy*, *24*(3), 175–180.

Arslanhan, M. D., Cengiz-Emek, S., Odabasi, E., Steib, E., Hamel, V., Guichard, P., & Firat-Karalar, E. N. (2023). CCDC15 localizes to the centriole inner scaffold and controls centriole length and integrity. *Journal of Cell Biology*, *222*(12).

Arslanhan, M. D., Gulensoy, D., & Firat-Karalar, E. N. (2020). A proximity mapping journey into the biology of the mammalian centrosome/cilium complex. *Cells*, *9*(6), 1390.

Aydin, Ö. Z., Taflan, S. O., Gurkaslar, C., & Firat-Karalar, E. N. (2020). Acute inhibition of centriolar satellite function and positioning reveals their functions at the primary cilium. *PLoS biology*, *18*(6), e3000679.

Badano, J. L., Teslovich, T. M., & Katsanis, N. (2005). The centrosome in human genetic disease. *Nature Reviews Genetics*, *6*(3), 194–205.

Begar, E., Seyrek, E., & Firat-Karalar, E. N. (2025). Navigating centriolar satellites: the role of PCM1 in cellular and organismal processes. *The FEBS Journal*, *292*(4), 688–708.

Berbari, N. F., O'Connor, A. K., Haycraft, C. J., & Yoder, B. K. (2009). The primary cilium as a complex signaling center. *Current biology*, *19*(13), R526–R535.

Bessis, M., & Breton-Gorius, J. (1958). On an pericentral inframicroscopic structure; electron microscopy of mammalian leukocytes. *Comptes rendus hebdomadaires des seances de l'Academie des sciences*, *246*(8), 1289–1291.

Bettencourt-Dias, M., & Glover, D. M. (2007). Centrosome biogenesis and function: centrosomics brings new understanding. *Nature reviews Molecular cell biology*, *8*(6), 451–463.

Bujakowska, K. M., Liu, Q., & Pierce, E. A. (2017). Photoreceptor Cilia and Retinal Ciliopathies. *Cold Spring Harb Perspect Biol*, *9*(10).

Clackson, T., Yang, W., Rozamus, L. W., Hatada, M., Amara, J. F., Rollins, C. T., Stevenson, L. F., Magari, S. R., Wood, S. A., Courage, N. L., Lu, X., Cerasoli, F., Jr., Gilman, M., & Holt, D. A. (1998). Redesigning an FKBP-ligand interface to generate chemical dimerizers with novel specificity. *Proc Natl Acad Sci U S A*, *95*(18), 10437–10442.

Comartin, D., & Pelletier, L. (2016). Organizational properties of the pericentriolar material. *The Microtubule Cytoskeleton: Organisation, Function and Role in Disease*, 43–77.

Conduit, P. T., Wainman, A., & Raff, J. W. (2015). Centrosome function and assembly in animal cells. *Nature reviews Molecular cell biology*, *16*(10), 611–624.

Conkar, D., Bayraktar, H., & Firat-Karalar, E. N. (2019). Centrosomal and ciliary targeting of CCDC66 requires cooperative action of centriolar satellites, microtubules and molecular motors. *Scientific reports*, *9*(1), 14250.

Dammermann, A., & Merdes, A. (2002). Assembly of centrosomal proteins and microtubule organization depends on PCM-1. *The Journal of cell biology*, *159*(2), 255–266.

Davis, E. E., & Katsanis, N. (2012). The ciliopathies: a transitional model into systems

biology of human genetic disease. *Curr Opin Genet Dev*, *22*(3), 290–303.

Deretic, J., Odabasi, E., & Firat-Karalar, E. N. (2023). The multifaceted roles of microtubule-associated proteins in the primary cilium and ciliopathies. *Journal of Cell Science*, *136*(23), jcs261148.

Doornbos, C., van Beek, R., Bongers, E., Lugtenberg, D., Klaren, P. H. M., Vissers, L., Roepman, R., & Oud, M. M. (2021). Cell-based assay for ciliopathy patients to improve accurate diagnosis using ALPACA. *Eur J Hum Genet*, *29*(11), 1677–1689.

Firat-Karalar, E. N., Rauniyar, N., Yates, J. R., & Stearns, T. (2014). Proximity interactions among centrosome components identify regulators of centriole duplication. *Current biology*, *24*(6), 664–670.

Fırat-Karalar, E. N., & Stearns, T. (2014). The centriole duplication cycle. *Philosophical Transactions of the Royal Society B: Biological Sciences*, *369*(1650), 20130460.

Firat-Karalar, E. N., & Stearns, T. (2015). Probing mammalian centrosome structure using BioID proximity-dependent biotinylation. In *Methods in cell biology* (Vol. 129, pp. 153–170). Elsevier

Fu, W., Wang, L., Kim, S., Li, J., & Dynlacht, B. D. (2016). Role for the IFT-A Complex in Selective Transport to the Primary Cilium. *Cell Rep*, *17*(6), 1505–1517.

Garcia-Gonzalo, F. R., Phua, S. C., Roberson, E. C., Garcia, G., Abedin, M., Schurmans, S., Inoue, T., & Reiter, J. F. (2015). Phosphoinositides regulate ciliary protein trafficking to modulate hedgehog signaling. *Developmental cell*, *34*(4), 400–409.

Garcia-Gonzalo, F. R., & Reiter, J. F. (2017). Open sesame: how transition fibers and the transition zone control ciliary composition. *Cold Spring Harbor perspectives in biology*, *9*(2), a028134.

Gheiratmand, L., Coyaud, E., Gupta, G. D., Laurent, E. M., Hasegan, M., Prosser, S. L., Gonçalves, J., Raught, B., & Pelletier, L. (2019). Spatial and proteomic profiling reveals centrosome-independent features of centriolar satellites. *The EMBO journal*, *38*(14), e101109.

Ghossoub, R., Molla-Herman, A., Bastin, P., & Benmerah, A. (2011). The ciliary pocket: a once-forgotten membrane domain at the base of cilia. *Biology of the Cell*, *103*(3), 131–144.

Gilula, N. B., & Satir, P. (1972). The ciliary necklace: a ciliary membrane specialization. *The Journal of cell biology*, *53*(2), 494–509.

Goetz, S. C., & Anderson, K. V. (2010). The primary cilium: a signalling centre during vertebrate development. *Nature Reviews Genetics*, *11*(5), 331–344.

Hagiwara, H., Ohwada, N., & Takata, K. (2004). Cell Biology of Normal and Abnormal. *International Review of Cytology: A Survey of Cell Biology*, *234*, 101.

Hall, E. A., Kumar, D., Prosser, S. L., Yeyati, P. L., Herranz-Pérez, V., García-Verdugo, J. M., Rose, L., McKie, L., Dodd, D. O., & Tennant, P. A. (2023). Centriolar satellites expedite mother centriole remodeling to promote ciliogenesis. *Elife*, *12*, e79299.

Handa, A., Voss, U., Hammarsjo, A., Grigelioniene, G., & Nishimura, G. (2020). Skeletal ciliopathies: a pattern recognition approach. *Jpn J Radiol*, *38*(3), 193–206.

Hirose, T., Ninomiya, K., Nakagawa, S., & Yamazaki, T. (2023). A guide to membraneless organelles and their various roles in gene regulation. *Nat Rev Mol Cell Biol*, *24*(4), 288–304.

Ho, E. K., & Stearns, T. (2021). Hedgehog signaling and the primary cilium: implications for spatial and temporal constraints on signaling. *Development*, *148*(9).

Hong, S.-R., Wang, C.-L., Huang, Y.-S., Chang, Y.-C., Chang, Y.-C., Pusapati, G. V., Lin, C.-Y., Hsu, N., Cheng, H.-C., & Chiang, Y.-C. (2018). Spatiotemporal

manipulation of ciliary glutamylation reveals its roles in intraciliary trafficking and Hedgehog signaling. *Nature communications*, *9*(1), 1732.

Hyland, R. M., & Brody, S. L. (2021). Impact of Motile Ciliopathies on Human Development and Clinical Consequences in the Newborn. *Cells*, *11*(1).

Jin, H., White, S. R., Shida, T., Schulz, S., Aguiar, M., Gygi, S. P., Bazan, J. F., & Nachury, M. V. (2010). The conserved Bardet-Biedl syndrome proteins assemble a coat that traffics membrane proteins to cilia. *Cell*, *141*(7), 1208–1219.

Joachim, J., Razi, M., Judith, D., Wirth, M., Calamita, E., Encheva, V., Dynlacht, B. D., Snijders, A. P., O'Reilly, N., & Jefferies, H. B. (2017). Centriolar satellites control GABARAP ubiquitination and GABARAP-mediated autophagy. *Current biology*, *27*(14), 2123–2136. e2127.

Kim, J., Krishnaswami, S. R., & Gleeson, J. G. (2008). CEP290 interacts with the centriolar satellite component PCM-1 and is required for Rab8 localization to the primary cilium. *Hum Mol Genet*, *17*(23), 3796–3805.

Kolos, J. M., Voll, A. M., Bauder, M., & Hausch, F. (2018). FKBP ligands—where we are and where to go? *Frontiers in pharmacology*, *9*, 1425.

Kubo, A., Sasaki, H., Yuba-Kubo, A., Tsukita, S., & Shiina, N. (1999). Centriolar satellites: molecular characterization, ATP-dependent movement toward centrioles and possible involvement in ciliogenesis. *The Journal of cell biology*, *147*(5), 969–980.

Kubo, A., & Tsukita, S. (2003). Non-membranous granular organelle consisting of PCM-1: subcellular distribution and cell-cycle-dependent assembly/disassembly. *Journal of Cell Science*, *116*(5), 919–928.

Kumar, D., & Reiter, J. (2021). How the centriole builds its cilium: of mothers, daughters, and the acquisition of appendages. *Current opinion in structural biology*, *66*, 41–48.

Lehman, J. M., Michaud, E. J., Schoeb, T. R., Aydin-Son, Y., Miller, M., & Yoder, B. K. (2008). The Oak Ridge Polycystic Kidney mouse: modeling ciliopathies of mice and men. *Developmental dynamics: an official publication of the American Association of Anatomists*, *237*(8), 1960–1971.

Liew, G. M., Ye, F., Nager, A. R., Murphy, J. P., Lee, J. S., Aguiar, M., Breslow, D. K., Gygi, S. P., & Nachury, M. V. (2014). The intraflagellar transport protein IFT27 promotes BBSome exit from cilia through the GTPase ARL6/BBS3. *Developmental cell*, *31*(3), 265–278.

Lin, Y.-C., Niewiadomski, P., Lin, B., Nakamura, H., Phua, S. C., Jiao, J., Levchenko, A., Inoue, T., Rohatgi, R., & Inoue, T. (2013). Chemically inducible diffusion trap at cilia reveals molecular sieve–like barrier. *Nature chemical biology*, *9*(7), 437–443.

Mabe, S., Nagamune, T., & Kawahara, M. (2014). Detecting protein-protein interactions based on kinase-mediated growth induction of mammalian cells. *Sci Rep*, *4*, 6127.

Mair, R., Gesteland, R., & Blank, D. (1982). Changes in morphology and physiology of olfactory receptor cilia during development. *Neuroscience*, *7*(12), 3091–3103.

Mill, P., Christensen, S. T., & Pedersen, L. B. (2023). Primary cilia as dynamic and diverse signalling hubs in development and disease. *Nat Rev Genet*, *24*(7), 421–441.

Mirvis, M., Stearns, T., & James Nelson, W. (2018). Cilium structure, assembly, and disassembly regulated by the cytoskeleton. *Biochem J*, *475*(14), 2329–2353.

Mitchison, H. M., & Valente, E. M. (2017). Motile and non-motile cilia in human pathology: from function to phenotypes. *The Journal of pathology*, *241*(2), 294–309.

Modarage, K., Malik, S. A., & Goggolidou, P. (2022). Molecular Diagnostics of Ciliopathies and Insights Into Novel Developments in Diagnosing Rare Diseases. *Br J Biomed Sci*, *79*, 10221.

Nijenhuis, W., van Grinsven, M. M., & Kapitein, L. C. (2020). An optimized toolbox for the optogenetic control of intracellular transport. *Journal of Cell Biology*, *219*(4), e201907149.

Nonaka, S., Tanaka, Y., Okada, Y., Takeda, S., Harada, A., Kanai, Y., Kido, M., & Hirokawa, N. (1998). Randomization of left–right asymmetry due to loss of nodal cilia generating leftward flow of extraembryonic fluid in mice lacking KIF3B motor protein. *Cell*, *95*(6), 829–837.

Odabasi, E., Batman, U., & Firat-Karalar, E. N. (2020). Unraveling the mysteries of centriolar satellites: time to rewrite the textbooks about the centrosome/cilium complex. *Molecular Biology of the Cell*, *31*(9), 866–872.

Odabasi, E., Gul, S., Kavakli, I. H., & Firat-Karalar, E. N. (2019). Centriolar satellites are required for efficient ciliogenesis and ciliary content regulation. *EMBO reports*, *20*(6), e47723.

Odle, R. I., Walker, S. A., Oxley, D., Kidger, A. M., Balmanno, K., Gilley, R., Okkenhaug, H., Florey, O., Ktistakis, N. T., & Cook, S. J. (2020). An mTORC1-to-CDK1 Switch Maintains Autophagy Suppression during Mitosis. *Mol Cell*, *77*(2), 228–240 e227.

Passmore, J. B., Nijenhuis, W., & Kapitein, L. C. (2021). From observing to controlling: Inducible control of organelle dynamics and interactions. *Current Opinion in Cell Biology*, *71*, 69–76.

Pazour, G. J., Baker, S. A., Deane, J. A., Cole, D. G., Dickert, B. L., Rosenbaum, J. L., Witman, G. B., & Besharse, J. C. (2002). The intraflagellar transport protein, IFT88, is essential for vertebrate photoreceptor assembly and maintenance. *Journal of Cell Biology*, *157*(1), 103–114.

Pedersen, L. B., & Rosenbaum, J. L. (2008). Chapter two intraflagellar transport (IFT): role in ciliary assembly, resorption and signalling. *Current topics in developmental biology*, *85*, 23–61.

Prasad, R. M., Jin, X., & Nauli, S. M. (2014). Sensing a sensor: identifying the mechanosensory function of primary cilia. *Biosensors*, *4*(1), 47–62.

Prigent, C., & Uzbekov, R. (2022). Duplication and segregation of centrosomes during cell division. *Cells*, *11*(15), 2445.

Prodanova Hadzhinesheva, V., Valcheva Chakarova, I., Metodieva Delimitreva, S., Dyankova Markova, M., Pantaleeva Nikolova, V., Sergeeva Mourdjeva, M., Istiliyanov Rashev, P., & Stefanova Zhivkova, R. (2018). Centriolar satellites associate with condensed chromatin in early mouse oocytes and undergo redistribution during transition to dictyate. *Biotechnology & Biotechnological Equipment*, *32*(6), 1622–1626.

Prosser, S. L., & Pelletier, L. (2020). Centriolar satellite biogenesis and function in vertebrate cells. *Journal of Cell Science*, *133*(1), jcs239566.

Prosser, S. L., Tkach, J., Gheiratmand, L., Kim, J., Raught, B., Morrison, C. G., & Pelletier, L. (2022). Aggresome assembly at the centrosome is driven by CP110–CEP97–CEP290 and centriolar satellites. *Nature Cell Biology*, *24*(4), 483–496.

Puram, S. V., Kim, A. H., Ikeuchi, Y., Wilson-Grady, J. T., Merdes, A., Gygi, S. P., & Bonni, A. (2011). A CaMKIIβ signaling pathway at the centrosome regulates dendrite patterning in the brain. *Nature neuroscience*, *14*(8), 973–983.

Quidwai, T., Wang, J., Hall, E. A., Petriman, N. A., Leng, W., Kiesel, P., Wells, J. N., Murphy, L. C., Keighren, M. A., Marsh, J. A., Lorentzen, E., Pigino, G., & Mill,

P. (2021). A WDR35-dependent coat protein complex transports ciliary membrane cargo vesicles to cilia. *Elife*, *10*.

Rai, A. K., Chen, J.-X., Selbach, M., & Pelkmans, L. (2018). Kinase-controlled phase transition of membraneless organelles in mitosis. *Nature*, *559*(7713), 211–216.

Reiter, J. F., & Leroux, M. R. (2017). Genes and molecular pathways underpinning ciliopathies. *Nat Rev Mol Cell Biol*, *18*(9), 533–547.

Ryan, E. L., Shelford, J., Massam-Wu, T., Bayliss, R., & Royle, S. J. (2021). Defining endogenous TACC3-chTOG-clathrin-GTSE1 interactions at the mitotic spindle using induced relocalization. *J Cell Sci*, *134*(3).

Sanchez, A. D., & Feldman, J. L. (2017). Microtubule-organizing centers: from the centrosome to non-centrosomal sites. *Curr Opin Cell Biol*, *44*, 93–101.

Satir, P., & Christensen, S. T. (2007). Overview of structure and function of mammalian cilia. *Annu. Rev. Physiol.*, *69*(1), 377–400.

Schatten, H. (2008). The mammalian centrosome and its functional significance. *Histochemistry and cell biology*, *129*, 667–686.

Schermelleh, L., Ferrand, A., Huser, T., Eggeling, C., Sauer, M., Biehlmaier, O., & Drummen, G. P. C. (2019). Super-resolution microscopy demystified. *Nat Cell Biol*, *21*(1), 72–84.

Schmidt, K. N., Kuhns, S., Neuner, A., Hub, B., Zentgraf, H., & Pereira, G. (2012). Cep164 mediates vesicular docking to the mother centriole during early steps of ciliogenesis. *Journal of Cell Biology*, *199*(7), 1083–1101.

Singla, V., & Reiter, J. F. (2006). The primary cilium as the cell's antenna: signaling at a sensory organelle. *science*, *313*(5787), 629–633.

Sorokin, S. (1962). Centrioles and the formation of rudimentary cilia by fibroblasts and smooth muscle cells. *The Journal of cell biology*, *15*(2), 363–377.

Stowe, T. R., Wilkinson, C. J., Iqbal, A., & Stearns, T. (2012). The centriolar satellite proteins Cep72 and Cep290 interact and are required for recruitment of BBS proteins to the cilium. *Molecular Biology of the Cell*, *23*(17), 3322–3335.

Tang, Z., Lin, M. G., Stowe, T. R., Chen, S., Zhu, M., Stearns, T., Franco, B., & Zhong, Q. (2013). Autophagy promotes primary ciliogenesis by removing OFD1 from centriolar satellites. *Nature*, *502*(7470), 254–257.

Tanos, B. E., Yang, H.-J., Soni, R., Wang, W.-J., Macaluso, F. P., Asara, J. M., & Tsou, M.-F. B. (2013). Centriole distal appendages promote membrane docking, leading to cilia initiation. *Genes & development*, *27*(2), 163–168.

Tollenaere, M. A., Mailand, N., & Bekker-Jensen, S. (2015). Centriolar satellites: key mediators of centrosome functions. *Cellular and molecular life sciences*, *72*, 11–23.

Veland, I. R., Awan, A., Pedersen, L. B., Yoder, B. K., & Christensen, S. T. (2009). Primary cilia and signaling pathways in mammalian development, health and disease. *Nephron Physiology*, *111*(3), p39–p53.

Viggars, M. R., Owens, D. J., Stewart, C., Coirault, C., Mackey, A. L., & Jarvis, J. C. (2023). PCM1 labeling reveals myonuclear and nuclear dynamics in skeletal muscle across species. *American Journal of Physiology-Cell Physiology*, *324*(1), C85–C97.

Wang, G., Chen, Q., Zhang, X., Zhang, B., Zhuo, X., Liu, J., Jiang, Q., & Zhang, C. (2013). PCM1 recruits Plk1 to the pericentriolar matrix to promote primary cilia disassembly before mitotic entry. *Journal of Cell Science*, *126*(6), 1355–1365.

Wang, L., Lee, K., Malonis, R., Sanchez, I., & Dynlacht, B. D. (2016). Tethering of an E3 ligase by PCM1 regulates the abundance of centrosomal KIAA0586/Talpid3 and promotes ciliogenesis. *Elife*, *5*.

Waters, A. M., & Beales, P. L. (2011). Ciliopathies: an expanding disease spectrum. *Pediatric nephrology*, *26*(7), 1039–1056.

Westlake, C. J., Baye, L. M., Nachury, M. V., Wright, K. J., Ervin, K. E., Phu, L., Chalouni, C., Beck, J. S., Kirkpatrick, D. S., & Slusarski, D. C. (2011). Primary cilia membrane assembly is initiated by Rab11 and transport protein particle II (TRAPPII) complex-dependent trafficking of Rabin8 to the centrosome. *Proceedings of the National Academy of Sciences*, *108*(7), 2759–2764.

Williams, C. L., Li, C., Kida, K., Inglis, P. N., Mohan, S., Semenec, L., Bialas, N. J., Stupay, R. M., Chen, N., & Blacque, O. E. (2011). MKS and NPHP modules cooperate to establish basal body/transition zone membrane associations and ciliary gate function during ciliogenesis. *Journal of Cell Biology*, *192*(6), 1023–1041.

Wirth, M., Zhang, W., Razi, M., Nyoni, L., Joshi, D., O'Reilly, N., Johansen, T., Tooze, S. A., & Mouilleron, S. (2019). Molecular determinants regulating selective binding of autophagy adapters and receptors to ATG8 proteins. *Nat Commun*, *10*(1), 2055.

Woodruff, J. B., Wueseke, O., & Hyman, A. A. (2014). Pericentriolar material structure and dynamics. *Philosophical Transactions of the Royal Society B: Biological Sciences*, *369*(1650), 20130459.

Wu, B., Long, C., Liu, J., Huang, X., Ma, S., Ma, Y., Wang, L., Jiang, Y., Yang, B., & Gong, C. (2025). A subset of evolutionarily conserved centriolar satellite core components is crucial for sperm flagellum biogenesis. *Theranostics*, *15*(14), 7025.

Xie, S., Naslavsky, N., & Caplan, S. (2023). EHD1 promotes CP110 ubiquitination by centriolar satellite delivery of HERC2 to the mother centriole. *EMBO reports*, *24*(6), e56317.

Yoshida, M. W., Yamada, M., & Goshima, G. (2019). Moss Kinesin-14 KCBP accelerates chromatid motility in anaphase. *Cell Structure and Function*, *44*(2), 95–104.

Zhao, H., Chen, Q., Li, F., Cui, L., Xie, L., Huang, Q., Liang, X., Zhou, J., Yan, X., & Zhu, X. (2021). Fibrogranular materials function as organizers to ensure the fidelity of multiciliary assembly. *Nat Commun*, *12*(1), 1273.

APPENDIX

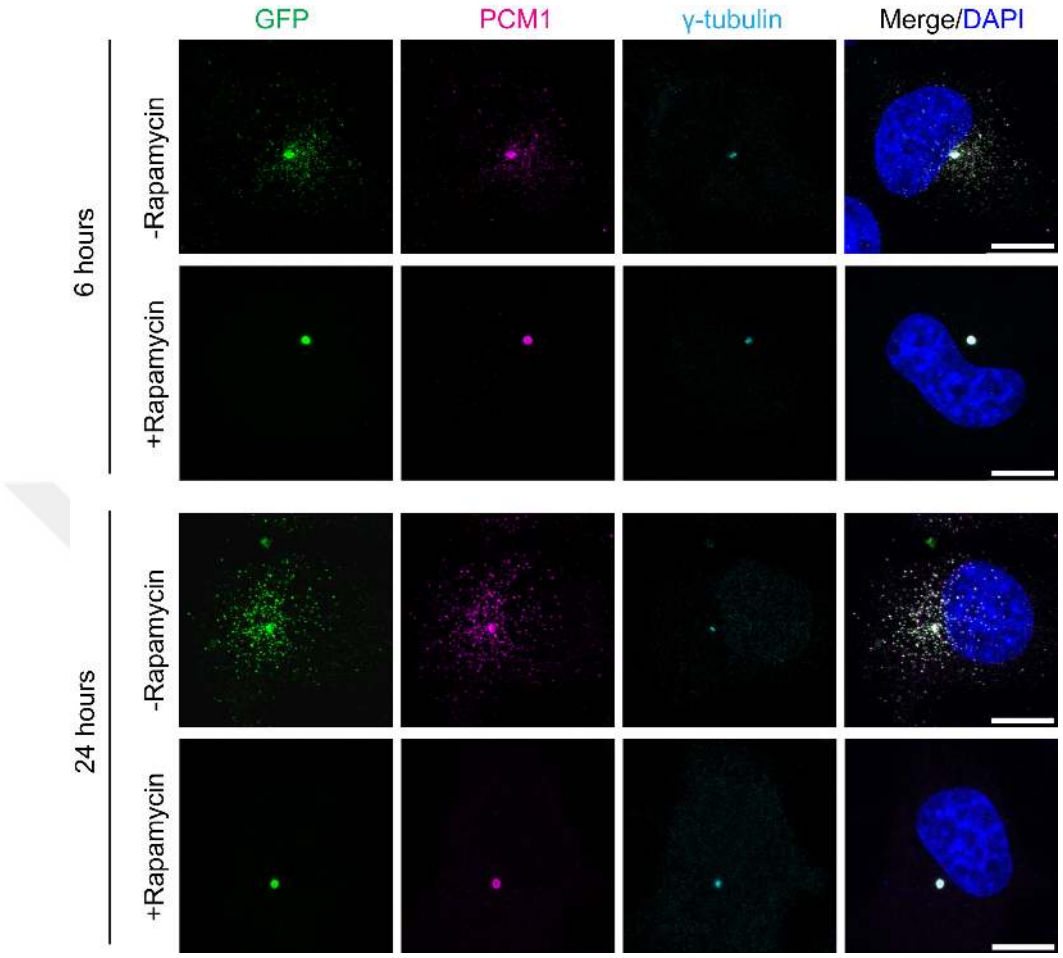

Appendix Figure 1 Satellite trafficking assay re-routes endogeneous PCM1 along with GFP-PCM1-FKBP.

Cells co-transfected with GFP-PCM1-FKBP and FRB-Flag-Kin14 were treated with rapamycin for 6 or 24 hours. Endogeneous PCM1 is recruited to the pericentrosomal region along with GFP-PCM1-FKBP. Scale bar: 10 μm.

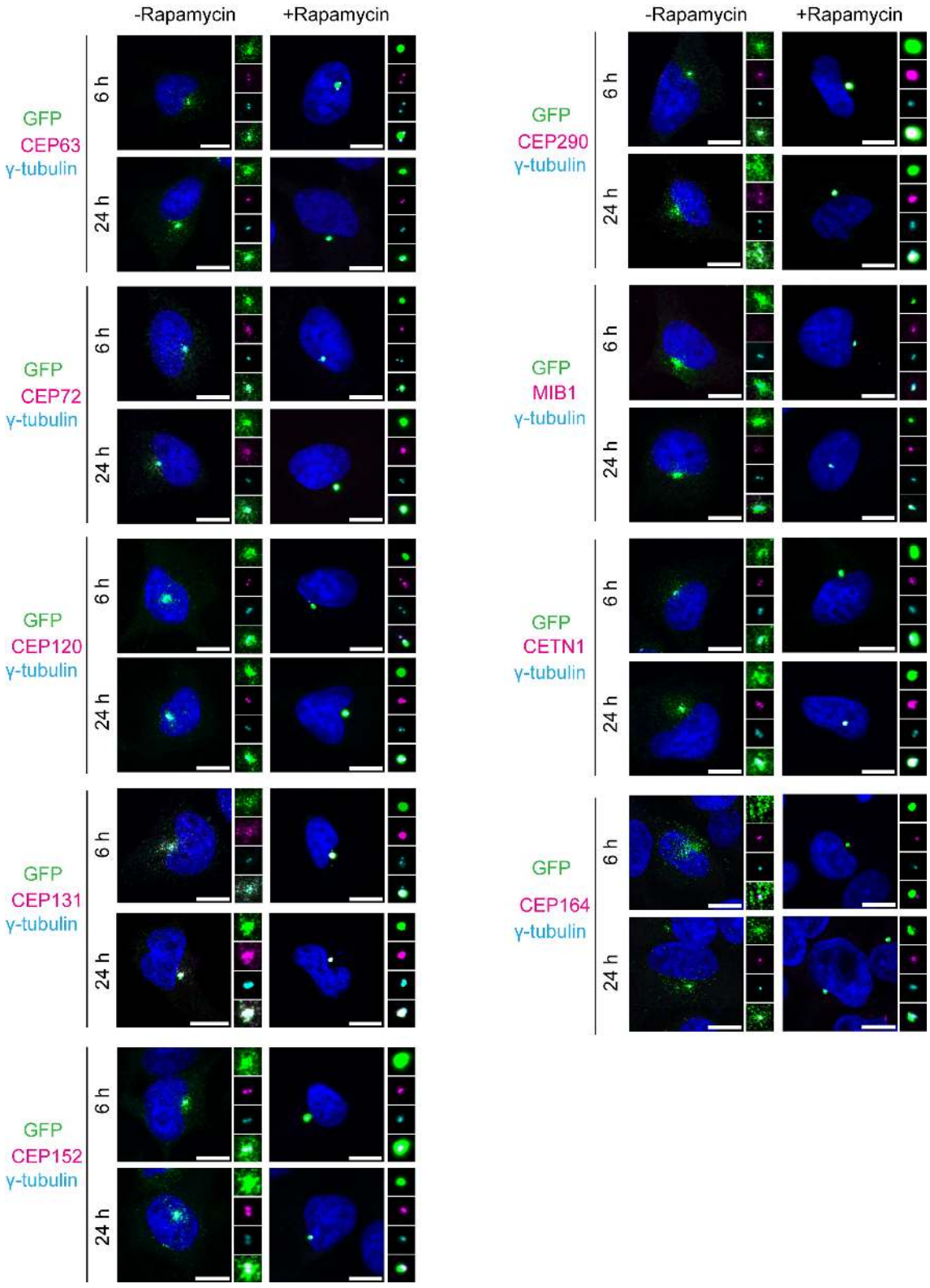

Appendix Figure 2 Centriolar satellites re-route client proteins to the centrosome. HeLa cells co-transfected with GFP-PCM1-FKBP and FRB-Flag-Kin14 were treated with rapamycin for 1 hour and fixed at 6 or 24 hours. Cells immunostained for GFP, γ-tubulin, and indicated client proteins. Insets show pericentrosomal region. Scale bar: 10 μm.

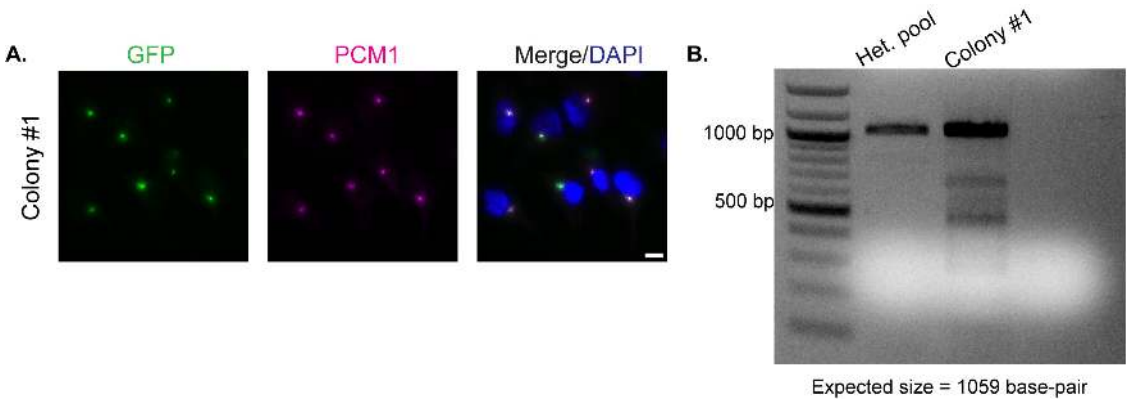

Appendix Figure 3 Confirmation of GFP-PCM1-FKBP knock in cell line.

A. Immunostaning of HeLa-hR26-GFP-PCM1-FKBP colony#1 cell line with GFP and PCM1. Scale bar: 10 μm. **B.** Confirmation of HeLa-hR26-GFP-PCM1-FKBP colony#1 cell line with genomic DNA PCR with primers specific to 5'homology arm and HygroB sequences.

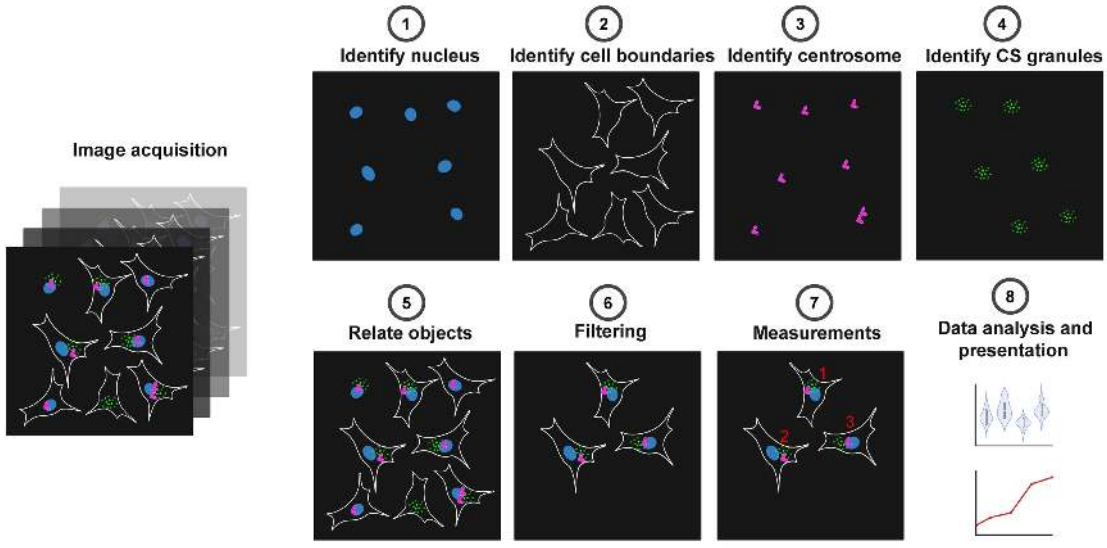

Appendix Figure 4 Centriolar satellite phenotypic assay pipeline.

Appendix Table 1. List of antibodies

Recognized Protein	Source	Brand	Product Code	Dilution
mNeonGreen	Rat	Homemade		1:1000
PCM1-N-Ab	Rabbit	Protein Tech	19856-1-AP	1:1000
PCM1-C-Ab	Rat	Homemade		1:1000
PCM1-C-Ab	Rabbit	Homemade		1:1000
Centrin (20H5)	Mouse IgG2a	Millipore	04-1624	1:500
SMO (E5)	Mouse IgG2a	Santa Cruz	sc-166685	1:1000
Acetylated tubulin	Mouse IgG2b	Santa Cruz	sc-23950	1:2000
CEP131	Rabbit	ProteinTech	25735-1-AP	1:1000
Arl13b	Rabbit	Protein Tech	17711-1-AP	1:2000
CEP290	Rabbit	Abcam	ab84870	1:1000
MIB1	Rabbit	Sigma	M5948	1:1000
GFP	Mouse IgG2a	Invitrogen	A11120	1:750
DYKDDDDK (Flag)	Rabbit	Protein Tech	20543-1-AP	1:500
DYKDDDDK (Flag)	Rabbit	Cell Signaling Technology	D6W5B	1:250
Gamma tubulin (GTU88)	Mouse IgG1	Sigma	T6557	1:1000
CEP63	Rabbit	Proteintech	16268 1 AP	1:1000
CEP72	Rabbit	Proteintech	19928 1 AP	1:1000
CEP120	Rabbit	Homemade		1:1000
CEP152	Rabbit	Bethyl	A302-479-A	1:1000
Centrin 1	Rabbit	Proteintech	12794 1 AP	1:1000
CEP164	Rabbit	Proteintech	22227 1 AP	1:1000
CEP164	Mouse IgG1	Homemade		1:1000
Alpha tubulin (DM1A)	Mouse IgG1	Sigma	T926	1:1000
Anti-Rat AlexaFluor 488	Goat	Thermo		1:2000
Anti-Rat AlexaFluor 568	Goat	Invitrogen	A11077	1:2000

Anti-Rat AlexaFluor 647	Goat	Invitrogen	A21146	1:2000
Anti-Rabbit AlexaFluor 488	Goat	Invitrogen	1971418	1:2000
Anti-Rabbit AlexaFluor 568	Goat	Invitrogen	A11011	1:2000
Anti-Rabbit AlexaFluor 633	Goat	Life technologies	A21071	1:2000
Anti-Mouse IgG1 AlexaFluor 594	Goat	Invitrogen	A21125	1:2000
Anti-Mouse IgG1 AlexaFluor 633	Goat	Invitrogen	A21126	1:2000
Anti-Mouse IgG2a AlexaFluor 594	Goat	Invitrogen	A21135	1:2000
Anti-Mouse IgG2a AlexaFluor 633	Goat	Life technologies	A21136	1:2000
Anti-Mouse IgG2b AlexaFluor 568	Goat	Life Technologies	A21144	1:2000
Anti-Mouse IgG2b AlexaFluor 633	Goat	Invitrogen	A21146	1:2000

Appendix Table 2 List of primers

hRosa26(Locus PCR) Genome 5'	GAGAAGAGGCTGTGCTTCGG
hRosa26(5'INT PCR) Splice Acceptor	CTGTGGGAGGAAGAGAAGAGGT
PCM1-FL-FW	CGCGGATCCGGTAGTATGGCCACAGGAGGAGGTC
PCM1-FL-REV	ATAAGAATGCGGCCGCTATACTCTGGGCTCCCACC
FKBP-F36V-FW	ATAAGAATGCGGCCGCTGGAGTGCAGGTGGAG
FKBP-F36V-REV	ATAAGAATGCGGCCGCTTCCAGTTTTAGAAGCTC